The effect of chemical reaction kinetics on the structure of gaseous detonations

by

Hoi Dick Ng

Department of Mechanical Engineering
McGill University
Montréal, Québec, Canada

June, 2005

A thesis submitted to the
Faculty of Graduate Studies and Research
in partial fulfillment of the requirements for the degree of
Doctor of Philosophy
in
Mechanical Engineering

Library and
Archives Canada

Published Heritage
Branch

395 Wellington Street
Ottawa ON K1A 0N4
Canada

Bibliothèque et
Archives Canada

Direction du
Patrimoine de l'édition

395, rue Wellington
Ottawa ON K1A 0N4
Canada

Your file Votre référence
ISBN: 978-0-494-21682-8
Our file Notre référence
ISBN: 978-0-494-21682-8

NOTICE:
The author has granted a non-exclusive license allowing Library and Archives Canada to reproduce, publish, archive, preserve, conserve, communicate to the public by telecommunication or on the Internet, loan, distribute and sell theses worldwide, for commercial or non-commercial purposes, in microform, paper, electronic and/or any other formats.

The author retains copyright ownership and moral rights in this thesis. Neither the thesis nor substantial extracts from it may be printed or otherwise reproduced without the author's permission.

AVIS:
L'auteur a accordé une licence non exclusive permettant à la Bibliothèque et Archives Canada de reproduire, publier, archiver, sauvegarder, conserver, transmettre au public par télécommunication ou par l'Internet, prêter, distribuer et vendre des thèses partout dans le monde, à des fins commerciales ou autres, sur support microforme, papier, électronique et/ou autres formats.

L'auteur conserve la propriété du droit d'auteur et des droits moraux qui protège cette thèse. Ni la thèse ni des extraits substantiels de celle-ci ne doivent être imprimés ou autrement reproduits sans son autorisation.

In compliance with the Canadian Privacy Act some supporting forms may have been removed from this thesis.

While these forms may be included in the document page count, their removal does not represent any loss of content from the thesis.

Conformément à la loi canadienne sur la protection de la vie privée, quelques formulaires secondaires ont été enlevés de cette thèse.

Bien que ces formulaires aient inclus dans la pagination, il n'y aura aucun contenu manquant.

Canada

> *"Magna opera Domini exquisita in omnes voluntates ejus"*
>
> *"The works of the Lord are great, sought out of all them that have pleasure therein".*
>
> *- Psalm CXI*

Abstract

In order to elucidate the effect of chemical kinetics on the dynamic structure of a detonation, an investigation is carried out by means of high-resolution numerical simulations of the reactive Euler equations. The chemical description ranges, with increasing complexity, from simplified single-step reaction kinetics to complex models with detailed chemical reaction rates.

To illustrate the unsteady dynamics of the detonation structure and its dependence on chemical kinetics, a one-dimensional pulsating detonation with one-step kinetics has been investigated. Different nonlinear dynamics of the pulsating front are observed by varying the global temperature sensitivity of the chemical process. Numerical results have suggested that the route to higher oscillation modes may follow closely the Feigenbaum scenario of a period-doubling cascade leading to the existence of chaos as observed in many generic nonlinear systems. The remarkable similarity between a simple nonlinear dynamical system and the pulsating detonation structure suggests that the use of a nonlinear oscillator model can be considered to explore the role of chemical kinetics on the instability spectrum of the oscillatory front.

To clarify the importance of chain-branching reactions and to resolve the drawbacks associated with the single-step Arrhenius model, a thorough analysis of the pulsating detonation using a two-step reaction mechanism, consisting of a thermally neutral induction step followed by a main reaction layer, has been carried out. It is found that the dynamics of detonation structure depend not only on the temperature sensitivity of the reaction but also the shape of the reaction zone characterized by the length of induction and main heat release layer. From the parametric study, a relevant non-dimensional stability parameter χ and its associated neutral stability curve have been determined. These results are further generalized to more complicated kinetic models of detonation in real gaseous mixtures. They provide a tool to elucidate different experimental observations on the detonation structure such as the cell regularity, the effect of argon dilution and the propagation mechanism. An improved model for the prediction of the characteristic cell size of a detonation is also formulated by including the present stability parameter χ.

To deduce a global method to examine the transient reaction structure of the detonation, the head-on collision problem of a detonation with a shock wave has been proposed. The present study concerned with the effect of chemical kinetics on the unsteady dynamics of the head-on collision phenomenon. Numerical simulations have demonstrated that the unsteady interaction involves a relaxation process consisting of a quasi-steady period and an overshoot for the transmitted detonation subsequent to the frontal collision, followed by the asymptotic decay to a CJ detonation. Due to the change of chemical kinetics as a result of the increase in the thermodynamic state of the reactive mixture from shock compression, the transmitted pulsating detonation can be stabilized with smaller amplitude and period oscillation. These observations are in agreement with experimental evidence obtained from smoked foils where significant decrease in detonation cell size after a region of relaxation is observed when the detonation collides head-on with a shock wave.

Résumé

Afin d'élucider l'effet de la cinétique chimique sur la structure dynamique d'une détonation, une étude est effectuée au moyen de simulations numériques à haute résolution des équations réactives d'Euler. Une gamme de mécanismes chimiques est utilisée et s'étend, en ordre croissant de complexité, de modèles cinétiques simplifiés à une seule réaction à des modèles complexes de réaction avec des taux de réaction chimiques détaillés.

Pour illustrer la dynamique instable de la structure des détonations et sa dépendance à la cinétique chimique, une détonation unidimensionnelle instable avec un modèle cinétique à une réaction a été étudiée. On observe une variété de dynamiques non linéaires du front en changeant la sensibilité globale du processus chimique. Les résultats numériques suggèrent que la transition à des modes plus élevés d'oscillation suit de près le scénario de Feigenbaum, soit une cascade de doublement de période menant à une solution chaotique, comme on peut l'observer dans plusieurs systèmes génériques non linéaires. La similitude remarquable entre un système dynamique non-linéaire simple et la structure d'une détonation unidimensionnelle instable suggère que l'utilisation d'un modèle d'oscillateur non linéaire puisse être employé pour explorer le rôle de la cinétique chimique sur les modes d'instabilité du front oscillant.

Pour clarifier l'importance des réactions de « chain-brainching » et pour résoudre les inconvénients liés aux modèles à une réaction d'Arrhenius, une analyse complète de la détonation unidimensionnelle instable utilisant un mécanisme à deux étapes de réaction, modèle se composant d'une étape thermiquement neutre d'induction suivie d'une zone principale de réaction, a été effectuée. On constate que la dynamique de la structure de détonation dépend non seulement de la sensibilité de la réaction à la température mais également de la forme de la zone de réaction caractérisée par les longueurs des zones d'induction et de réaction. À partir d'une étude paramétrique, un paramètre de stabilité non dimensionnel approprié, χ, et la courbe de stabilité neutre associée ont été déterminés. Ces résultats ont ensuite été généralisés à des modèles cinétiques plus compliqués de détonation dans de vrais mélanges gazeux. Ces résultats fournissent un outil pour expliquer différentes observations expérimentales de la structure des détonations, telle que la régularité des cellules, l'effet de la dilution avec de l'argon et le mécanisme de propagation. Un modèle amélioré pour la prédiction de la taille caractéristique des cellules d'une détonation est également formulé en incluant le paramètre de stabilité actuel, χ.

Pour déduire une méthode globale d'analyse de la structure de réaction des détonations, on étudie le problème de collision frontale d'une détonation avec une onde de choc. La présente étude s'est penchée sur l'effet de la cinétique chimique sur la dynamique instable du phénomène de collision frontale. Les simulations numériques ont démontré que l'interaction implique un processus de relaxation, composé d'une période quasi-stationnaire et suivi d'une augmentation soudaine de la vitesse de la détonation transmise. Cette interaction est suivie de l'affaiblissement asymptotique à une détonation de type Chapman-Jouguet (CJ). En raison du changement de la cinétique chimique dû à l'augmentation de l'état thermodynamique du mélange réactif compressé par une onde de choc, une détonation initialement instable peut être stabilisée, exhibant ainsi une plus petite amplitude d'oscillation et une période plus courte, grâce à son interaction frontale avec une onde de choc. Ces observations sont en accord avec les résultats expérimentaux obtenus à partir de « smoked foils » où, lorsque la détonation se heurte à une onde choc, une diminution significative de la taille des cellules de détonation, après une région de relaxation, est observée.

Acknowledgments

First and foremost, I would like to express deep gratitude to my supervisor, Prof. John Lee, for his good advice and constructive criticism, availability and guidance throughout the entire course of my graduate studies. His way of thinking in fundamental physics and unique attitude to science certainly inspired me on how to become a good research scientist.

This work could not have been completed without the help of many people. I would like to thank Nikolaos Nikiforakis for teaching and providing me all the computational tools I need for my research. His warm hospitality during my visit at University of Cambridge is also greatly appreciated. I am especially grateful to Prof. Andrew Higgins and Matei Radulescu, for stimulating numerous interesting ideas of this thesis and nursing it through to completion with a wealth of helpful suggestions.

The assistance from all members of the Shock Wave Physics Group is gratefully acknowledged. Special thanks to Jenny Chao, for proofreading many of my manuscripts and being a friendly neighbor at the office. I acknowledge to Prof. Eugene Timofeev for providing his characteristics algorithm. Many thanks also go to Vincent Tanguay, Charles Kiyanda, Sam Goroshin and Barbara Botros for making my graduate studies more pleasant with their unique perspective on a variety of both scientific and non-scientific topics of discussion.

Grateful acknowledgment is also due to many researchers around the globe: Prof.

Mark Short, Gary Sharpe, Bala Varatharajan, Randy Chue, Kiumars Mazaheri, Prof. Jiming Yang, Jean-Philippe Dionne, Fan Zhang, Max Romano, Kelvin Bates for their valuable advice, assistance and numerous fruitful discussions on the field of detonation physics and scientific computing.

I also want to extend my full gratitude to my family, all my friends, brothers and sisters in Montreal Chinese Alliance Church for their support and encouragement. Finally, I would like to acknowledge the Natural Sciences and Engineering Research Council of Canada (NSERC) and Fonds de recherche sur la nature et les technologies (FQRNT) for their financial support.

Chapter 3 of the present thesis contains materials, which appear in "Nonlinear dynamics and chaos analysis of one-dimensional pulsating detonations," *Combust. Theory Model.* **9**, 159-170. (2005). The thesis author was the primary researcher in that publication.

Chapter 4 of the present thesis contains materials, which appear in "Numerical investigation of the instability for one-dimensional Chapman-Jouguet detonations with chain-branching kinetics," *Combust. Theory Model.*, In press. (2005). The thesis author was the primary researcher in that publication.

Chapter 5 of the present thesis contains materials, which appear in "The effect of argon dilution on the stability of acetylene/oxygen detonations," *Proc. Combust. Inst.* **29**, 2825-2831. (2002). The thesis author was the secondary researcher in that publication.

Chapter 7 and Appendix C of the present thesis contain materials, which appear in "Head-on collision of a detonation with a planar shock wave," *Proc. 24th Int. Sym. Shock Waves*, Vol. 2, 745-750. (2004). The thesis author was the primary researcher in that publication.

Contents

List of Figures

List of Tables

Glossary

A	Proportionality factor of the cell size correlation
c	Sound speed
C_{p_i}	Specific heat at constant pressure of the i^{th} species
C_{v_i}	Specific heat at constant volume of the i^{th} species
D	Detonation velocity
e	Specific internal energy
E	Total energy of the mixture per unit mass
E_a	Global activation energy
E_I	Activation energy of the induction process
E_R	Activation energy of the heat release process
f	Detonation overdriven factor
$\mathbf{F}(\mathbf{U})$	Convective flux in the x-direction
$\mathbf{G}(\mathbf{U})$	Convective flux in the y-direction
h_i	Specific enthalpy of the i^{th} species
h_i^f	Heat of formation of the i^{th} species
K	pre-exponential constant
K_I	Reaction rate constant of the induction process
K_R	Reaction rate constant of the heat release process
k_j^f	Forward reaction rate constant for reaction j

k_j^b	Backward reaction rate constant for reaction j
$k_j^{equil.}$	Equilibrium constant
l_{driver}	Length of the driver gas section
L_{c_i}, L_{s_i}	Operators for the convective and reactive source terms
$L_{1/2}$	Half-reaction zone length
l_h	Hydrodynamic thickness
M	Mach number
W_i	Molecular weight of the i^{th} species
N_s	Total number of chemical species
N_{reac}	Total number of chemical reactions
p	Pressure
Q	Chemical energy release
q_j	Net rate of progress for reaction j
R	Universal gas constant
$\mathbf{S}(\mathbf{U})$	Source term
t	Time
T	Temperature
T_B	Chain-branching cross-over temperature
u	Particle velocity in the x-direction
$\mathbf{U}$	Conserved variable
v	Particle velocity in the y-direction
x	Distance along first coordinate direction
X_i	Chemical species
$[X_i]$	Species concentration
y	Distance along second coordinate direction
Y_i	Species mass fraction

Acronyms

AMR	Adaptive Mesh Refinement
CFD	Computational Fluid Dynamics
CFL	Courant - Friedrichs - Lax
CJ	Chapman - Jouguet
ENO	Essentially Non-Oscillatory
FORCE	First-Order Centered
MUSCL	Monotone Upwind Scheme for Conservation Laws
MUSTA	Multi-Stage Predictor-Corrector Approach
RH	Rankine - Hugoniot
SLIC	Slope Limited Centered
SWACER	Shock Wave Amplification by Coherent Energy Release
TVD	Total Variation Diminishing
WAF	Weighted Average Flux
VN	von Neumann
ZND	Zel'dovich - von Neumann - Döring

Greek symbols

α_j	Temperature exponent in the kinetic rate law
β	Reaction progress variable
χ	Non-dimensional stability parameter
δ	Temperature jump across the shock front
Δ_i	Slope vector in the MUSCL reconstruction
Δ_I	Characteristic induction length
Δ_R	Characteristic reaction length
ε_I	Reduced activation energy of the induction process

ε_R	Reduced activation energy of the heat release process
γ	Ratio of specific heats
λ	Detonation cell size
μ_i	Location of bifurcation points
ν'_{ij}, ν''_{ij}	Forward and backward stoichiometric coefficients
Ω	Chemical reaction rate
ξ	Reaction progress variable for the induction process
ϕ	Equivalent ratio
Φ	Unsteady part of the energy in the oscillator model
Ψ	Unsteady part of the heat release rate in the oscillator model
ρ	Density
$\dot{\sigma}$	Thermicity
$\dot{\omega}_i$	Net mass production/consumption rate of the i^{th}species
τ	Induction time
ν	Specific volume

Subscripts

L	Left
R	Right
o	Initial condition, unburnt mixture properties
s	Post-shock condition
p	Product
r	Reactant
ref	Reference scale
max	Maximum

Chapter 1

Introduction

Although gaseous detonation waves have been studied extensively for many years, the development of successful theories for the prediction of practical properties in a given explosive mixture such as detonation limits, critical tube diameter or initiation energy (Lee 1984) remains a challenge. It is known that the ability to describe the detonation propagation mechanism and to predict these dynamic parameters can only be resolved by understanding the physical and chemical processes inside the non-equilibrium structure of the detonation wave. However, knowledge of many aspects of this structure remains qualitative due to its complexity where gasdynamic effects are strongly coupled with the fast chemical reactions. In the present thesis, the objective is to contribute to a better description of the detonation structure, and in particular, to investigate the influence of chemical reaction kinetics on the instability of detonation fronts and on the different dynamic parameters.

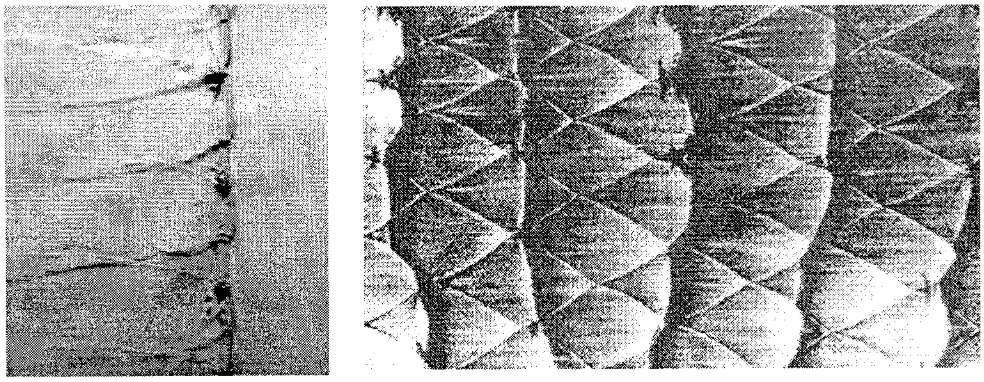

Figure 1.1. Schlieren photograph and smoked foil showing the cellular structure for $2H_2$-O_2-2Ar detonation (Radulescu 2003; Strehlow 1969).

1.1 Detonation structure

The classical model for the structure of detonation waves was independently proposed in the early 1940's by Zel'dovich (1940), von Neumann (1942) and Döring (1943). The ZND theory postulates that a detonation structure consisted of a planar leading shock wave followed by an exothermic chemical reaction zone. The combustible mixture is first compressed to a high temperature by the leading shock front and thereby, causing auto-ignition and initiating the chemical reactions after an induction time. The subsequent expansion of the high-pressure reacting gases provides the momentum change to sustain the propagation of the leading shock front. Thus, the ZND model provides the basic propagation mechanism, i.e. the detonation is sustained by the chemical energy release caused by auto-ignition via adiabatic shock compression and the work done by the expansion behind the shock front. Knowledge of the elementary reactions and their respective rate constants also permits the detailed time evolution of the various chemical species and the thermodynamic state in the reaction zone to be determined.

The steady ZND model describes the one-dimensional or laminar structure of a detonation wave, but it is generally not applicable to experimentally observed self-propagating detonation waves, which are three-dimensional and non-steady. It has now been established, both experimentally and theoretically, that self-sustained detonations in most combustible mixtures are inherently unstable, leading to different unsteady and multi-dimensional features. The multi-dimensional unsteady structure of self-sustained detonation waves was conclusively demonstrated from experiments carried out in the 50's and early 60's using optical visualizations (Voitsekhovskii *et al.* 1958; White 1961; etc.) and smoked foil technique (Denisov & Troshin 1959; Shchelkin & Troshin 1965; Strehlow *et al.* 1967; etc.). The unsteady structure consists of an ensemble of interacting transverse shock waves sweeping back and forth across the leading front. Their mutual interactions form the classical triple shock Mach interaction configuration (Courant & Friedrichs 1946). The trajectories of these triple points can be recorded on a smooth surface coated with a carbon soot deposit and have a characteristic fish scale or cellular pattern as the detonation propagates by it. The cellular structure is indeed a manifestation of the instability of the front caused by the unsteady coupling between the chemical reactions and the gasdynamic flow field. A photograph of a detonation front and an example of a soot foil are given in figure 1.1.

The cellular structure of gaseous detonations can be attributed to the onset of chemical-gasdynamic instabilities. Theoretical stability analyses (e.g. Zaidel 1961; Erpenbeck 1964; Lee & Stewart 1990; etc.) have shown that the laminar ZND structure is inherently unstable to small perturbations. These theoretical studies indicate that a large number of unstable modes contribute to the overall detonation structure. These modes can interact in a nonlinear manner to produce a complex unstable detonation structure. One-dimensional unstable structure of detonation waves was first studied numerically using the method of characteristics by Fickett & Wood as early as 1966. Since then, more thorough studies on one-dimensional detonations

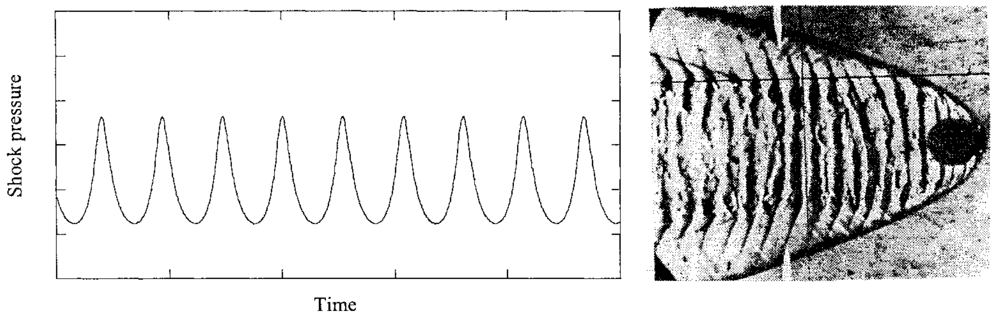

Figure 1.2. a) Numerically computed pulsating detonation front and b) shock-induced oscillation from a hypersonic projectile into a reactive mixture (Alpert & Toong 1972).

have been carried out by different researchers (Abouseif & Toong 1982; Moen *et al.* 1984; etc.). The results of these studies all showed that in a one-dimensional configuration, the manifestation of instability to small disturbances results in a longitudinal pulsating structure of the detonation front (see figure 1.2a). Investigations of the nonlinear oscillatory behavior of one-dimensional detonations thus provide a first step in elucidating the nature of the self-sustained cellular detonation structure and interpreting the instability mechanism. Also noted that the phenomenon of the periodic longitudinal pulsation of one-dimensional detonations is reminiscent to the bow shock instability observed experimentally off the forward surface of a hypersonic spherical or blunt body object traveling into reactive atmosphere, where the strength of the leading shock wave fluctuates in a periodic manner, as illustrated in figure 1.2b (McVey & Toong 1971; Alpert & Toong 1972; etc.).

Multi-dimensional simulations of the detonation structure have also been performed by several researchers since the early 80's (Taki & Fujiwara 1978; Oran & Boris 1987; Fujiwara & Reddy 1989; Bourlioux & Majda 1992; etc.). The early two-dimensional simulations demonstrated that under standard conditions, perturbation on the ZND wave by spatial density inhomogeneities or local explosion behind the

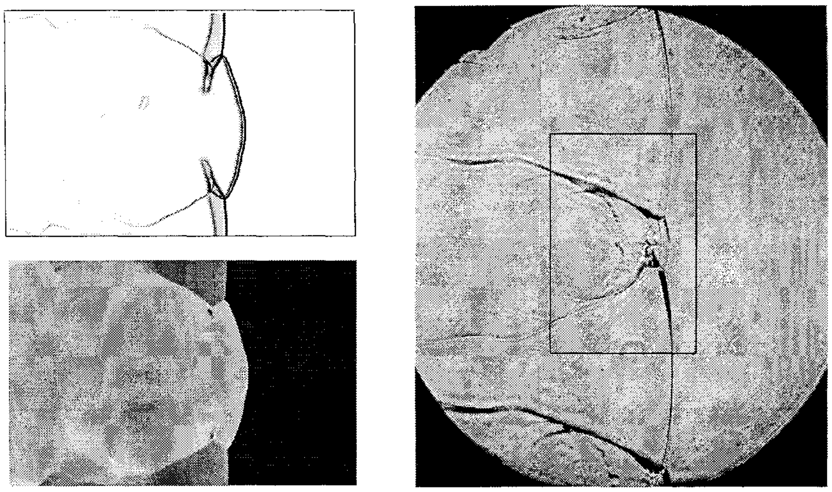

Figure 1.3. Comparison of the detailed configuration of the cellular detonation front between numerical simulations from the present study and experimental results (Austin *et al.* 2004).

shock leads to the development of unstable cellular structure. A comparison between numerical simulations and experimental results is given in figure 1.3 showing the unsteady configuration of the transient incident shock, Mach stem and transverse reflected waves. Although current capability of numerical simulations can essentially reproduce the same qualitative features of the cellular detonation as revealed in real experiments, interpretation of the tremendous amount of information that is being generated from the computation remains difficult. The issue of obtaining sufficient numerical resolution for achieving highly resolved details on the multi-dimensional detonation structure for quantitative analysis is still unresolved.

In spite of the extensive efforts to study the behavior of detonations thus far, a complete quantitative theory capable of describing the coupled chemical hydrodynamic interactions responsible for the dynamic structure of detonations is not yet achieved. This stems largely from the fact that the associated phenomena are highly complex and involve many aspects of combustion and wave processes. The origin or nature of the unstable detonation front, such as the role of instability and the detailed chemical kinetics processes within the reaction zone structure, remains poorly understood. It is therefore important to identify the key ingredients and understand their influences so that the detonation structure can be correctly characterized.

1.2 The effect of chemistry

Since the discovery of the detailed unsteady detonation structure, it has become clear that characteristics of the unstable detonation front are strongly influenced by the chemistry of the combustible mixture. Experimentally, it is shown the nature of transverse waves and the cell regularity of detonations are dependent on the chemical systems, which can undergo different chemical reactions with different kinetics. As Strehlow (1969) pointed out, significant differences on the unstable structure can be observed in mixtures with different chemical composition. For example, sensitive mixtures like H_2-O_2 or high temperature systems such as fuel-oxygen mixtures highly diluted with a monotonic gas such as argon are generally observed to produce remarkably regular or more organized structure having weak transverse waves. However, for less sensitive hydrocarbon fuel-oxygen mixtures such as CH_4-O_2 or fuel-air mixtures without dilution, the cell patterns recorded on the smoked foil can be extremely irregular or disorganized and the detonation structure consists of strong transverse waves. Figure 1.4 shows some smoked foil records for the purpose of making a qualitative comparison of the effect of chemical system on structure.

The role of chemical kinetics on the detonation structure was also illustrated later by Libouton *et al.* (1975). They have shown experimentally how slight changes in the chemical kinetics process, caused by inhibiting species added in traces to the original mixture, can modify the cellular structure of detonations. The added compound only caused inhibition effects on several reaction steps in the chemical kinetic mechanism

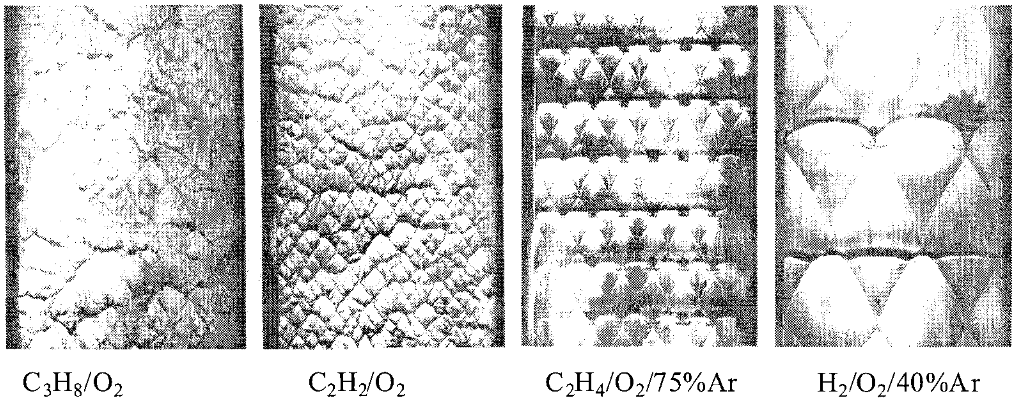

Figure 1.4. Experimental smoked foil records for different types of combustible mixture (Voitsekhovskii *et al.* 1966).

and it does not significantly modify the overall thermodynamic properties of the system. Their early tentative explanation is that the presence of additives in trace amounts has a similar effect of increasing the overall activation energy of the system and thus causing an increase in the detonation cell width.

Attempts have also been made to characterize the regularity of the cellular detonation structure using the concept of global activation energy E_a/RT_s (where E_a is the dimensional activation energy of the reaction, R is the gas constant and T_s is the post shock temperature of a steady ZND wave). Ul'yanitskii (1981) and Manzhalei (1977) reported a qualitative correlation between the cell regularity and the global activation energy of the mixture. This perhaps provides the simplest link explaining the role played by chemical kinetics on the observed detonation structure. They show that mixtures with higher activation energy generally have a more irregular structure.

Numerical simulations using the single-step Arrhenius reaction rate model tend to support this feature of chemical kinetics on the detonation structure. For a single-step

Arrhenius model, the chemical kinetics is solely controlled by the global activation energy. A closer look at this parameter of activation energy basically describes the steepness of the reaction time-temperature dependence. Large values of the overall activation energy give large fluctuations in the reaction rate with small temperature change, and thus rendering the system unstable. The unsteady coupling between the leading detonation front and the energy release from the chemical reaction can create an unstable feedback loop that results in the spontaneous and various nonlinear instabilities of the propagating detonation. Numerical results show that the one-dimensional unstable pulsating structure changes from harmonic oscillations to nonlinear and eventually to highly aperiodic as the value of the activation energy is increased from its value at the stability limit (Bourlioux *et al.* 1991; He & Lee 1995; Sharpe & Falle 1999; etc.). Similarly, the recent two-dimensional simulations by Gamezo *et al.* (1999) have demonstrated that increasing the activation energy of the combustible mixture results in more irregular structures characterized by stronger triple points, larger variations of the local shock velocity inside the detonation cell, and higher frequency of appearance and disappearance of triple points.

Overall, the past experimental and numerical investigations clearly indicate the strong dependence of the unstable detonation structure on the temperature sensitivity of the reactions. However, a more quantitative analysis of cell regularity made by Shepherd *et al.* (1986) who used peaks in the power spectral density computed from digital images processing technique of soot foils to identify the frequency present, found that the overall activation energy (E_a/RT_s) as a stability parameter given by the single step Arrhenius reaction model fails to account for the observed variations in a systematic way. As an example, it can be shown from kinetic calculations that the global activation energy (E_a/RT_s) for acetylene-oxygen mixtures with different degree of argon dilutions does not change significantly, while there is a large variation in the regularity of detonation structure as shown in figure 1.5 illustrating the cell size distribution for acetylene-oxygen detonations with different amounts of argon.

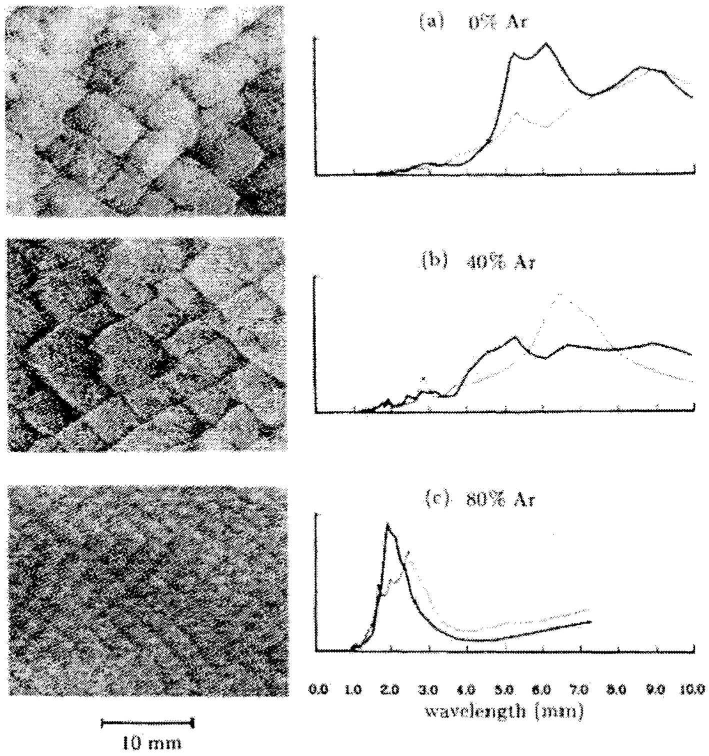

Figure 1.5. Cell size distribution for acetylene-oxygen detonations with different amounts of argon dilution (Shepherd *et al.* 1986).

No doubt any parameter that characterizes the sensitivity of the system such as the activation energy can provide some measure of the regularity of the detonation structure, but it is obvious that the detailed description of the detonation structure cannot be fully obtained by this single parameter and important features of the chemical process on the non-equilibrium structure may be discarded. The chemical reaction kinetics should perhaps be examined more closely and other important chemical kinetic parameters should be introduced in order to characterize the detonation front. But it becomes clear that this can only be achieved if a detailed investigation using more detailed chemical kinetic mechanisms is carried out.

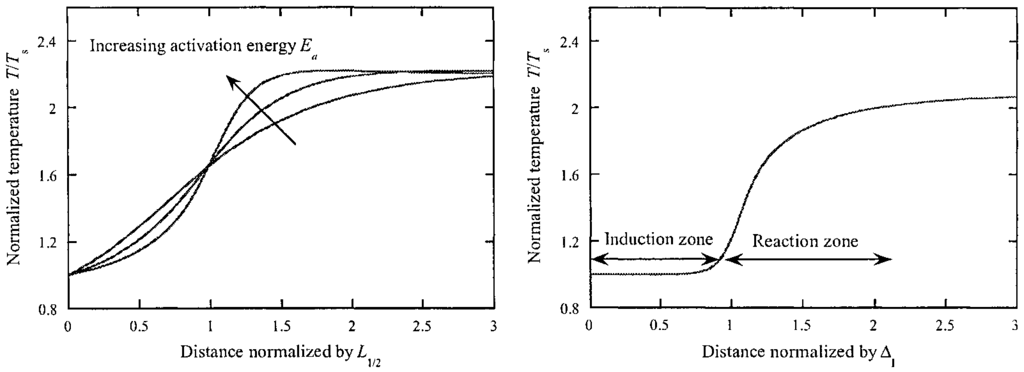

Figure 1.6. Temperature profiles of the ZND detonation structure computed using (a) the one-step kinetic model with different values of activation energy and (b) the detailed kinetic mechanism for H_2-O_2 mixture.

1.3 Importance of the chemical kinetic model

In spite of the recognition of the necessity to consider more details of the chemical kinetics in the study of detonation dynamics, this is often one of the most important aspects that has been underestimated in most of the previous theoretical and numerical investigations. The majority of these studies have been conducted for the simplest one-step Arrhenius description for the chemical reaction structure, where the reactant is simply assumed to transform into the product via a first-order irreversible Arrhenius reaction. As discussed above, the kinetic aspect of the reaction can be varied only by changing the global activation energy of the mixture. Despite the fact that the use of such a model simplifies the analysis and reveals some interesting global features of the phenomenon, it is indeed very limited and has several drawbacks when attempting to study the complex interaction between the gasdynamics and chemical kinetic processes involved in the detonation phenomena of real systems. Some results obtained by using a one-step chemistry model may not even be in qualitative agreement with experimental observations.

In practice, the chemical kinetics for typical hydrocarbon mixtures are known to be chain-branching type, which proceed by a sequence of different types of chemical reaction stages. The reaction zone structure generally characterized by two characteristic zones: a thermally neutral region of radical accumulation that exists at the start of the chemical reactions corresponding to chain-initiation and chain–branching reactions; and a main reaction layer to that of chain-recombination or chain–termination reactions where radicals recombine to form the product and release chemical energy. While the detonation instability has been widely studied both theoretically and numerically using a one-step Arrhenius kinetics, such a simple reaction model cannot reproduce the features of real detonation governed by chain-branching kinetics described above. It is difficult or even impossible to choose its chemical kinetic parameters in such a way that the computed reaction zone structure gives close quantitative agreement with that calculated using realistic chemistry for typical combustible mixtures. A comparison of the temperature profile inside the reaction zone computed using both the one-step model and detailed chemical kinetics for H_2-O_2 is given in figure 1.6.

The use of single-step Arrhenius kinetics fails for the determination of dynamic parameters from numerical simulations, which is perhaps the most important aspect in detonation studies. Mazaheri (1997) in his numerical study of direct blast initiation of detonations shows that a detonation will always be initiated after a sufficiently long time even with a small amount of initiation source energy. This often yields the non-physical result that initiation of detonation can always be achieved via any arbitrary strength of shock wave. Within the single-step chemistry description, a system without losses will always react to completion and the total chemical energy of the mixture is always released. It therefore results in the difficulty of defining an unique value of minimum energy required to directly initiate a detonation, which has been measured experimentally. To illustrate the problem of using a single-step reaction rate law, the initiation processes of planar detonation for different initiation

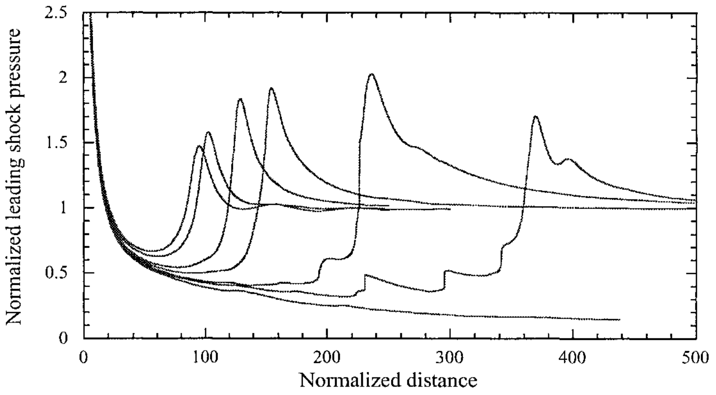

Figure 1.7. Leading shock pressure versus position for direct initiation using one-step kinetic rate law for different initiation energies (Ng & Lee 2003).

energies are given in figure 1.7, obtained previously by Ng & Lee (2003). Note that if one waits long enough, all blast waves originated from different energy sources will eventually result in detonation initiation. No sharp cut-off can be obtained with a single-step model to permit a definitive value of the critical energy to be determined. Since the one-step model provides no mechanism for quenching of the reaction, causing initiation to always occur. Equivalently, it is also impossible to predict the detonability limit for a specific mixture, i.e. the limit at which self-sustained detonation wave no longer exists.

Some studies have revealed that complexities in the chemistry model can resolve some of the problems inherent in the one-step kinetic model and may also have significant influences on the dynamics of detonation waves. For instance, von Neumann (1942) and more recently Sharpe & Falle (2000) and Dionne (2000) pointed out that pathological detonations, i.e. detonations that can travel at a velocity greater than the Chapman-Jouguet (CJ) value, are possible when the chemical kinetic mechanism involves a competition between exothermic and endothermic reaction steps. Examples are detonations in H_2-Cl_2 mixture (Dionne 2000). Such non-ideal detonations are possible when there are more than one-step kinetics present in the chemical model.

It has been shown that reaction models that are qualitatively different to the simplified thermally sensitive one-step kinetics lead to qualitative difference in the detonation ignition mechanism. Investigations carried by Dold & Kapila (1991) and more recently by Sharpe (2002) on the problem of shock-induced initiation of detonation using asymptotic analysis and numerical simulations have shown that the sequence of development of the detonation behind an initiating shock wave is qualitatively different when the chemistry is modeled by a radical chain-branching multi-step reaction mechanism having separate induction and main heat release kinetics from that of a global one-step model. The evolution process may also be different in different fuels governed by chain-branching chemistry, such as hydrogen-oxygen or hydrocarbon-oxygen, for the same initial disturbance. A similar observation was also revealed recently by Sharpe & Short (2003) in investigating the evolution to detonation from a temperature gradient. These analyses thus suggest that a one-step model may probably not be adequate for describing detonation initiation in typical combustible mixtures, which are mostly known to burn via a radical chain-branching process and the effect of chemical kinetics is critical in understanding these phenomena.

To address the influence of chain-branching kinetics on the pulsating structure of one-dimensional detonations, Short & Dold (1996) conducted linear stability studies of a weakly overdriven detonation wave using the same three-step reaction model as Dold & Kapila. In parallel with the linear stability analyses, Short & Quirk (1997) carried out direct numerical simulations to simulate the non-linear pulsating detonation structure driven by the same three-step chain-branching reaction. Although they showed that similar mechanisms for the regular and irregular modes of oscillatory behavior for both the three-step reaction model and the standard one-step reaction model, the pulsating structure is now governed by a bifurcation parameter in the chain-branching model, which controls the ratio of the chain-branching induction length to the length of the recombination zone. The use of the three-step chain-branching reaction also has a distinct advantage over the standard one-step Arrhenius model because multi-step chemical kinetics can provide a chemical mechanism that causes detonation to quench and permits a well-defined detonability limit for propagation. The chain-branching reaction kinetics features the so-called cross-over temperature T_B, a temperature limit below which the chain-branching reactions become ineffective, resulting in a sudden decrease in the radical generation, thus the global reaction rate and causing quenching of energy release and a failure to maintain the coupling between the leading shock with the chemical reaction zone. Similar observations for the propagation of overdriven detonations with branched-chain kinetics were also obtained more recently by Sánchez *et al.* (2001) by integrate the nonlinear evolution equations derived under certain asymptotic limits.

This chemical mechanism from multi-step chemical kinetic scheme, which cannot be described by the one-step Arrhenius reaction model, also provides explanations for some experimental observations. As shown recently by Ng & Lee (2003), the use of a multi-step chain-branching reaction mechanism for the blast initiation problem permits a more clear value for the critical initiation energy to be determined. From the chemical kinetic consideration, a criterion for defining a critical direct initiation energy can also be obtained, based on the blast wave generated by the source not decaying below the chain-branching cross-over temperature before the onset of detonation occurs.

1.4 Objective of the thesis

Past experimental and numerical studies have thus brought out the significant influence of chemical kinetics on the dynamic structure of detonations. Despite considerable research, how the chemistry controls the detonation structure is still not well understood. At the present time, there is no unique characteristic parameter or length scale which models correctly both the gasdynamics and chemical reaction processes within the structure of detonation waves. The lack of such parameter has indeed prevented current models for the prediction of different dynamic detonation parameters from being quantitatively correct. It can be achieved only if the connection between the unstable cellular structure and chemical kinetics is fully realized.

There is evidence that different characteristics of the cellular structures such as the cell regularity and the strength of transverse waves can be explained by studying the nature of instability within the reaction zone. Some success has indeed been achieved to characterize and relate the cell regularity with a stability parameter on the basis of a single-step Arrhenius model. However, the single-step chemistry description as discussed previously is far from being complete to model the interaction of gasdynamics and chemical kinetics within the structure of detonation waves. In view of recent studies, it appears that the chain-branching type reaction mechanism is significant to describe the chemical kinetics that typically occurs in real gaseous detonations. However, the extent to which this type of reaction kinetics affects the instability and the dynamic structure of detonations is not clear.

The objective of the present research is thus to clarify the influence of chemical kinetics on structures of cellular detonations and their characteristic features. In particular, the questions that will be addressed are: Why does the cellular detonation structure display different degrees of regularity under the influence of chemistry? How important is the complexity of the reaction mechanism in studying the dynamic structure of the detonation? Can some relevant chemical kinetic parameter be introduced to characterize the dynamics of the detonation structure and its cell regularity? What does the answer of these questions imply towards the modeling of detonation waves? These critical issues will be addressed in the present thesis through a numerical investigation.

Due to the unsteady nature of the detonation structure and the important nonlinear coupling between the gasdynamics and chemical kinetics within it, it becomes clear that the easier approach to study the detailed flow structure is numerical simulations. Numerical simulations permit one to extract relevant detailed information in the flow field whereas experimentally, only few parameters can be measured and sometimes the measurement may not even be accurate. In real experiments, only results of the full three-dimensional structure can be studied and also many parameters, such as different kinetic parameters, cannot be readily varied. As a result, many aspects of the phenomenon cannot be identified separately or studied in details. Alternatively, one can easily reduce the dimension of the problem from numerical simulations to first understand the fundamental mechanism governing the phenomenon and then extend the concepts to higher dimension. A number of high-resolution numerical schemes are well-developed nowadays. Complex sets of chemical kinetic rate equations can now be solved simultaneously with the conservation equations within current computational capabilities and the full nonlinear solutions can be accurately obtained at various conditions without imposing any asymptotic approximations. The capability of numerical simulation in providing detailed information of the highly transient and unstable event within the detonation structure as well as the flexibility to vary different conditions thus justify the methodology used for the present investigation.

The role of chemical kinetics on the unsteady detonation structure can be addressed by investigating numerically its effect on the corresponding instability problem. Since important characteristics of the instability phenomenon essentially remain on different numbers of dimension, most computations and analyzes can be realized on the basis of the one-dimensional unsteady detonations where instability manifests itself in the form of a nonlinear pulsating detonation wave. Furthermore, a one-dimensional geometry permits highly resolved numerical simulations to be performed, which are necessary for describing the highly non-linear detonation phenomena and difficult to achieve in multi-dimensional simulations.

Insight on the formation of cellular structure and its regularity under the influence of chemical kinetics can be obtained by investigating the instability spectrum and how different unstable modes are being developed. Numerical simulations carried out with chemical kinetic model ranging from simplified single-step reaction to complex descriptions with detailed chemical reaction schemes will help to examine to what level of complexity in the chemical kinetics description is required to yield a minimum number of kinetic parameters for the characterization of detonation stability. The implications of these numerical investigations on the real dynamics of detonation structure can be illustrated by comparing with experimental observations. The present research should provide how the effect of chemical kinetics could be explored and linked toward the modeling of the unsteady detonation structure.

Chapter 2

Problem formulation and numerical methodology

The methodology used in the present investigation is numerical simulations. It is important to formulate the mathematical model and assess the numerical technique used for detonation simulation, which involves many aspects of the highly transient and unstable events inside the reaction structure. This chapter is therefore devoted to the detailed description of the mathematical formulation and the numerical method to solve the governing equations. To demonstrate its robustness and accuracy, the present numerical scheme is assessed via a number of benchmarks tests and possible improvements are also suggested.

2.1 Mathematical model

The full unsteady nonlinear dynamics of detonations are modelled by solutions of the inviscid compressible, time-dependent Euler equations, which are expressed as the conservation equations for mass, momentum and energy:

$$\frac{\partial \rho}{\partial t} + \nabla \cdot (\rho \mathbf{V}) = 0 \tag{2.1}$$

$$\frac{\partial (\rho \mathbf{V}_i)}{\partial t} + \nabla \cdot (\rho \mathbf{V}_i \mathbf{V}) + \frac{\partial p}{\partial \mathbf{x}_i} = 0 \tag{2.2}$$

$$\frac{\partial (\rho E)}{\partial t} + \nabla \cdot ((\rho E + p)\, \mathbf{V}) = 0 \tag{2.3}$$

$$\frac{\partial (\rho Y_i)}{\partial t} + \nabla \cdot (\rho Y_i \mathbf{V}) = \rho \Omega_i (\rho, p, Y_i) \tag{2.4}$$

where ρ is the mass density, $\mathbf{V} = (u, v, w)$ is the velocity vector, p is the pressure, Y_i is the mass fraction of a reactant and E is the total energy per unit mass which is the sum of internal energy and kinetic energy:

$$E = e(\rho, p, Y_i) + \frac{1}{2}\mathbf{V}^2 \tag{2.5}$$

To complete the governing equations, it requires the specification of an equation of state of the form $e(\rho, p, Y_i)$ and a chemical reaction mechanism to describe the chemical production/consumption rates $\Omega_i(\rho, p, Y_i)$ for species i. The effect of chemical kinetics is thus modeled in the mass conservation of mixture species by introducing different rate laws for the reactions. The liberation of chemical energy, which is reflected from the change in internal energy of the mixture $e(\rho, p, Y_i)$, affects the gasdynamics of the flow defining the structure of a detonation wave.

2.1.1 Steady-state ZND equations

The steady-state solution of the Euler equations can be readily solved to yield the steady ZND model for detonation structures. In order to do so, equations 2.1-2.4 are usually rewritten in terms of a reference frame attached to the moving shock and all time derivative $\partial/\partial t$ are set to zero for a steadily propagating wave. This gives:

$$\begin{aligned}
\frac{d}{dx'}\left(\rho u'\right) &= 0 && (2.6)\\
\frac{d}{dx'}\left(\rho u'^2+p\right) &= 0 && (2.7)\\
\frac{d}{dx'}\left[\left(\rho E+p\right)u'\right] &= 0 && (2.8)\\
\frac{d}{dx'}\left(\rho u' Y_i\right) &= \rho\Omega_i \qquad (i=1,\ldots,N_s) && (2.9)
\end{aligned}$$

where x' and u' is the relative distance and particle velocity in the shock-attached coordinate (i.e. $u' = D - u$ where D is the steady detonation velocity). For an ideal gas, E can be expressed in the following form in terms of the mixture specific enthalpy h:

$$E = h - \frac{p}{\rho} + \frac{u'^2}{2} \tag{2.10}$$

and the ideal gas equation of state allows to write:

$$E = h - R_s T + \frac{u'^2}{2} \tag{2.11}$$

where R_s is the specific gas constant. It is possible to express equations 2.6-2.9 in a more convenient form for integration (see Appendix B), which are given by:

$$\begin{aligned}
\frac{dp}{dt'} &= -\rho u'^2 \frac{\dot{\sigma}}{1-M^2} && (2.12)\\
\frac{d\rho}{dt'} &= -\rho \frac{\dot{\sigma}}{1-M^2} && (2.13)\\
\frac{du'}{dt'} &= u' \frac{\dot{\sigma}}{1-M^2} && (2.14)\\
\frac{dY_i}{dt'} &= \Omega_i \qquad (i=1,\ldots,N_s) && (2.15)
\end{aligned}$$

in which M is the flow Mach number ($M = u'/c$ where c is the local sound speed) and the thermicity parameter $\dot{\sigma}$ has been used to denote the non-dimensional energy release rate:

$$\dot{\sigma} = \sum_{i=1}^{N_s} \left(\frac{W}{W_i} - \frac{h_i}{C_p T} \right) \frac{dY_i}{dt'} \tag{2.16}$$

where W is the mean molar mass of the mixture, C_p is the mixture specific heat at constant pressure and h_i is the specific enthalpy of species i. One can notice that the term $(1 - M^2)$ appears in these ZND equations (i.e., equations 2.12-2.15), indicating a potential singularity. To avoid a singularity in the solution, the thermicity must vanish as the flow becomes sonic (i.e. Mach number $M = u'/c$ approaches one). Hence for a ZND detonation wave traveling at the CJ velocity, the equilibrium state is reached at the sonic plane as given by the Chapman-Jouguet (CJ) sonic condition.

The above system of ZND equations is indeed formulated for complete detailed chemistry. It is possible to make further simplification by considering simple models of the mixture properties, which have been often used in studying the solutions of the reactive flow equations. The simplest model treats the combustible system as an ideal mixture of polytropic gases all having the same (constant) heat capacity (or γ =constant). The simplest chemical kinetic model is often described by one or multi-step reaction mechanism given as:

$$A \rightarrow B, \; B \rightarrow C \ldots$$

where each reaction step i is governed by a progress variable β_i and its rate of change generally has an Arrhenius temperature-dependent form. i.e.

$$\frac{d\beta_i}{dt'} = \Omega_i \sim \exp\left(E_i/RT\right) \tag{2.17}$$

where E_i is the activation energy associated with each step of the reaction mechanism. Using the polytropic equation of state also gives:

$$E = \frac{p}{(\gamma - 1)\rho} + \frac{u'^2}{2} + \sum_{i=1}^{N_{reac}} \beta_i Q_i \tag{2.18}$$

where Q_i denotes the chemical heat release in each of the reaction i. The thermicity parameter $\dot{\sigma}$ in the ZND equations can be easily shown to reduce to the following form:

$$\dot{\sigma} = \sum_{i=1}^{N_{reac}} (\gamma - 1)\frac{Q_i}{c^2}\frac{d\beta_i}{dt'} \tag{2.19}$$

In order to integrate the ZND equations in all cases, the unique detonation velocity must first be obtained. The post-shock states can then be computed from the Rankine-Hugoniot (shock jump) condition in the shock coordinate, which serve as initial conditions for the integration of equations 2.12 - 2.15 for the thermodynamic profiles within the detonation structure. For ideal CJ detonations, the detonation velocity can be readily determined from the global conservation laws and equilibrium thermodynamics. The exothermicity vanishes when the flow reaches chemical equilibrium. However in the case of non-ideal detonations involving a competition between exothermic and endothermic reactions (i.e. pathological detonations), the eigenvalue solution is found by iterating for the detonation velocity that satisfies the generalized CJ criterion. The generalized CJ criterion requires both the numerator and denominator of equations 2.12 - 2.15 vanish simultaneously to seek a singularity-free solution. Therefore, the heat release rate must become zero at the transition from exothermic to endothermic reactions when the flow becomes sonic relative to the shock front. In this case, the sonic plane is achieved prior to complete chemical equilibration.

2.2 Description of the numerical method

Unlike the steady ZND equations which are a coupled set of ordinary differential equations, the full unsteady reactive Euler equations are described by a set of partial differential equations and must be solved using some reliable numerical method.

These unsteady governing equations describing the dynamics of a detonation wave indeed express a system of hyperbolic conservation laws with additional source terms account for the chemical reactions. A variety of efficient high-resolution numerical schemes for hyperbolic systems of partial differential equations has been devised in the recent years. Many of these modern high-resolution numerical schemes are often based on upwind differencing, which are generally most suitable for the numerical solution of systems of hyperbolic conservation laws as they introduce characteristic information regarding the local directionality of the flow along the discontinuous interfaces of the spatial cells. Nevertheless, these upwind differencing schemes generally require the solution of the corresponding local Riemann problem to evaluate the flux terms at the cell interfaces and this in turn greatly complicates the upwind algorithm. Furthermore, the quality of the global solution depends quite crucially on the particular Riemann solver being used (Toro 2003). It sometimes lacks of generality in a sense that small modifications of the physics of a model can lead to major changes in the implementation of higher-order Godunov upwind methods and their Riemann solvers.

In contrast, it is possible to construct centered schemes, which do not require information to be provided about the Riemann problem of the evolved equations. No intricate and time-consuming Riemann solvers and related characteristic decomposition are necessary, which are the building block of the high-resolution upwind schemes. In recent years, central differencing schemes for the approximate solution of hyperbolic systems of conservation laws received a lot of attention (Nessyahu & Tadmor 1990). The main feature of such centered schemes is simplicity: they usually have a low computational cost and have less user-adjusted parameters. Due to their simple structure, the methods can be applied very easily to any hyperbolic system in flux-conservative form. While central schemes are usually more simple and flexible than a Riemann-solver based integration method, there is a cost of an increase in numerical diffusion. Thus, the numerical results (discontinuities and rarefaction waves) are slightly more smeared than would be expected if a Riemann-solver based method were used at a similar resolution. Nevertheless, centered schemes do not compromise the qualities of the high-resolution family, albeit at a small loss of 'sharpness' of the solution (Anile *et al.* 2000).

In the context of detonation studies, a full description of the phenomena requires reliable and highly resolved numerical simulations. As a result, these simulations are often very computationally intensive. An increasing attention is also recently devoted for the inclusion of a more detailed chemical kinetic description in the simulation of multi-dimensional detonation problem. For these reasons, a centered scheme is revisited here in the context of detonation simulation due to its low computational cost, ease of implementation and generality. A well-established high-resolution centered scheme, namely the slope limiter centered (SLIC) scheme by Toro is considered in this investigation (Toro 1997; Toro & Billet 2000). This particular numerical scheme has been used in other disciplines such as hydrodynamical semiconductor simulations (Anile *et al.* 2000), which also involve highly nonlinear phenomena.

2.2.1 Slope limiter centered scheme

The numerical method used here for approximating the solution of hyperbolic conservation laws employs the finite volume approach where the integral formulation of the conservation laws is discretized directly in the physical space. Consider a 1-D system of partial differential equations written in conservative form,

$$\frac{\partial \mathrm{U}}{\partial t}+\frac{\partial \mathbf{F}\left(\mathrm{U}\right)}{\partial x}=0 \tag{2.20}$$

where $\mathbf{U}$ is the vector of conserved variables and $\mathbf{F}(\mathbf{U})$ the convective fluxes. The resulting update finite volume formula derived by considering the equivalent integral formulation,

$$\oint\left[\mathbf{U}dx+\mathbf{F}\left(\mathrm{U}\right)dt\right]=0 \tag{2.21}$$

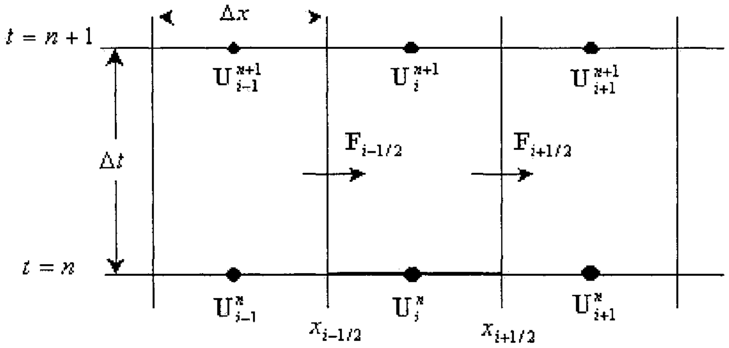

Figure 2.1. Geometrical illustratoin of the finite volume update formula.

can be written as:

$$\mathbf{U}_i^{n+1} = \mathbf{U}_i^n + \frac{\Delta t}{\Delta x}\left[\mathbf{F}_{i-1/2} - \mathbf{F}_{i+1/2}\right] \tag{2.22}$$

where $\mathbf{U}_i^{n+1}$ and $\mathbf{U}_i^n$ are the conserved variables at the next and current time-levels, $n+1$ and n, respectively. $\mathbf{F}_{i-1/2}$ and $\mathbf{F}_{i+1/2}$ are the numerical fluxes at the interfaces of the computational cells of the discretized space. For a known value of Δx (based on the desired resolution) and Δt (based on CFL stability criterion), the vector of conserved variables $\mathbf{U}$ can be advanced, from time level t^n to t^{n+1} if the fluxes are known. This can be represented schematically in figure 2.1. To this end the centered scheme uses a nonlinear combination of a good second (or higher)-order scheme with a first-order monotone scheme.

The slope limiter centered scheme described here is a combination of the second-order MUSCL-Hancock and the first-order centered (FORCE) scheme (Toro 1997; Toro & Billet 2000). In the MUSCL-Hancock approach, a second-order scheme can be achieved by reconstructing the data as piecewise linear function in every cell. Such a modification gives the boundary extrapolated values for cell i

$$\mathbf{U}_i^L = \mathbf{U}_i^n - \frac{1}{2}\mathbf{\Delta}_i, \qquad \mathbf{U}_i^R = \mathbf{U}_i^n + \frac{1}{2}\mathbf{\Delta}_i \tag{2.23}$$

where $\mathbf{\Delta}$ is a slope vector. These new boundary values are then evolved in time by half a time-step using the usual conservative formula

$$\bar{\mathbf{U}}_i^L = \mathbf{U}_i^L + \frac{1}{2}\frac{\Delta t}{\Delta x}\left[\mathbf{F}(\mathbf{U}_i^L) - \mathbf{F}(\mathbf{U}_i^R)\right], \bar{\mathbf{U}}_i^R = \mathbf{U}_i^R + \frac{1}{2}\frac{\Delta t}{\Delta x}\left[\mathbf{F}(\mathbf{U}_i^L) - \mathbf{F}(\mathbf{U}_i^R)\right] \quad (2.24)$$

Instead of relying on the solution of the Riemann problem, the inter-cell numerical fluxes in the finite volume formula (equation 2.22) are evaluated using the first-order centered (FORCE) scheme, which is a combination of the first-order Lax-Friedrichs and second-order Richtmyer fluxes

$$\mathbf{F}_{i+1/2}^{force} = \mathbf{F}_{i+1/2}^{force}(\bar{\mathbf{U}}_i^R, \bar{\mathbf{U}}_{i+1}^L) = 0.5\left[\mathbf{F}_{i+1/2}^{LF}(\bar{\mathbf{U}}_i^R, \bar{\mathbf{U}}_{i+1}^L) + \mathbf{F}_{i+1/2}^{Ri}(\bar{\mathbf{U}}_i^R, \bar{\mathbf{U}}_{i+1}^L)\right] \quad (2.25)$$

where the first-order Lax-Friedrichs flux $\mathbf{F}^{LF}$ is given by:

$$\mathbf{F}_{i+1/2}^{LF} = \mathbf{F}_{i+1/2}^{LF}(\bar{\mathbf{U}}_i^R, \bar{\mathbf{U}}_{i+1}^L) = 0.5\left[\mathbf{F}(\bar{\mathbf{U}}_i^R) + \mathbf{F}(\bar{\mathbf{U}}_{i+1}^L)\right] + 0.5\frac{\Delta x}{\Delta t}\left[\bar{\mathbf{U}}_i^R - \bar{\mathbf{U}}_{i+1}^L\right] \quad (2.26)$$

and the second-order Richtmyer flux $\mathbf{F}^{Ri}$ is found by first evaluating an intermediate state $\mathbf{U}^{Ri}$

$$\mathbf{U}_{i+1/2}^{Ri} = \mathbf{U}_{i+1/2}^{Ri}(\bar{\mathbf{U}}_i^R, \bar{\mathbf{U}}_{i+1}^L) = 0.5\left[\bar{\mathbf{U}}_i^R + \bar{\mathbf{U}}_{i+1}^L\right] + 0.5\frac{\Delta t}{\Delta x}\left[\mathbf{F}(\bar{\mathbf{U}}_i^R) - \mathbf{F}(\bar{\mathbf{U}}_{i+1}^L)\right] \quad (2.27)$$

which is then used to compute $\mathbf{F}_{i+1/2}^{Ri} = \mathbf{F}^{Ri}(\mathbf{U}_{i+1/2}^{Ri})$. The resulting numerical scheme is second-order accurate in space and time. So to avoid spurious oscillations in the vicinity of steep gradients, the slope $\mathbf{\Delta}$ is "limited" using a slope limiter function. The solution is then updated by evaluating the conservative finite volume formula (equation 2.22). For further details on this high-resolution non-oscillatory centered scheme, as well as different slope limiter function and validation problems for non-reactive compressible flow, see the textbook by Toro (1997).

2.2.2 Method of fractional steps

The governing equations for the chemically reactive flow problem are generally of the form:

$$\frac{\partial \mathbf{U}}{\partial t} + \frac{\partial \mathbf{F}\left(\mathbf{U}\right)}{\partial x} = \mathbf{S}\left(\mathbf{U}\right) \quad (2.28)$$

where an additional source term $\mathbf{S}(\mathbf{U})$ appears in the formulation in order to model the chemical energy release from the reactions. Therefore, the method of fractional steps is adopted for the numerical integration to treat separately the hydrodynamics process and the chemical reaction process, where the homogeneous hyperbolic part of equation 2.28, i.e.

$$\frac{\partial \mathbf{U}}{\partial t} + \frac{\partial \mathbf{F}(\mathbf{U})}{\partial x} = 0 \tag{2.29}$$

is first solved by using the SLIC scheme (with initial and boundary conditions as specified for the complete system). The remaining ordinary differential equations describing the chemical reactions

$$\frac{d\mathbf{U}}{dt} = \mathbf{S}(\mathbf{U}) \tag{2.30}$$

are then integrated implicitly using conventional techniques. To maintain second-order accuracy, the Strang splitting method (Strang 1964) is used with the following algorithm:

$$\mathbf{U}_i^{n+1} = L_C^{\Delta t/2} L_S^{\Delta t} L_C^{\Delta t/2} \mathbf{U}_i^n \tag{2.31}$$

where L_C and L_S denote the operator for the convective and reactive source terms, respectively.

2.3 Numerical scheme validation

To evaluate the performance of the described SLIC method together with the operator splitting in the context of detonation simulation, it is assessed against several numerical examples of time-dependent problems as benchmark tests, including the simulations of one-dimensional pulsating instabilities of planar detonations and two-dimensional cellular detonations with simple chemistry, as well as detonation initiation by reflected shock with a realistic detailed hydrogen-oxygen-argon chemical kinetic mechanism.

2.3.1 One-dimensional pulsating detonation with simplified single-step chemistry

Instabilities associated with the one-dimensional planar ZND structure have been revealed by Erpenbeck (1962, 1964) via a linear stability analysis. The non-linear intrinsic oscillatory behavior of one-dimensional detonations with simple chemistry has also been shown numerically by Fickett & Wood (1966) using the method of characteristics. Since then, more thorough studies on one-dimensional pulsating detonations have been carried out by numerous researchers (see, for example, Bourlioux *et al.* 1991; He & Lee 1995; Sharpe & Falle 1999; etc.). Because of the extensive numerical examination of this canonical 1-D unsteady detonation problem over the past, it is used widely as a benchmark problem for high-resolution numerical schemes for detonation simulations. Therefore, this problem is used to evaluate the performance of the described SLIC method together with the operator splitting in the context of detonation simulation. The propagation of detonation wave with a single-step, irreversible chemical reaction can be modeled by the Euler equations coupled with a species equation. In one space dimension, the governing equations can be written in non-dimensional form as

$$\frac{\partial \mathbf{U}}{\partial t} + \frac{\partial \mathbf{F}\left(\mathbf{U}\right)}{\partial x} = \mathbf{S}\left(\mathbf{U}\right) \tag{2.32}$$

where the conserved variable **U**, the convective flux **F** and reactive source term **S** are, respectively,

$$\mathbf{U} = \begin{pmatrix} \rho \\ \rho u \\ \rho E \\ \rho\beta \end{pmatrix} \qquad \mathbf{F}\left(\mathbf{U}\right) = \begin{pmatrix} \rho u \\ \rho u^2 + p \\ \left(\rho E + p\right) u \\ \rho u \beta \end{pmatrix} \qquad \mathbf{S}\left(\mathbf{U}\right) = \begin{pmatrix} 0 \\ 0 \\ 0 \\ \rho\Omega \end{pmatrix} \tag{2.33}$$

with

$$E = \frac{p}{(\gamma - 1)\rho} + \frac{u^2}{2} + \beta Q \tag{2.34}$$

$$T = \frac{p}{\rho} \tag{2.35}$$

$$\Omega = -K\beta \exp\left(\frac{-E_a}{T}\right) \tag{2.36}$$

In the above equations, ρ, u, p, T and E are density, particle velocity, pressure, temperature and total energy per unit mass, respectively. The variable β is the reaction progress variable, which varies between 1 (for unburned reactant) and 0 (for product). The mixture is assumed to be ideal and calorically perfect (with constant specific heat ratio γ). The parameter Q and E_a represent the non-dimensional heat release and activation energy, respectively. These variables have been made dimensionless with reference to the uniform unburned state ahead of the detonation front.

$$\rho = \frac{\tilde{\rho}}{\tilde{\rho}_o}, \quad p = \frac{\tilde{p}}{\tilde{p}_o}, \quad T = \frac{\tilde{T}}{\tilde{T}_o}, \quad u = \frac{\tilde{u}}{\sqrt{\tilde{R}\tilde{T}_o}}, \quad Q = \frac{\tilde{Q}}{\tilde{R}\tilde{T}_o}, \quad E_a = \frac{\tilde{E}_a}{\tilde{R}\tilde{T}_o}$$

The pre-exponential factor K is an arbitrary parameter that merely defines the spatial and temporal scales. It is chosen such that the half-reaction length $L_{1/2}$, i.e. the distance required for half the reactant to be consumed in the steady ZND wave, is scaled to unit length. Hence,

$$x = \frac{\tilde{x}}{\tilde{L}_{1/2}}, \quad t = \tilde{t} \cdot \frac{\sqrt{\tilde{R}\tilde{T}_o}}{\tilde{L}_{1/2}}, \quad K = \tilde{K} \cdot \frac{\tilde{L}_{1/2}}{\sqrt{\tilde{R}\tilde{T}_o}}$$

In the present study of instabilities of 1-D unsteady detonations, the simulations were always initialized by imposing the corresponding steady ZND solution onto the computational grids. The computational setup follows Bourlioux *et al.*(1991) by fixing the dimensionless parameters with the values $Q = 50$, $\gamma = 1.2$, $E_a = 50$ and overdriven factor $f = 1.6$ (i.e. $f = (D/D_{cj})^2$ where D is the detonation velocity of the equivalent steady ZND detonation and D_{cj} is the minimum Chapman-Jouguet detonation velocity) so that detailed comparison can be made. According to a number of linear stability analyses (Bourlioux *et al.*1991; Lee & Stewart 1991), the corresponding ZND profile has a single instability mode. Various numerical computations also

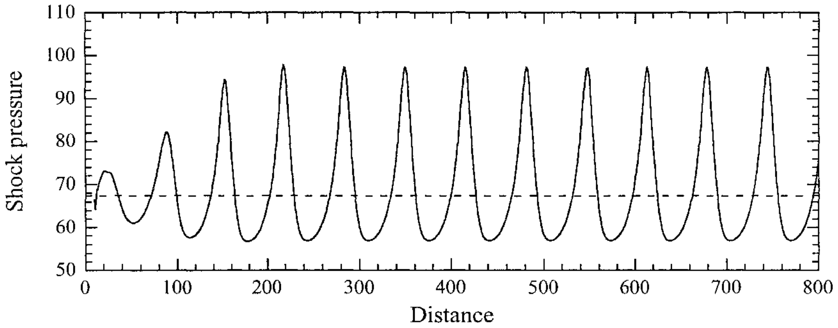

Figure 2.2. Pressure behind the shock front versus position for the overdriven detonation with $Q = 50$, $\gamma = 1.2$, $E_a = 50$ and $f = 1.6$, using 20 grid points per $L_{1/2}$. The dashed line indicates the steady-state ZND value of the von Neumann pressure P_{vn}.

show that the nonlinear manifestation of this instability is a regular periodic pulsating detonation (Bourlioux *et al.*1991; He & Lee 1995; etc.). Figure 2.2 shows the leading shock pressure versus position plot generated using the SLIC scheme. Note that there is no perturbation applied to the ZND initial condition but the instability grows quickly from the numerical startup error (e.g. adjustment in the shock capturing). After the transient development, it correctly predicts the single instability mode of the detonation front.

Following the work by Hwang *et al.* (2000), a convergence study for the peak pressure magnitude behind the overdriven detonation reached during the limit-cycle pulsations is performed. The present results are compared with those published previously for other various numerical schemes (Bourlioux *et al.* 1991; Quirk 1994; Papalexandris *et al.* 1997; Hwang *et al.* 2000; Toro 1997) and they are presented in figure 2.3, showing the peak shock pressure vs. the relative mesh spacing (i.e., a relative mesh spacing of 0.5 corresponds to a resolution of 20 grid points per $L_{1/2}$). From this graph, it can be noticed that the SLIC scheme, like the other schemes, converges to approximately the peak pressure value of $\sim$ 98.6 as first predicted by Fickett &

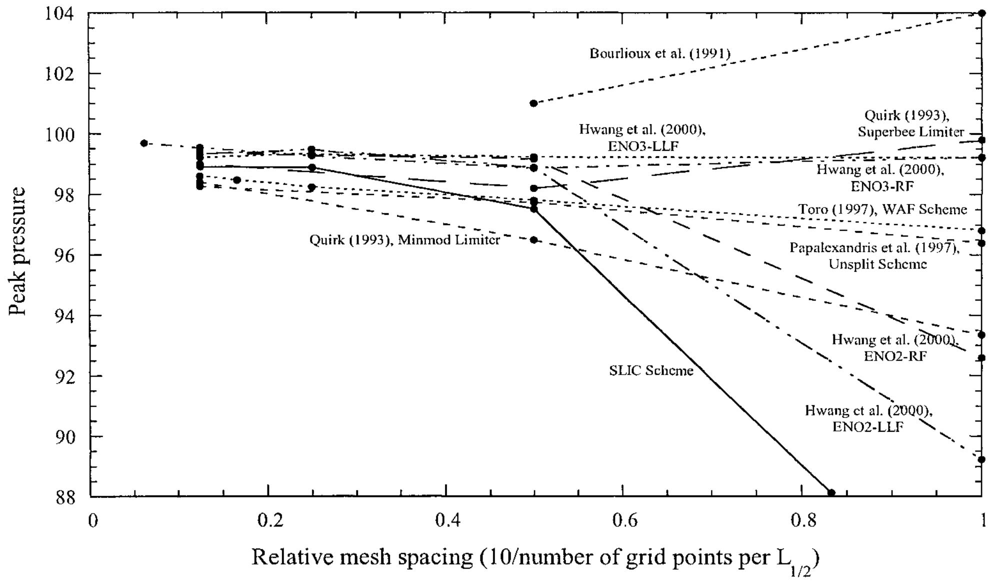

Figure 2.3. Comparison of peak pressure behind the shock front as a function of relative mesh spacing among different numerical schemes for the overdriven pulsating detonation ($Q = 50$, $\gamma = 1.2$, $E_a = 50$ and $f = 1.6$).

Wood (1966). Nevertheless, one may notice that the SLIC scheme approaches the correct value at a slightly higher resolution compared to other Riemann-solver based methods. At low resolution (less than 20 cells per $L_{1/2}$), the SLIC method is less accurate. This is to be expected because the SLIC method is more diffusive than Riemann-solver based method and the numerical results are slightly more smeared. Since the effects of numerical diffusion are decreased as the solution resolution increases, therefore, higher resolution for SLIC is generally necessary to accurately converge to the solution than would be expected if a Riemann-solver based methods were used.

Beside the convergence in peak pressure, it is also important to consider the period of oscillation for the pulsating detonations (see Hwang *et al.* 2000). Figure 2.4

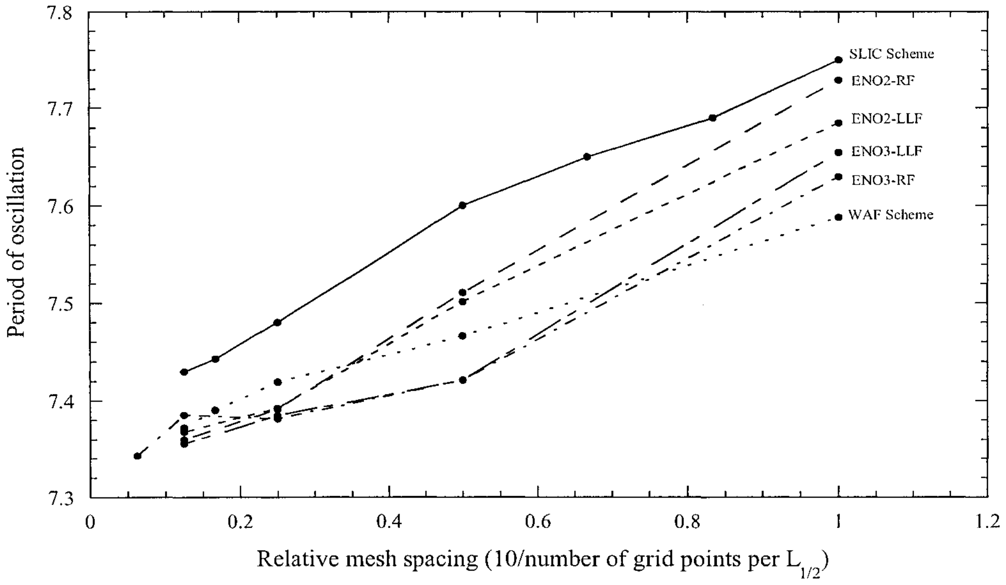

Figure 2.4. Comparison of the period of pressure oscillation as a function of relative mesh spacing obtained by different ENO schemes (Hwang *et al.* 2000), the WAF scheme (Toro 1997) and the present SLIC scheme for the overdriven pulsating detonation ($Q = 50$, $\gamma = 1.2$, $E_a = 50$ and $f = 1.6$).

compares the period of pressure oscillation with the relative mesh spacing obtained by the SLIC scheme as well as different ENO (Essentially Non-Oscillating) schemes used by Hwang *et al.* (2000). The period of oscillation is determined by taking the average of several cycles between successive pressure peaks. The results show that the present SLIC scheme approaches to a period in the range 7.4-7.5 at high resolutions. These are comparable with the non-linear stability analysis by Erpenbeck (1967), which predicted a period of 7.41-7.49. However, it is interesting to note that the value at high numerical resolutions is slightly different to that obtained by different ENO schemes, which indicates that the predicted period depends on the numerical schemes. Overall, it is found recently by Hwang *et al.* (2000), that a reaction zone resolution of at least 20 points per $L_{1/2}$ is usually required for accurate resolution of the detonation wave with an overdrive of $f = 1.6$ if an upwind numerical scheme is used. Similar conclusion can be made here using the SLIC scheme. Above this numerical resolution, both centered and upwind achieve the same accuracy.

2.3.2 Two-dimensional cellular detonation simulation with simplified single-step chemistry

It is well established that multi-dimensional detonation waves generally exhibit a complex and unsteady reaction zone structure. Two-dimensional detonation waves are characterized by an ensemble of interacting transverse waves sweeping laterally across the leading shock front of the detonation wave. The interactions of incident shocks, Mach stems and transverse waves form a characteristic cellular pattern, producing so-called detonation cells. In the present study, two-dimensional simulations were also conducted to validate the present SLIC scheme. In 2-D case, the reactive Euler equations (equations 2.32 - 2.36) extends to the form:

$$\frac{\partial \mathbf{U}}{\partial t} + \frac{\partial \mathbf{F}(\mathbf{U})}{\partial x} + \frac{\partial \mathbf{G}(\mathbf{U})}{\partial y} = \mathbf{S}(\mathbf{U}) \tag{2.37}$$

$$\mathbf{U} = \begin{pmatrix} \rho \\ \rho u \\ \rho v \\ \rho E \\ \rho\beta \end{pmatrix} \mathbf{F}(\mathbf{U}) = \begin{pmatrix} \rho u \\ \rho u^2 + p \\ \rho uv \\ (\rho E + p) u \\ \rho u\beta \end{pmatrix} \mathbf{G}(\mathbf{U}) = \begin{pmatrix} \rho v \\ \rho uv \\ \rho v^2 + p \\ (\rho E + p) v \\ \rho v\beta \end{pmatrix} \mathbf{S}(\mathbf{U}) = \begin{pmatrix} 0 \\ 0 \\ 0 \\ 0 \\ \rho\Omega \end{pmatrix} \tag{2.38}$$

$$E = \frac{p}{(\gamma - 1)\rho} + \frac{(u^2 + v^2)}{2} + \beta Q \tag{2.39}$$

where an additional convective flux term $\mathbf{G}$ and velocity component v are included for the transverse direction. Analogously to the fractional step operator splitting approach, one can obtain a second-order splitting scheme as follows:

$$\mathrm{U}_i^{n+1} = L_{C_X}^{\Delta t/2} L_{C_Y}^{\Delta t/2} L_S^{\Delta t} L_{C_Y}^{\Delta t/2} L_{C_X}^{\Delta t/2} \mathrm{U}_i^n \tag{2.40}$$

where the convective operators L_{C_X} and L_{C_Y} were of the same form as the one-dimensional convective vector in equation 2.29, and integrated with the same one-dimensional flow solver.

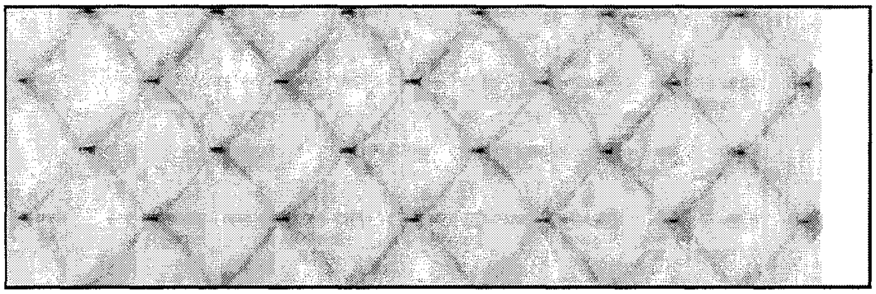

Figure 2.5. Numerical smoked foil record for the overdriven detonation with Q = 50, γ = 1.2, E_a = 10 and f = 1.2, using 24 grid points per $L_{1/2}$ and channel width = 10 half reaction lengths (shown twice).

For meaningful comparison, this study performs the test problem considered in prior studies (Bourlioux & Madja 1992; Helzel 2000; Quirk 1994) with parameter set to Q = 50, γ = 1.2, E_a = 10 and f = 1.2. This corresponds to the case of high energy release and low activation energy, producing a regular cell pattern with a complex structure of transverse waves. The same degree of numerical resolution as Bourlioux & Madja (1992), i.e. 24 cells per $L_{1/2}$, is used in the present study so that direct comparison can be made. The solution for the planar steady ZND wave is imposed as initial data and perturbed by introducing a small curvature into the front to accelerate the growth of transverse instability. The width of the computational

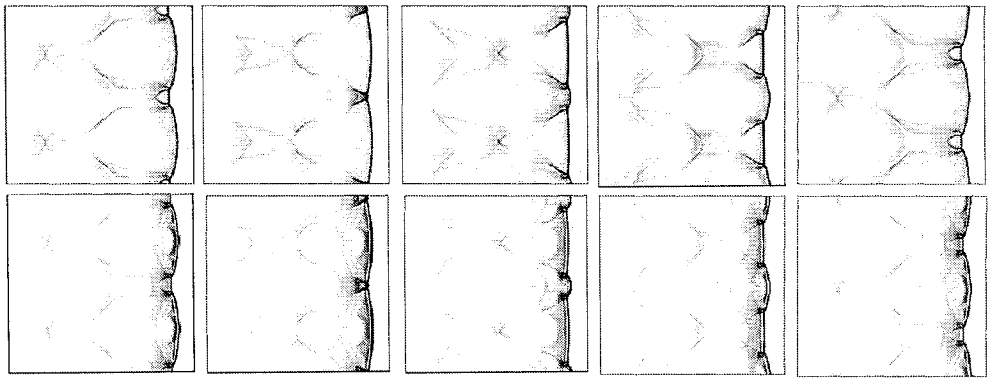

Figure 2.6. Sequence of five Schlieren-type plots showing the pressure (top) and density (bottom) flow field behind the shock for the overdriven detonation with $Q = 50$, $\gamma = 1.2$, $E_a = 10$ and $f = 1.2$, using 24 grid points per $L_{1/2}$ and channel width = 10 half reaction lengths (shown twice).

domain is 10 half-reaction zone lengths. Periodic boundary conditions are used along the top and bottom boundaries.

The cellular pattern so obtained is shown in figure 2.5. This is a typical "numerical smoked foil" showing the time-integrated maximum pressure contour from the numerical simulation, which corresponds to the trajectories of the triple shock interactions (i.e. triple point). The obtained transverse characteristic length scale, i.e., the cell size, is in agreement with that found in other published literature, which has a value of 10 for the given channel width. To look at the flow field behind the detonation front in more detail, figure 2.6 shows a sequence of Schlieren-type or gradient plots of pressure and density. They are very similar to Bourlioux's results and most of the characteristics of the flow field can be correctly resolved. More importantly, these results indicate the capability of the present computational method for producing highly complex simulation of multi-dimensional detonation cell phenomena. Nevertheless, it is worth noting that to resolve all the various length scales involved in the problem, a higher resolution than the one used here is indeed required as pointed out in the paper by Sharpe (2001).

2.3.3 Detonation initiation with detailed chemistry

So far, the numerical scheme is assessed against one and two-dimensional time-dependent detonations with only simple one-step Arrhenius chemistry. This section extends the numerical scheme to include multi-species and performs simulations to validate the SLIC method coupled with detailed realistic chemistry. To include detailed chemistry, the one-dimensional Euler equations (equations 2.32 -2.35) can be modified to account for compressible flows with more than one species, which become:

$$\frac{\partial \mathbf{U}}{\partial t} + \frac{\partial \mathbf{F}(\mathbf{U})}{\partial x} = \mathbf{S}(\mathbf{U}) \tag{2.41}$$

$$\mathbf{U} = \begin{pmatrix} \rho_1 \\ \vdots \\ \rho_{N_s} \\ \rho u \\ \rho E \end{pmatrix} \quad \mathbf{F}(\mathbf{U}) = \begin{pmatrix} \rho_1 u \\ \vdots \\ \rho_{N_s} u \\ \rho u^2 + p \\ (\rho E + p) u \end{pmatrix} \quad \mathbf{S}(\mathbf{U}) = \begin{pmatrix} \rho \Omega_1 \\ \vdots \\ \rho \Omega_{N_s} \\ 0 \\ 0 \end{pmatrix} \tag{2.42}$$

where N_s is the total number of species being considered and ρ_i are the density of the i^{th} chemical species. The total density of the gas mixture ρ is therefore given by:

$$\rho = \sum_{i=1}^{N_s} \rho_i \tag{2.43}$$

The total energy per unit mass for the gas mixture is designated by E, which can be written as

$$E = e + \frac{u^2}{2} \tag{2.44}$$

where e is the specific internal energy of the mixture and is calculated based on a mass-weighted average of the internal energy per unit mass of each species e_i

$$e = \sum_{i=1}^{N_s} Y_i e_i \tag{2.45}$$

where $Y_i = \rho_i/\rho$ is the mass fraction of i^{th} species. For a mixture of perfect gases, each gas species has its partial pressure p_i and the equation of state for multi-species flow is therefore written as:

$$p = \sum_{i=1}^{N_s} p_i = \rho R T \sum_{i=1}^{N_s} \frac{Y_i}{W_i} \tag{2.46}$$

where $R = 8.314\mathrm{J/mol^\circ K}$ is the universal gas constant and W_i is the molecular weight of the i^{th} species. In addition, the internal energy, enthalpy, and specific heats are functions of the temperature only. Here, all gaseous species are also assumed to be thermally perfect of which the specific heats are non-constant functions of temperature. In this case, the enthalpy of each species is given by:

$$h_i(T) = h_i^f + \int_0^T C_{p_i}(T)\,dT \tag{2.47}$$

where $h_i^f = h_i(0)$ is the heat of formation and $C_{p_i}(T)$ is the specific heats at constant pressure of the i^{th} species, which are generally tabulated as a function of temperature for many gases. Using the following thermodynamic relation:

$$e = h - \frac{p}{\rho} = \sum_{i=1}^{N_s} Y_i h_i(T) - \frac{p}{\rho} = \sum_{i=1}^{N_s} Y_i h_i^f + \int_0^T \sum_{i=1}^{N_s} Y_i C_{p_i}(T)dT - \frac{p}{\rho} \tag{2.48}$$

and the ideal gas equation of state, the total energy per unit mass for the gas mixture can be rewritten as:

$$E = \sum_{i=1}^{N_s} Y_i h_i(T) - RT \sum_{i=1}^{N_s} \frac{Y_i}{W_i} + \frac{u^2}{2} \tag{2.49}$$

which gives an implicit relation for determining the temperature T from the conserved variable, but requiring an iteration procedure.

For the chemical kinetic model, Ω_i is the production rate of the i^{th} species, which can also be expressed as

$$\Omega_i = \frac{\dot{w}_i W_i}{\rho}$$

where $\dot{w}_i$ denotes the net molar production/destruction rate of i^{th} species due to chemical reaction. It is generally derived from a given detailed chemical reaction mechanism of elementary reactions, having the form:

$$\sum_{i=1}^{N_s} \nu'_{ij} X_i \Leftrightarrow \sum_{i=1}^{N_s} \nu''_{ij} X_i \qquad j = 1, ..., N_{reac} \tag{2.50}$$

where ν'_{ij} and ν''_{ij} are respectively the forward and backward stoichiometric coefficients of species X_i in the j^{th} reaction. N_{reac} is the total number of chemical reactions in the mechanism. Subsequently, the net molar production rate of species i can be expressed by:

$$\dot{w}_i = \sum_{j=1}^{N_{reac}} \left(\nu''_{ij} - \nu'_{ij}\right) q_j \tag{2.51}$$

where q_j is the net rate of progress for reaction j and can be written as:

$$q_j = k_j^f \prod_{i=1}^{N_s} [X_i]^{\nu'_{ij}} - k_j^b \prod_{i=1}^{N_s} [X_i]^{\nu''_{ij}} \tag{2.52}$$

where k_j^f and k_j^b are respectively the forward and backward reaction rate constant for reaction j. $[X_i]$ is the mole concentration of species i. The forward rate coefficients is generally given by the Arrhenius form:

$$k_j^f(T) = K_{f_j} T^{\alpha_j} \exp\left(\frac{-E_{a_j}}{RT}\right) \tag{2.53}$$

with the pre-exponential constant K_{f_j}, the temperature exponent α_j and activation energy E_{a_j}. Knowing the forward reaction rate, the corresponding backward rate can be found by chemical equilibrium consideration and calculated by:

$$k_j^b(T) = \frac{k_j^f(T)}{k_j^{equil.}(T)} \tag{2.54}$$

where the $k_j^{equil.}(T)$ is equilibrium constant based on thermodynamic calculation. In this work, the rate $\dot{w}_i$ as well as other thermodynamic data for each gaseous species, such as the values of the enthalpy $h_i(T)$, the specific heats $C_{p_i}(T)$ or $C_{v_i}(T)$, etc., were obtained from the CHEMKIN package (Kee *et al.* 1989).

2.3.4 Detonation initiation by reflected shock in hydrogen-oxygen-argon mixture

The present study addresses the detonation initiation process for a hydrogen-oxygen-argon mixture due to reflection of a shock wave in a shock tube closed at one end. The initial conditions for the computations correspond to the evolution of a strong ignition case by Oran *et al.* (1982). This particular one-dimensional example has also been used extensively in the past to test numerical schemes (Deiterding 2000; Im *et al.* 2002; etc.). and thus, data are available in the literature so that direct comparison can be made with the results obtained from the present computations. The general configuration is a shock tube of length $l = 12$ cm filled with stoichiometric hydrogen-oxygen-argon mixture of molar ratios 2:1:7. Initially, an incident shock wave is created, which propagates through the shock tube from right to left. Once the incident shock is reflected at the end wall, a detonation wave is formed by the reflected shock heating after some induction period. For the computation, the calculation is performed in Cartesian geometry covered with 4800 uniform numerical cells. The hydrogen-oxygen-argon chemistry is modeled with the same 9 species and 24-step reaction mechanism, which was developed in reference (Oran *et al.* 1982).

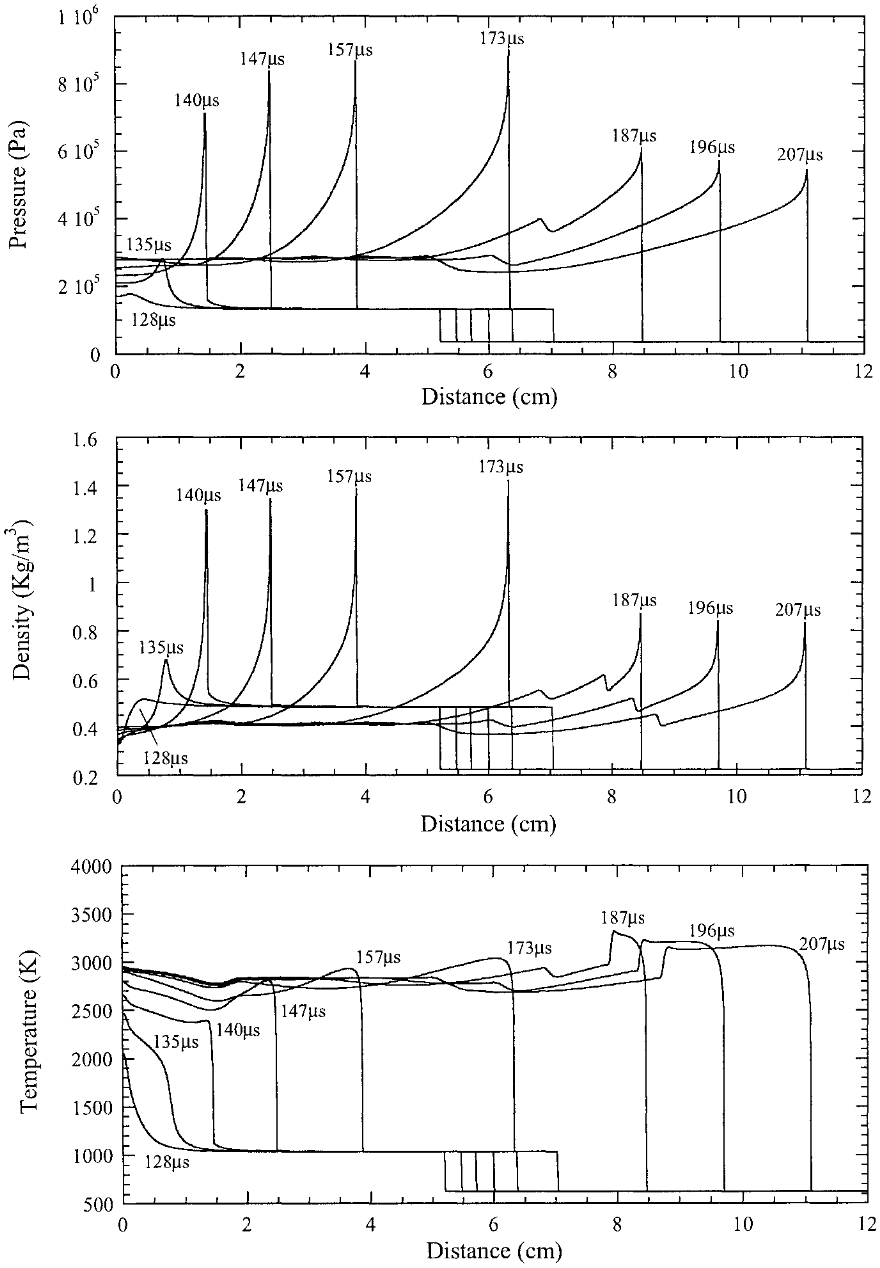

Figure 2.7. Pressure (top); density (middle); and temperature (bottom) profiles showing the time evolution of the detonation intiation process by reflected shock.

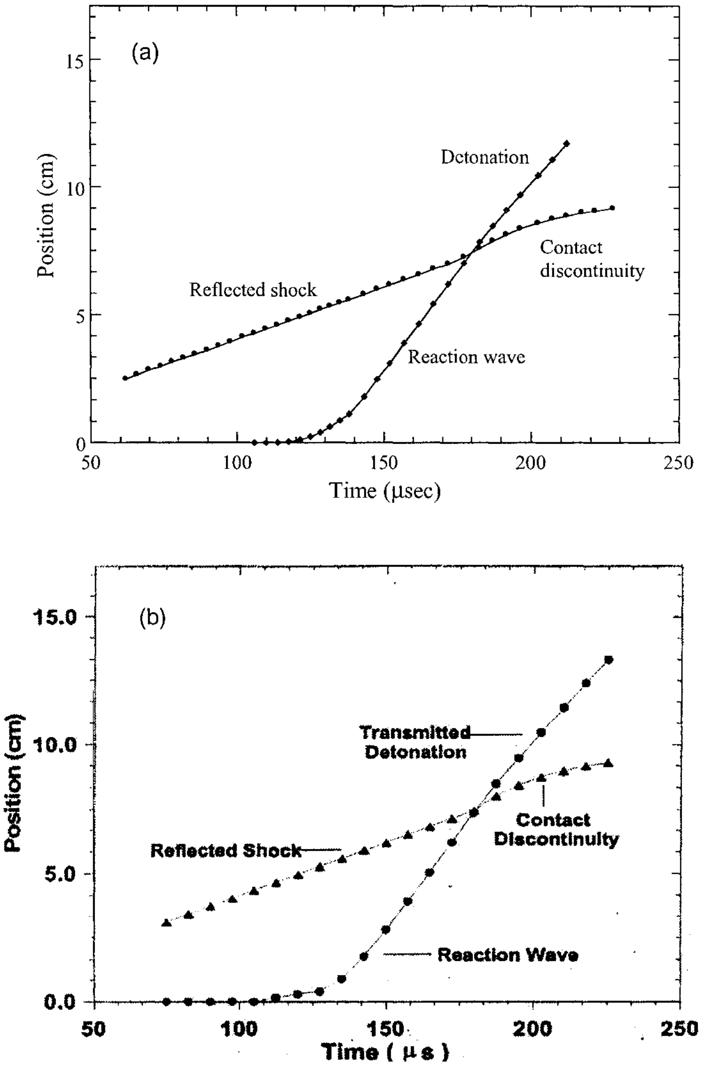

Figure 2.8. Wave diagram for the detonation initiation process by reflected shock. Comparison between (a) the present result and (b) that obtained by Im *et al.* (2002).

To look at the flow evolution for the detonation initiation after the shock reflection from the end wall, figure 2.7 shows the pressure, density and temperature profiles at subsequent time interval. These transient results obtained during different stages of the initiation process, i.e. the ignition, development and final onset of detonation, are found to be in good agreement with those from the literature (Oran *et al.* 1982; Im *et al.* 2002; etc.). After its formation behind the reflected shock, the detonation wave eventually catches up and merges with the reflected shock, causing a split into 3 waves (i.e., the rarefaction, contact surface and the detonation front). Note that these different waves are clearly captured by the present numerical schemes, as shown in the density profile of figure 2.7.

Figure 2.8 shows the trajectory of different waves in the flow field, including the position of the shock front, reaction wave, transmitted detonation and the contact discontinuity due to the merging of the shock with reaction wave. For comparison, results obtained by Im *et al.* (2002) is also shown in figure 2.8b. Very good agreement is found between these two wave diagrams. Furthermore, the result shows that the time when the detonation and reflected shock wave merge is at a value of approximately 180μsec, which also agrees with previous studies (Oran *et al.* 1982; Deiterding 2000; Im *et al.* 2002;). Here, the comparison with previous numerical results from literatures illustrates the similar accuracy of the present approach using this SLIC scheme for the simulation with detailed chemistry.

2.4 An improved SLIC scheme

For moderate grid resolution, the present study has demonstrated on several benchmark test problems that the centered SLIC method can lead to accurate approximations of detonation waves, comparable to those obtained using different best upwind schemes but has the advantage of lower computational cost and simplicity without the use of Riemann-solver. Nevertheless, it is discussed earlier that the SLIC method used in this study cannot achieve the same accuracy at coarser spatial resolutions due to large dissipative nature of the centered scheme. In this section, a possible way to improve the SLIC scheme for low-resolution simulations is addressed, while retaining its advantages of simplicity, robustness and generality.

A computational technique based on a multi-stage predictor-corrector (MUSTA) approach has been recently proposed by Toro (2003) to construct numerical flux for the use in finite volume methods. The idea is that in the predictor step, a simple and robust numerical flux is used to open the Riemann fan without making use of precise knowledge of the structure of the solution of the Riemann problem. It extracts the relevant information for the corrector step, which involves the final inter-cell flux evaluation. The attractiveness of this approach is that the implementations can rely on centered fluxes at each stage (Toro 2003). This procedure is expected to produce a numerical flux very close to that of the upwind method of Godunov scheme. Hence, the use of MUSTA approach opens up a possibility to improve existing centered scheme.

Using the MUSTA approach, an improved SLIC scheme is obtained here by replacing the single evaluation process of the inter-cell numerical flux with a multi-stage FORCE$^{\kappa}$ scheme. It is derived by applying the centered FORCE flux described in equation 2.25 for both the multi-stage predictor and the corrector in the MUSTA approach (Toro 2003). By starting with $\kappa = 1$, $\mathbf{U}_i^{(1)} = \bar{\mathbf{U}}_i^R$, $\mathbf{U}_{i+1}^{(1)} = \bar{\mathbf{U}}_{i+1}^L$, $\mathbf{F}_{i+1/2}^{(force^1)} = \left(\bar{\mathbf{U}}_i^R, \bar{\mathbf{U}}_{i+1}^L\right)$ given by equations 2.25 - 2.27, the general algorithm for the κ-stage FORCE scheme is given as:

Open Riemann fan:

$$\mathbf{U}_i^{(\kappa+1)} = \mathbf{U}_i^{(\kappa)} - \frac{\Delta t}{\Delta x}\left[\mathbf{F}_{i+\frac{1}{2}}^{(force^{\kappa})}\left(\mathbf{U}_i^{(\kappa)}, \mathbf{U}_{i+1}^{(\kappa)}\right) - \mathbf{F}\left(\mathbf{U}_i^{(\kappa)}\right)\right] \tag{2.55}$$

$$\mathbf{U}_{i+1}^{(\kappa+1)} = \mathbf{U}_{i+1}^{(\kappa)} - \frac{\Delta t}{\Delta x}\left[\mathbf{F}\left(\mathbf{U}_{i+1}^{(\kappa)}\right) - \mathbf{F}_{i+\frac{1}{2}}^{(force^{\kappa})}\left(\mathbf{U}_i^{(\kappa)}, \mathbf{U}_{i+1}^{(\kappa)}\right)\right] \tag{2.56}$$

Flux evaluation:

$$\mathbf{F}_{i+\frac{1}{2}}^{\left(force^{\kappa+1}\right)} = \mathbf{F}_{i+\frac{1}{2}}^{(force^{\kappa})}\left(\mathbf{U}_i^{(\kappa+1)}, \mathbf{U}_{i+1}^{(\kappa+1)}\right) \tag{2.57}$$

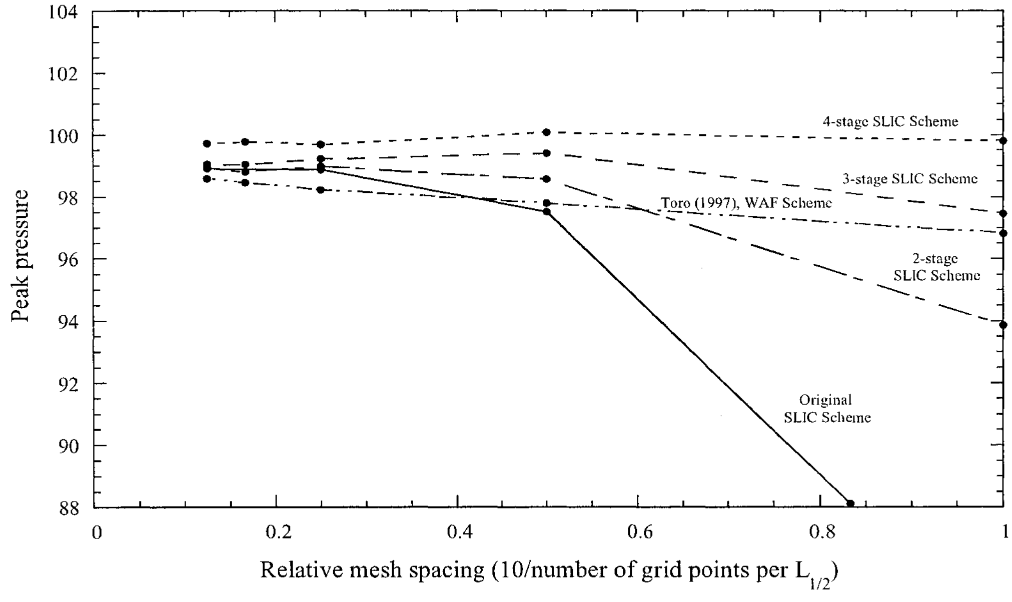

Figure 2.9. Comparison of peak pressure behind the shock front as a function of relative mesh spacing between the original SLIC scheme, modified κ-stage SLIC scheme and WAF scheme for the overdriven pulsating detonation ($Q = 50$, $\gamma = 1.2$, $E_a = 50$ and $f = 1.6$).

To illustrate the performance of the multi-stage SLIC scheme, the canonical problem of the one-dimensional pulsating overdriven detonations discussed in previous section is again considered here. Similarly, figures 2.9 and 2.10 show the peak pressure amplitude and the period of oscillation as a function of relative mesh spacing of the overdriven detonation computed using the original SLIC scheme, the improved κ-stage SLIC scheme (κ =2, 3 and 4) and the 2$^{\text{nd}}$ order upwind WAF scheme for comparison. The improvement using the MUSTA approach can be readily shown in these plots. The multi-stage SLIC schemes are clearly able to predict more accurate results for a given mesh spacing (clearly at low resolution) than the original SLIC

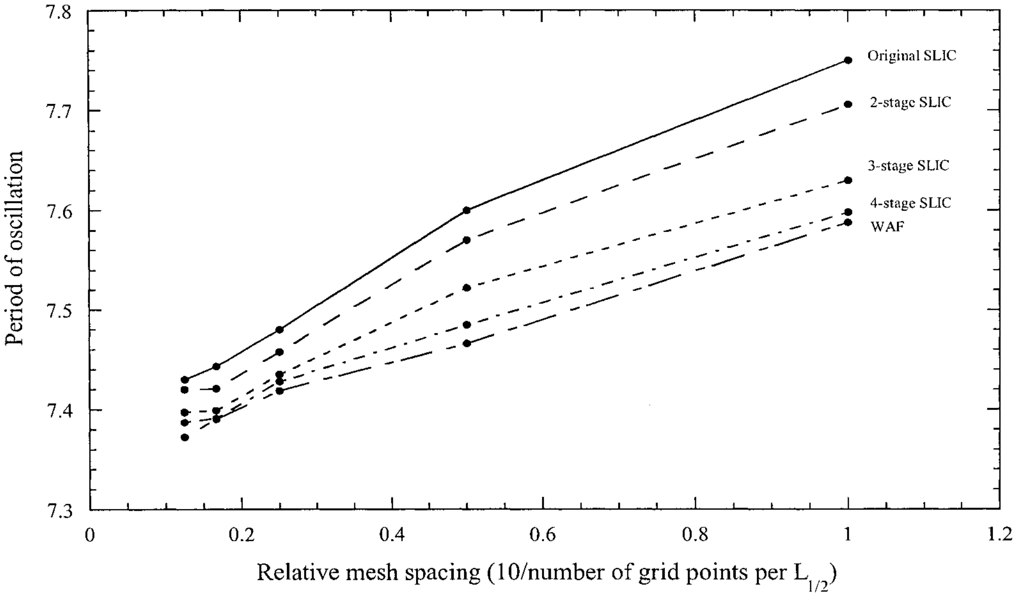

Figure 2.10. Comparison of the period of pressure oscillation as a function of relative mesh spacing between the original SLIC scheme, modified κ-stage SLIC scheme and WAF scheme for the overdriven pulsating detonation (Q = 50, γ = 1.2, E_a = 50 and f = 1.6).

scheme. By increasing the number of stages in the modified SLIC scheme, the results approach faster to the converged value of peak pressure $P \sim 99$ and oscillation period of $\sim$ 7.4 at coarser grid resolution. For the 3- and 4-stage SLIC schemes, they are able to achieve the correct peak pressure with a relatively coarse resolution (10 points per $L_{1/2}$) and have indeed similar accuracy (or even better) to that of the upwind (WAF) method. It should be pointed out that although better accuracy can be achieved as the number of stages is increased, at the same time the computational time for evaluating the inter-cell numerical flux is also increased, which can become comparable to most existing Riemann-solver based upwind schemes. Nevertheless, the multi-stage approach retains the simplicity, robustness and generality of centered scheme. In this study, it is also found that the 3-stage scheme should be sufficiently accurate and is probably the preferred scheme to be used for practical high-speed flow computations.

2.5 Adaptive mesh refinement

It is shown in previous sections the necessity of having fine resolutions in the simulations of detonation waves in order to ensure that detailed features within the reaction zone structure are properly resolved. However, the use of very small time steps and uniform fine grid of cells in a long computational domain requires a much larger amount of computer resources. For detonation problems, high resolutions are in fact only needed in part of the computational domain as most reactions are completed in a narrow region in the vicinity of detonation front. It is thus more economical to refine only in this region and use coarser resolutions elsewhere, hence reducing the computational demands without sacrificing accuracy.

The adaptive mesh refinement method (AMR) originally developed by Berger & Oliger (1984) is adopted in the present numerical investigation as a technique for manipulating the local resolution of numerical simulations in response to the behavior of the evolved solution. The basic idea is to refine automatically, both in space and in time, regions of the computational domain in which high resolution is needed to resolve developing features, while leaving less interesting parts of the domain at lower resolutions. The AMR strategy provides a means for concentrating effort to computationally demanding regions and dramatically improves the computational efficiency of numerical simulations. The AMR method has been widely applied for adaptive computations of hyperbolic conservation laws on Cartesian grids (Plewa 1999).

The Berger-Oliger AMR algorithm follows a patch-based strategy. At regular intervals during the computation, a refinement criterion or an error indicator is applied

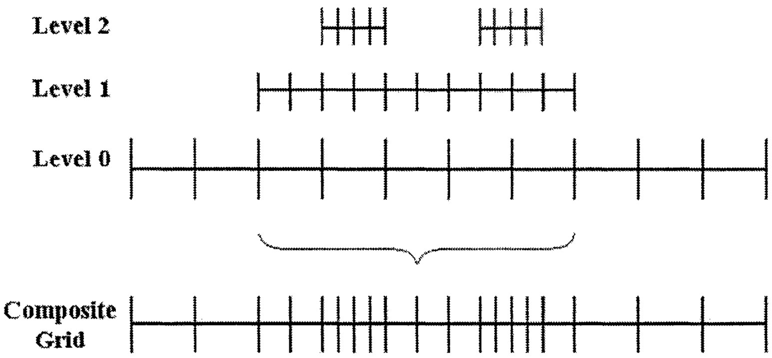

Figure 2.11. Adaptive grid arrangement in one-dimensional configuration.

to the current numerical solution to flag those cells that require higher resolution and then cluster them into several rectangular grids or patches. These selected regions are then refined by overlaying sub-grids of higher resolutions. The refinement process can be repeated recursively from coarser ones until no refinement is needed or the finest refinement level is reached. A hierarchical of embedded overlaying grid patches is constructed. For instance, figures 2.11 and 2.12 show the resulting adaptive grid hierarchy in one- and two-dimensional configuration. Each sub-grid at different refinement level in the hierarchy is uniform and its solution can be advanced individually using the numerical integration scheme with time step adaptively modified by the same refinement factor as in space. More accurate solutions at finer level grids are projected back onto the coarser meshes when they both advanced to the same time step. In order to follow moving features of the flow, all adaptively refined sub-grids are regenerated after a specific number of time steps on the base grid level. The re-gridding procedure in the AMR algorithm therefore dynamically creates, moves and destroys sub-grids in the hierarchy so that refined regions occur only where they are needed as the computation progresses.

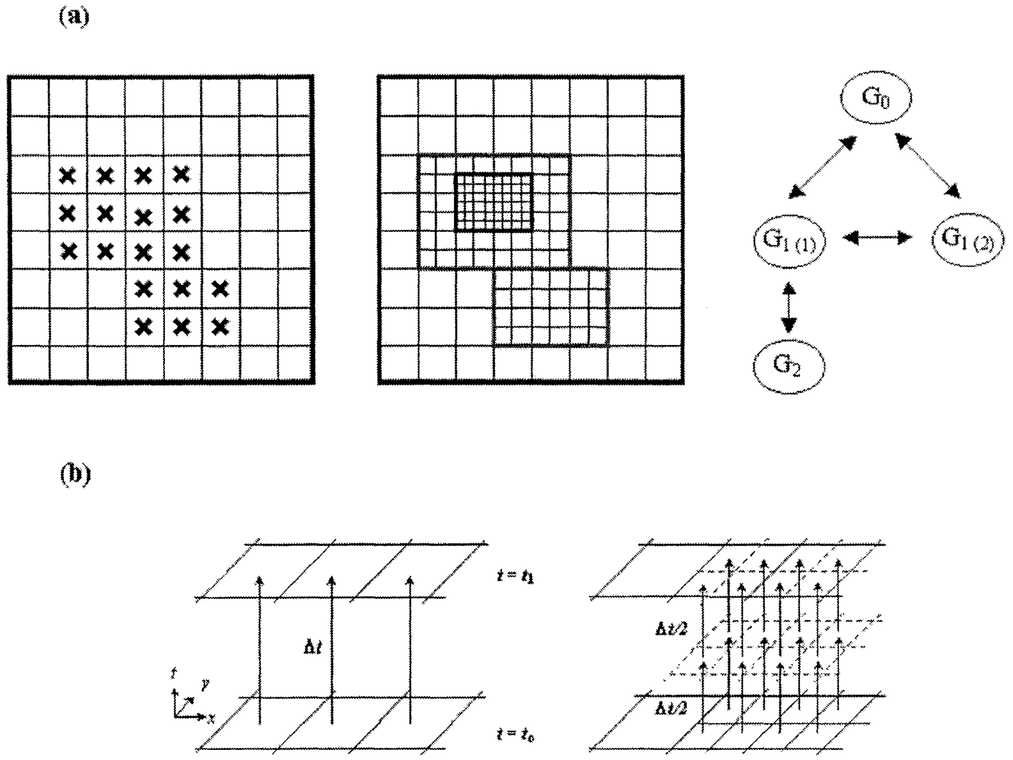

Figure 2.12. Hierarchical series of Cartesian grids for adaptive refinement in two-dimensional configuration.

Further technical details of the AMR algorithm applying to general hyperbolic systems of conservation laws can be found in articles by Berger & co-workers (Berger & Oliger 1984; Berger & Colella 1989; Berger & LeVeque 1998; etc.) and are not discussed in any depth here. In the present study, the finite-volume integration method has been implemented in an existing framework AMR C++ code developed by Hern (1999).

To illustrate the efficiency of local adaptive refinement, figure 2.13 and 2.14 show some examples of both one and two-dimensional computations applied for the detonation test problem where the reactive Euler equations are solved using the SLIC

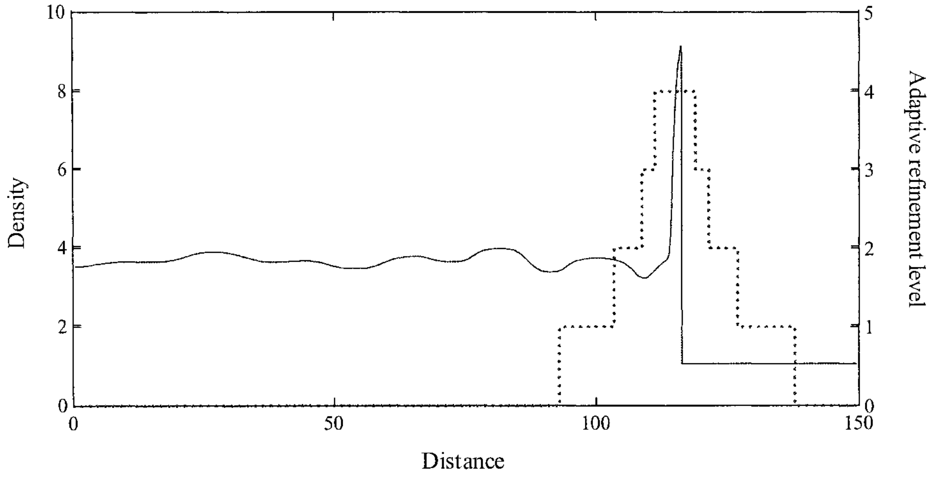

Figure 2.13. Pressure profile of a one-dimensional detonation structure. Dashed lines indicate the level of refinement at the computation domain.

scheme with the AMR framework. For both configurations, the AMR computation was done with 2 levels of refinement and refinement ratio of 2 in each case. The refinement criterion was based on the local density gradient. Cells are flagged for refinement if:

$$\frac{1}{\rho_{i,j}}\sqrt{\left(\frac{\rho_{i+1,j}-\rho_{i-1,j}}{x_{i+1}-x_{i-1}}\right)^2+\left(\frac{\rho_{i,j+1}-\rho_{i,j-1}}{y_{j+1}-y_{j-1}}\right)^2} > \epsilon$$

Figure 2.13 shows the pressure profile of a one-dimensional detonation structure and the dashed lines indicate how the refinement levels adapt over the computational domain. Most of the refinements were done near the leading shock front where the local gradient is largest. For the two-dimensional simulations with AMR, figure 2.14 shows snapshots of density contour (top), computational meshes (middle) and density Schlieren plot (bottom) at two different times and demonstrates how the grids are adaptively refined in both space and time.

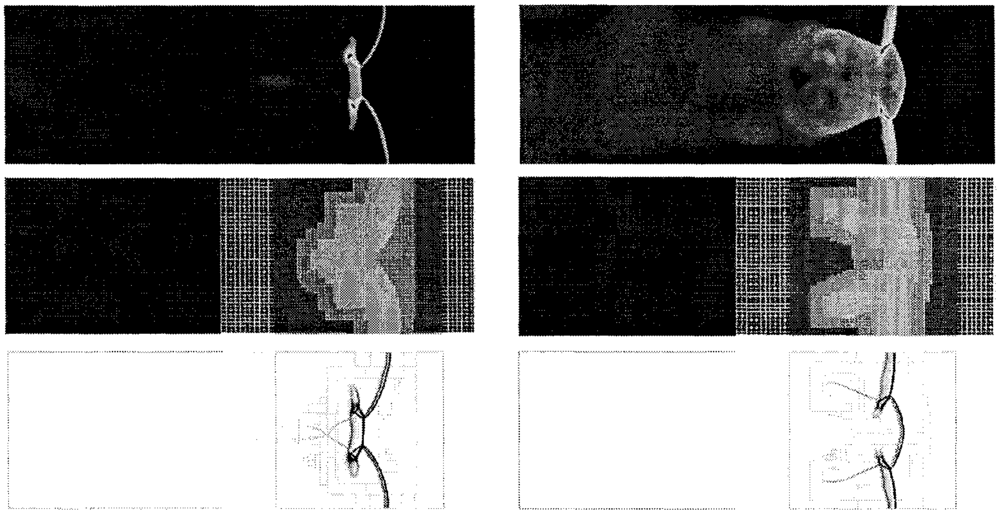

Figure 2.14. Snapshots of density contour (top); grid arrangement (middle); and Schlieren plot (bottom); of the two-dimensional cellular detonation at different times.

2.6 Summary

In this chapter, the mathematical model governing the dynamics of detonation structure is described. The applicability of a high-order centered scheme, namely the SLIC scheme, to solve the governing equations for the simulation of transient detonation waves is also presented. The SLIC method belongs to the high-resolution class of methods, which is conservative, explicit, second-order accurate in space and time. The SLIC method is 'limited' such that in the numerical solution any discontinuities are well-resolved and are not accompanied by the spurious oscillations, which occur typically for unlimited second-order schemes. In this study, this centered scheme is applied to several canonical problems of time-dependent detonation waves with both the simple and complex chemistry. Detailed comparisons with previous published results reveal that the quality of the results obtained from this simple numerical scheme is comparable with those of the upwind schemes at typical resolution used in literature.

The motivation to use this centered scheme comes from the fact that it does not require information about the characteristic structure of the hyperbolic equation system to be provided. Therefore, it generally has a lower computational cost and simple structure compared to most Riemann-solver based methods. However, Riemann-solver based methods typically have the advantage when it comes to accuracy and this is more transparent for computations with coarser spatial resolution in the present study. Here, a possible way to improve the accuracy of the centered schemes using Toro's MUSTA approach is discussed. By constructing the numerical flux based on a multi-stage predictor-corrector fashion, the modified κ-stage SLIC scheme achieves the accuracy of upwind methods even for low-resolution simulations but retains the simplicity and robustness of centered methods.

From the formulation of centered method, it is also apparent that once a skeleton algorithm for the scheme is coded, any system of hyperbolic conservation laws can be solved, simply by typing the corresponding vectors of the conserved variables and the numerical fluxes for the system. Indeed, this is convenient when the method is used for the numerical solution of detonation wave with detailed chemistry or multi-phase components. One should also realize that the flexibility of the scheme generalizes straightforwardly to higher dimensions.

The SLIC scheme is also incorporated easily with adaptive mesh refinement without any implementation complications. The Berger & Oliger's adaptive refinement technique improves the efficiency of numerical simulations of systems of partial differential equations by allowing the size of time steps and grids to vary adaptively according to the requirement of the evolving solution. Computational resources are not wasted in maintaining uninteresting parts of the solution at unnecessarily high resolutions. Therefore, by combining with the AMR algorithm, the present numerical method provides a robust and effective tool for the present computational studies.

Chapter 3

The one-dimensional pulsating detonation structure

3.1 Introduction

To elucidate the unstable structure of detonations and how it is affected by chemical kinetics, this chapter addresses the simplest problem of one-dimensional, time-dependent dynamics of planar detonations with simplified chemistry. Although advances in scientific computing now permit direct numerical simulations of reproducing multi-dimensional cellular detonation structure, the one-dimensional unsteady detonation should retain the essential physical features that could shed light on many peculiarities of multi-dimensional detonations, and yet is much simpler to investigate. In the one-dimensional treatment, the dynamic structure manifests itself through longitudinal pulsation.

Since the pioneering work of Fickett & Wood (1966), the one-dimensional pulsating detonation has been extensively studied via computational investigations by various researchers (Abouseif & Toong 1982; Moen *et al.* 1984; Bourlioux *et al.* 1991;

He & Lee 1995; etc.). These numerical studies are mostly carried out using a single-step Arrhenius law for the reaction rate and capable to demonstrate the evolution of unstable one-dimensional detonation evolves into an oscillatory wave controlled by chemical kinetics and gasdynamic parameters (such as activation energy, the degree of overdrive, heat of reaction, specific heat ratio). Another important conclusion is that the calculated stability boundary and the frequency of the oscillations agreed well with the results as predicted from linear stability analyses (Erpenbeck 1964; Lee & Stewart 1990; Sharpe 1997; etc.).

Recent advances in computation now permit high-resolution numerical simulation of idealized, one-dimensional Chapman-Jouguet (CJ) detonations (He & Lee 1995; Short & Quirk 1997; Sharpe 2000; Sharpe & Falle 1999). Such simulations make it possible to examine the long-time evolution of the longitudinal instability and explore the role of chemical kinetics on the instability spectrum far from the stability limit. One of the interesting characteristics in many of these simulations is that varying a chemical parameter can cause the temporal pattern of the pulsation to pass from regularly periodic to highly irregular or so-called chaotic structures. How the instability pattern approaches chaos in the Chapman-Jouguet detonation under the influence of chemical kinetics remains unclear. To this end, a general interpretation of the large amount of data that is generated by such numerical simulations remains highly desirable for further insight.

Many of the nonlinear features that arise from 1-D pulsating detonations as results of some variations in the reaction kinetics have remarkable resemblance to those found in simple nonlinear dynamical systems such as the nonlinear oscillator (Zhang *et al.* 1998). Perhaps the simplest-known nonlinear system is the logistic equation, i.e., $X_{n+1} = r \cdot X_n \cdot (1 - X_n)$, a single-parameter iterative formula having a growth and a decay term. It has been shown to capture the essence of a whole class of real world phenomena, e.g. population dynamics (May 1973, 1976). While having a simple form, the logistic model gives remarkable insight into a wealth of nonlinear phenomena. The behavior of this system depends critically on the control parameter r and exhibits in certain regions sudden and dramatic changes in response to small variations in r. There is a substantial body of literature on this kind of simple equations, on which a considerable amount of analytical techniques and nonlinear concepts have been developed in the field of nonlinear science. Much of these methodologies have been extended to deal with more complicated dynamical systems (Feigenbaum 1978, 1983).

Although similarities between a simple nonlinear dynamical system and 1-D pulsating detonation have been previously recognized by several authors (Bourlioux *et al.* 1991; Zhang *et al.* 1998; Short & Quirk 1997; Sharpe 2000; etc.), nevertheless a detailed study using classical theories of nonlinear dynamics and chaos to describe detonation instability has not been carried out. In this chapter, very long-term numerical simulations of an idealized pulsating detonation using single-step Arrhenius chemical kinetics are performed. A wide spectrum of instability dynamics resulted from the change of the global activation energy is presented and examined using classical nonlinear dynamic theories. Analysis of the pulsating structure by drawing the similarity to the dynamics of non-linear oscillators also provides some insight about the effect of chemical kinetics.

3.2 Computational results

The reactive Euler equations with a single-step Arrhenius kinetics as given by equations 2.32-2.36 are solved using the SLIC scheme to simulate the inviscid, one-dimensional propagation of a detonation wave. The computations are initialized by the steady solution of the ZND detonation. An effective numerical resolution of 128 points per half-reaction zone length of the steady ZND detonation $L_{1/2}$ is used,

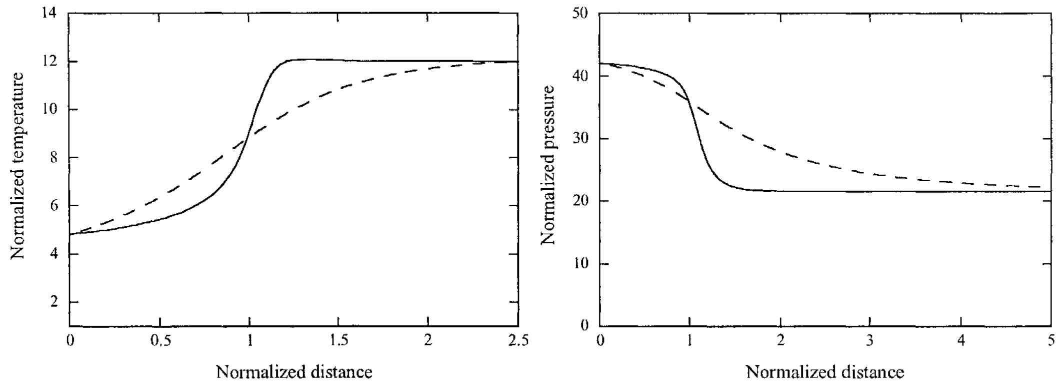

Figure 3.1. Steady ZND detonation profiles for a mixture with $Q = 50$, $\gamma = 1.2$, $f = 1.0$ and two values of activation energies $E_a = 25.0$ (dashed lines); and $E_a = 50.0$ (solid lines).

unless specified, in this study to ensure the detailed features of the pulsating front are properly resolved. This investigation also follows previous studies to fix the dimensionless parameters with the values $Q = 50$, $\gamma = 1.2$ while varying activation energy E_a as a control parameter so that detailed comparisons can be made with prior results found in literature. ZND profiles computed using two activation energies are shown in figure 3.1. In both cases, temperature begins to raise immediately behind the leading shock front. From these curves, it can be seen that increasing E_a has an effect of steepening the temperature profile of the steady ZND structure. Hence, the wave should be more sensitive to temperature perturbation at higher E_a, which will lead to different instability phenomena as discussed previously in Chapter 1. One interesting remark can be made from these ZND profiles is that by having extremely high value of activation energy E_a, the thermally neutral induction zone can indeed be roughly approximated. However, it will only result a very thin heat release zone. Therefore, using one-step Arrhenius kinetics, independent variation of these two characteristic zone lengths is not possible.

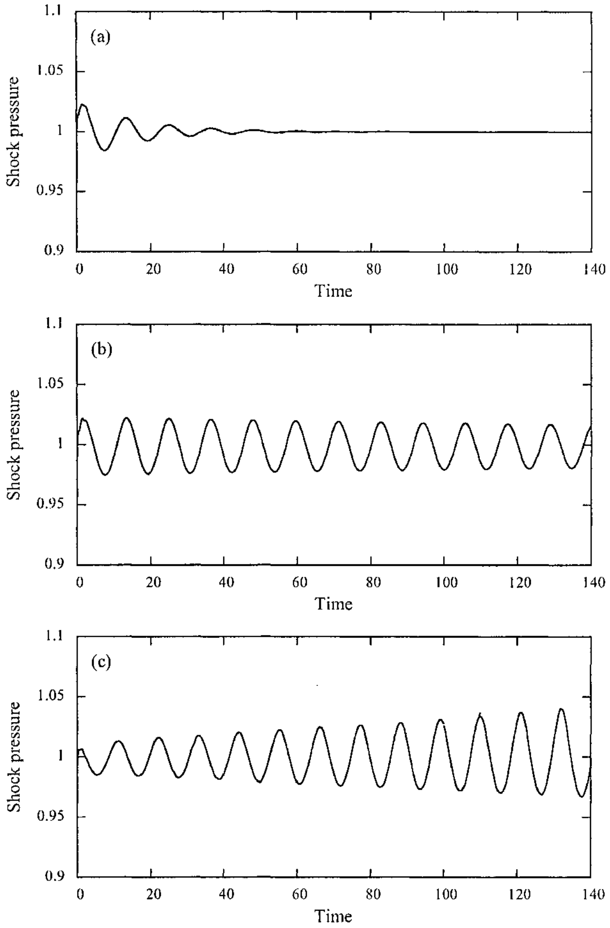

Figure 3.2. Leading shock pressure history for activation energies close to the stability limit (a) $E_a = 24.00$; (b) $E_a = 25.24$; and (c) $E_a = 25.28$.

Typical results of the early transient development obtained from the numerical simulations are shown in figure 3.2. Following previous studies, the leading shock pressure behind the evolving 1-D detonation wave normalized by the von Neumann pressure P_{vn}, i.e., the post-shock pressure in the corresponding steady ZND solution, is plotted for different activation energies E_a. For very low activation energy ($E_a <$ 25.26), the oscillation due to the initial perturbation damps out with time and the propagating detonation is stable after the long-term evolution (figure 3.2a & 3.2b). The stability boundary, above which there is a gradual increase in the amplitude of leading shock pressure oscillations with time, is found to be around E_a = 25.26 - 25.27. The detonation wave with activation energy above this boundary is thus unstable, as illustrated in figure 3.2c. The stability limit value obtained from the present simulation is in good agreement with the prediction of the linear analysis ($E_a = 25.28$) and those numerically determined by other researchers (Sharpe 1997; Sharpe & Falle 1999; etc.).

Figure 3.3 shows the long-term nonlinear evolution of the pulsating detonation after the initiation transient has passed by plotting the leading shock front history as well as the phase plot. As pointed out by Sharpe (2000), it is important to allow the detonation to run for thousands of half-reaction times to ensure the correct final nonlinear behavior of the detonation propagation has been reached. For an activation energy close to the stability limit, the oscillation demonstrates a regular harmonic oscillatory behavior with constant period (figure 3.3a). By systematically increasing the activation energy, instability of the detonation front evolves away from a single-mode oscillation to a period-two oscillation after some transient development, as shown in figure 3.3b. Different modes of oscillation begin to appear as the value of activation energy is continuously increased (see figure 3.3c & 3.3d). Note that the peak amplitudes are used here to define the oscillation modes or periods. For example, a period-two oscillation should have two different values of peak amplitudes. In the present study, oscillation up to period-sixteen can be identified from the computational results. It should be pointed out that evidence for period-sixteen oscillation shown in figure 3.4 is achieved by doubling the numerical resolutions as used for the other cases and it is difficult to determine exactly where the period-sixteen oscillation mode occurs. At very high activation energy, the oscillation then becomes very irregular, as illustrated in figure 3.5 for the case of activation energy $E_a = 30.00$. These numerical results showing the long-time nonlinear evolution are in good agreement with those available in literature computed using different numerical methods, such as Bourlioux's PPM method with conservative front tracking (Mazaheri 1997) and other shock-capturing Godunov-type schemes (Sharpe 2000). Hence, the present computations provide reliable raw data for further time series analysis using different methods of nonlinear dynamics.

It should be pointed out that higher modes of oscillation greater than period-sixteen are difficult to distinguish in the present study due to various limitations associated with the numerical simulations. For example, it can be seen from figure 3.4 that there are only small variations in peak amplitude and distance between limit cycles for period-sixteen oscillation. In order to identify higher oscillation modes, the peak of the oscillation must be captured very accurately. This can be achieved numerically only if both the grid resolution Δx and time step Δt approach zero. Furthermore, to locate the next occurrence of bifurcation, a much smaller increment of activation energy E_a is necessary, i.e., at least $\Delta E_a = 0.0001$ or smaller. However, these requirements will readily give principal difficulties in both the computational efficiency as well as the accuracy and stability of the numerical scheme. With a small incremental step size in these parameters, the numerical error (e.g. truncation error) will become significant and thus will limit the identification of higher bifurcation sequence. Similarly, another concern is the accuracy of numerical results for very high activation energy (i.e. E_a of the order of 30.00 or higher). It has been shown in literature that there is no converged solution for very high activation energy (He & Lee 1995; Sharpe 2000; etc.). This fact casts some doubts on the reliability of numerical simulation for very unstable detonations, which are so dependent on the details of the numerical method, grid resolution, initial conditions, etc. Due to this uncertainty about the numerical results for highly unstable detonations, the present analyses are thus carried out for the computational results with activation energy E_a no more than 30.00.

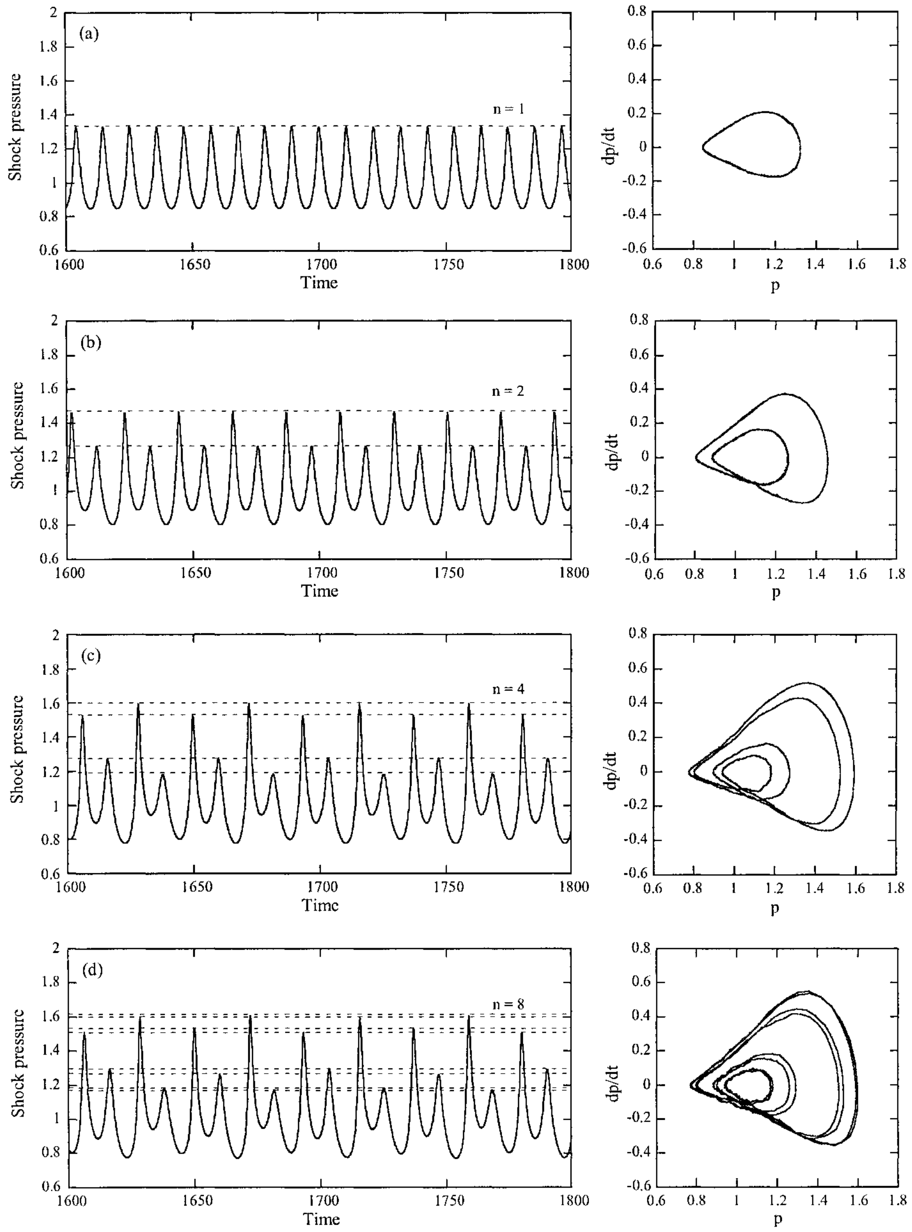

Figure 3.3. Leading shock pressure history and its phase plot showing different modes of oscillation for varying activation energies: (a) $E_a = 27.00$; (b) $E_a = 27.40$; (c) $E_a = 27.80$; and (d) $E_a = 27.82$.

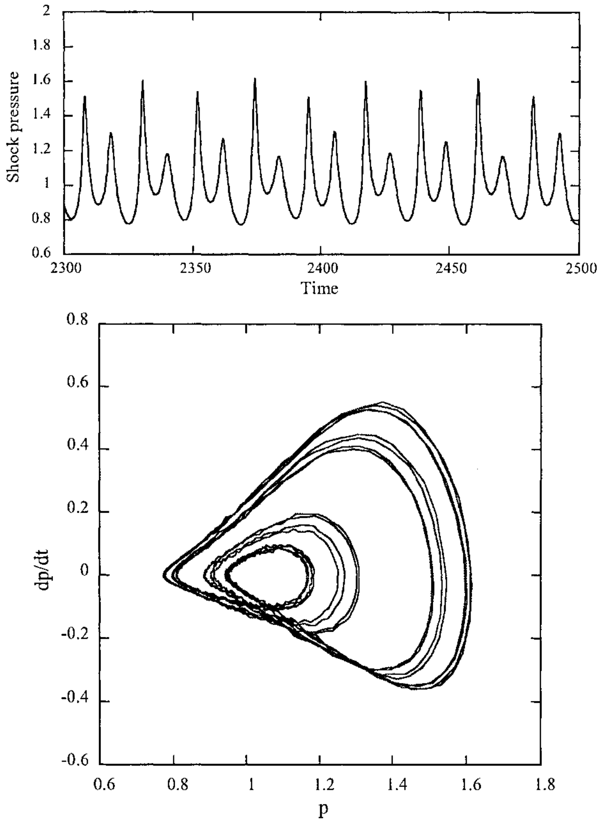

Figure 3.4. Leading shock pressure history and phase plot showing the period-sixteen mode of oscillation for $E_a = 27.845$.

3.3 Autonomous structure of the pulsating detonation

It is interesting to note that if one computes the average velocity of the pulsating detonation over several cycles of oscillation, it is very close to the theoretical value determined from the solution of the steady one-dimensional conservation equations based on the Chapman-Jouguet criterion as shown in figure 3.6. The fact that the time averaged pulsating detonation velocity agrees with the steady theoretical

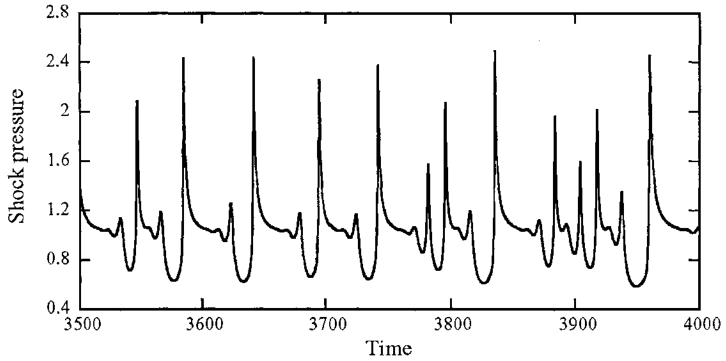

Figure 3.5. Leading shock pressure history for a highly irregular case of activation energy $E_a = 30.00$.

solution within 1% suggests that the structure may indeed be independent of the flow field behind the detonation. Equivalently, a rear boundary must exist separating the detonation complex from the non-steady mean expansion flow in the products as pointed out by Taylor (1950).

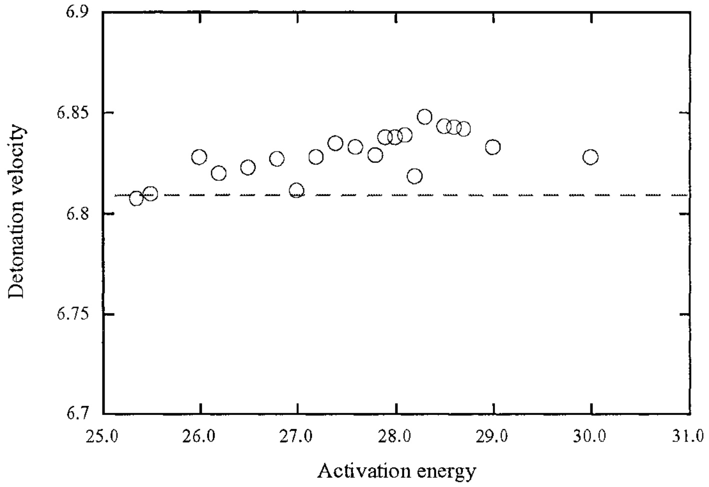

Figure 3.6. Time-averaged velocity of the oscillatory detoantion front.

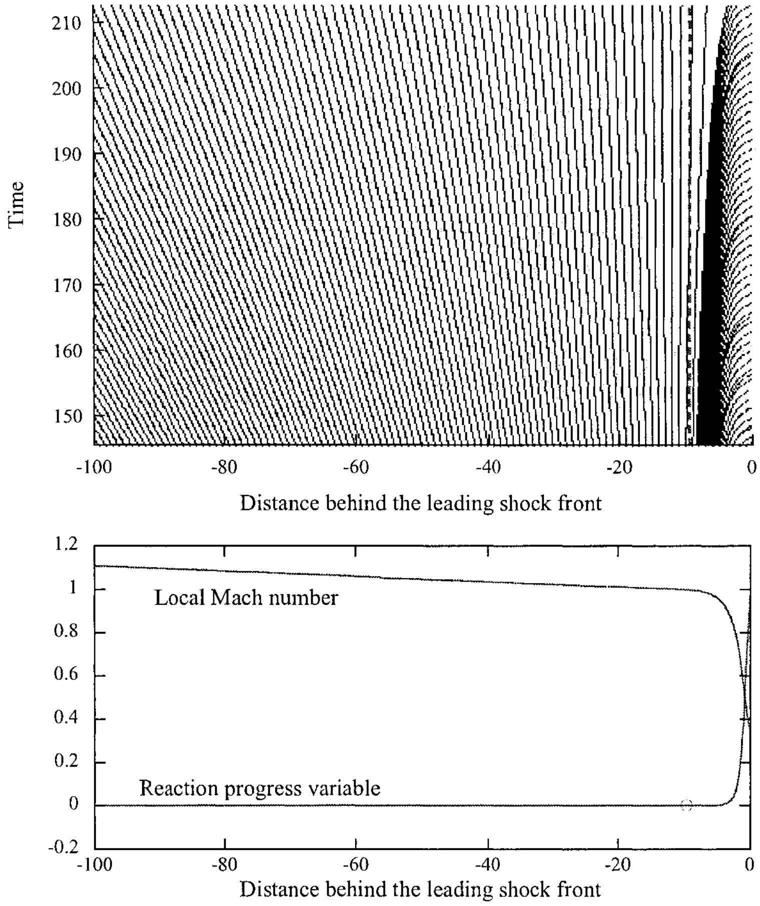

Figure 3.7. Profiles showing the $u' + c$ characteristic lines at the shock-fixed frame (top); and the Mach number and reaction progress variable behind the shock (bottom). The dashed line shows the location where the reaction progress variable $\beta \sim 10^{-5}$.

To further investigate the existence of a complex boundary in the unsteady detonations, the following analyzes in more details two computational results of $E_a = 24$ and $E_a = 27$, which respectively yield the stable and unstable solutions. For activation energy $E_a = 24$, the unsteady solution approaches asymptotically to a steady-state value. Figure 3.7a gives the $x' - t$ diagram showing the $u' + c$ characteristic lines behind the leading shock front at which the coordinate is fixed (i.e. u' is the particle velocity in the shock-attached frame). From this plot, one can see a limiting characteristic which acts as a boundary such that the characteristics lines of the nonsteady expansion at the downstream flow field are incapable of penetrating and influencing the detonation structure. For the case of low activation energy such as $E_a = 24$ where only a steady-state structure is approached asymptotically, the vertical limiting characteristic corresponds to the notion of a "sonic surface" as postulated from the steady concepts. Figure 3.7b gives profiles of the stable detonation structure showing its distribution of reaction progress variable and Mach number measured relative to the leading shock. Across the shock, the Mach number decreases to a subsonic value and then rises to a value 1 downstream of the structure. The location of the sonic point also approximates the end of the chemical reaction ($\beta \sim 10^{-5}$). This agrees with the ideal Chapman-Jouguet condition, which requires that the end of the reaction must approach a sonic condition. For the stable solution obtained with $E_a = 24$, the detonation structure agrees with the steady-state ZND solution where the notion of a limiting characteristic coincides with that of a "sonic surface".

On the other hand, instability of the detonation with higher activation energy $E_a = 27$ leads to an oscillatory solution and thus, there is no steady bounding sonic surface for the unstable transient pulsating detonation. Nevertheless, there still exists a rear limiting characteristic for the pulsating detonation despite its unstable propagation, as also shown recently by Kasimov & Stewart (2004). This limiting characteristic can be seen again from the $x' - t$ diagram showing the $u' + c$ characteristic lines (figure 3.8). As the front evolves, the domain of influence of the shock front is essentially bounded by a limiting characteristic and the shock. Consequently, any trailing unsteady expansion waves or perturbations represented by characteristic lines have again no influence on the continuous dynamics of the flow ahead of the limiting characteristic and on the motion of the shock front. This information boundary thus ensures the self-contained and autonomous nature of the unstable detonation. The notion of this limiting characteristic can have significant implications on the analytical treatment of unsteady detonation waves as it may provide a closure condition for the boundary-value problem encountered from the derivation of evolution equation using asymptotic analysis (Kasimov 2004).

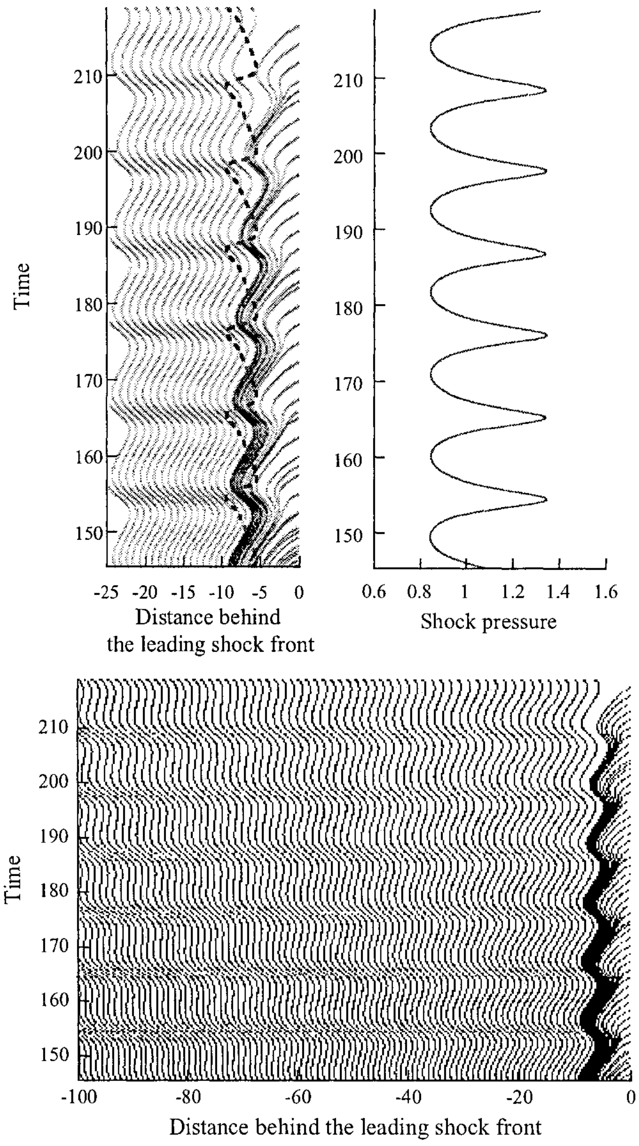

Figure 3.8. Profiles showing the leading shock pressure history and the $u'+c$ characteristic lines at the shock-fixed frame for an unstable detonation. The dashed line shows the location where the reaction progress variable $\beta \sim 10^{-5}$.

On the same plot, the location where the reaction progress variable has been depleted to $\beta = 10^{-5}$ is also indicated by the dashed line. It is noted that the location where the chemical reaction is essentially completed does not necessary coincide with the limiting characteristic. The distance of the rear boundary from the leading shock is found to be sometimes longer than the reaction zone length. This implies that unlike the steady one-dimensional ZND detonation, it is not sufficient to require the termination of chemical reactions to define the self-contained system for unstable detonation. Thermodynamic and hydrodynamic equilibrium may require a longer span to be achieved. It is thus important to note that a meaningful autonomous structure must include both the thermodynamic and hydrodynamic equilibrium within it.

Experimentally, the distance from the leading shock to the rear information boundary in an average sense is generally referred to as "hydrodynamic thickness" of real cellular detonations (Soloukhin 1969; Lee *et al.* 1969). Recent study also suggests that the hydrodynamic thickness may perhaps provide a suitable length scale to characterize the detonation structure within which various chemical and gasdynamic mechanisms responsible for sustaining the unstable detonation are contained. It should have significant implications for understanding the propagation and developing models of real multi-dimensional detonations, which are always non-steady and highly unstable (Radulescu & Lee 2005).

3.4 Nonlinear dynamics and chaos analysis

An important observation from the above analysis is that the one-dimensional unsteady detonation is not always a stable ZND wave propagating at a constant velocity, but one that oscillates around the time-average steady-state solution. Its degree of instability varies according to the chemical kinetics parameter. To further explore the different oscillatory nature of the pulsating detonation resulted from the variation of activation energy, different nonlinear dynamic analyses will be carried out in this section.

3.4.1 Power spectral density

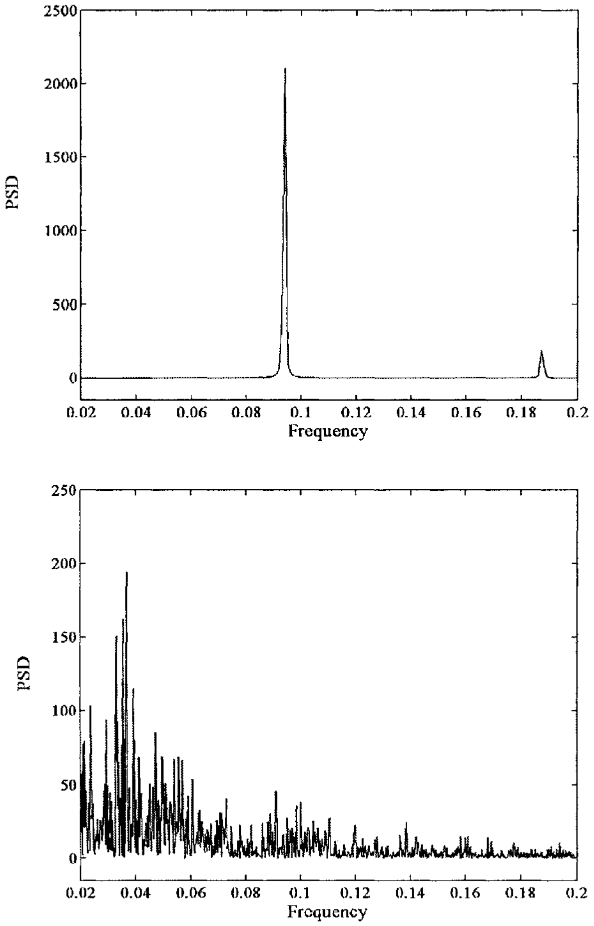

Figure 3.9. Power spectral density of the leading shock pressure history for activation energies (*a*) $E_a = 27.00$; and (*b*) $E_a = 30.00$.

To distinguish the regularity of the pulsating detonation front, it may be of interest to look at the power spectral density (PSD). The PSD describes how the power (or variance) of a time series is distributed with frequency. Mathematically, it is defined as the Fourier Transform of the autocorrelation sequence of the time series. The PSD of the leading shock pressure history for the low activation energy case ($E_a = 27.00$) can be found in figure 3.9a. The plot shows a very large spike at one dominant frequency mode. In other words, the energy is concentrated at this frequency leading to a very regular oscillation. It should be pointed out that the small amplitude peak at the right side of the frequency spectrum is not the consequence of numerical noise, but rather the second harmonic of the system with exactly two times the fundamental frequency.

On the other hand, with a large activation energy ($E_a = 30.00$), there are no clear power spikes, meaning the energy is distributed over a wide range in the frequency spectrum (figure 3.9b). This may provide an indication of the existence of chaos in the system. Nevertheless, a closer examination of the results is required in order to definitively demonstrate the existence of chaos in the system, and not just an example of numerical noise in the data.

3.4.2 Bifurcation diagram

The computational results indicate that the cyclic pulsations change from harmonic oscillations to nonlinear and eventually to highly irregular as the value of the activation energy is systematically increased from its value at the stability limit. An alternative way to represent the computational results in order to illustrate the transition pattern is to construct a bifurcation diagram, as shown in figure 3.10. It is a useful diagnostic tool used to characterize changes in the dynamics of a system as a function of a varying parameter. Here, a bifurcation diagram is generated by plotting the amplitudes of the peaks of the leading shock pressure against the activation energy. As before, measurements are only made after the initiation transient

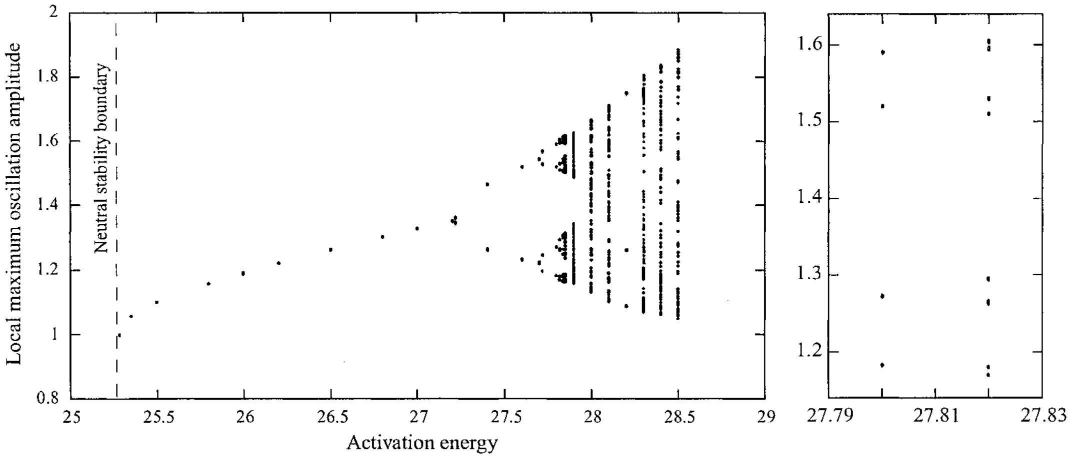

Figure 3.10. Bifurcation diagram for the one-step Arrhenius kinetic model with varying E_a.

has disappeared. In this form, a bifurcation diagram would display the repeating magnitude of the oscillation as a single point. The principal features in this diagram are the vertical windows that identify the ranges of the activation energy of different oscillation modes. A number of distinct regions of different types of behaviour can be observed in the resulting diagram.

i	Activation energy E_a	Oscillation mode	Feigenbaum number
0	25.27	1	–
1	27.22	2	–
2	27.71	4	3.98
3	27.82	8	4.46
4	27.845	16	4.40

Table 3.1. Values of bifurcation limits and Feigenbaum numbers obtained using the one-step Arrhenius kinetic model.

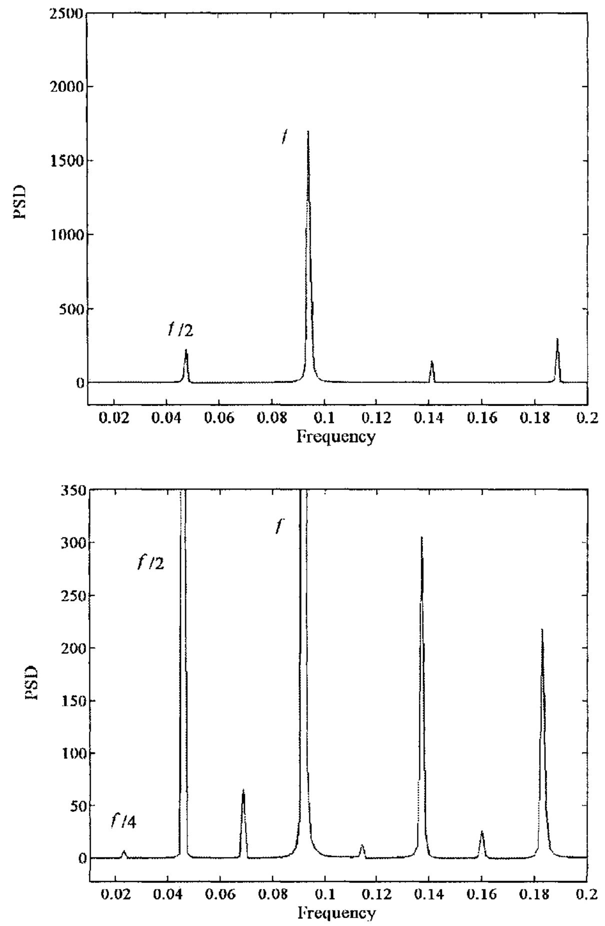

Figure 3.11. Power spectral density of the leading shock pressure history for activation energies (*a*) $E_a = 27.40$; and (*b*) $E_a = 27.80$.

At low activation energy below the neutral stability limit, the detonation front is stable and hence no oscillation amplitude is recorded. Above this limit, the propagating front starts to oscillate and a single peak pressure amplitude can be found, represented by a single point in the bifurcation diagram. The amplitude of the oscillation continues to grow and a period-doubling bifurcation occurs. Further bifurcation processes follow as the activation energy continues to increase. At each bifurcation i, the appearance of a subharmonics with $f/2^i$ where f is the fundamental frequency can also be seen in the PSD. (For example, see figure 3.11a and 3.11b for the oscillations with period-two and period-four, respectively.) This cascade of period-doubling bifurcations can eventually lead to a very irregular oscillation with different peak amplitudes.

3.4.3 Route to higher oscillation modes

In nonlinear dynamics, a number of scenarios were proposed and proved to describe the route to higher or eventually to irregular oscillation modes (Eckmann 1981). In this study of 1-D pulsating detonation, the corresponding bifurcation diagram indicates that the early stage of the pattern transition follows the generic pattern of the period-doubling. This evidence suggests that the route may indeed follow closely Feigenbaum scenario, which involves successive subharmonic bifurcations (Feigenbaum 1983). It is interesting to note that the bifurcations come faster and faster until the system becomes aperiodic.

Table 3.1 shows the value of activation energy where transition occurs. To further characterize the bifurcation diagram and provide evidence for the validity of Feigenbaum scenario describing the 1-D pulsating detonation phenomenon, these values are used to determine the Feigenbaum number (Feigenbaum 1978), which is defined as the ratio between the spacing of successive bifurcations, i.e.:

$$\delta = \frac{\mu_i - \mu_{i-1}}{\mu_{i+1} - \mu_i} \tag{3.1}$$

where μ_i is location of the bifurcation point. For similar bifurcation processes occurred in logistic model as well as other simple nonlinear dynamical systems, Feigenbaum discovered a universal feature that the bifurcations should be occurring at a ratio that converges to a natural constant that is approximately 4.669 in the asymptotic limit where the number of bifurcations go to infinity, independent of the particular system. It may be worthwhile to point out this convergent Feigenbaum cascade of bifurcations has also been observed in a number of experimental studies of different types: Rayleigh-Bénard experiment on the flow in a flat convective layer of liquid heated from below; experiments on circular Couette flow; acoustic cavitation noise; driven nonlinear semiconductor oscillator; shallow water waves in a resonator; optical turbulence in a hybrid optically bistable system; Belousov-Zhabotinskii reaction in a well-stirred flow reactor; etc. (Hao 1984). Some values of the Feigenbaum number for the present bifurcation diagram are shown in table 3.1, which also appear to be in reasonable agreement to this universal value. Unfortunately, the Feigenbaum number for further bifurcation points cannot be measured since the identification of higher bifurcation sequences is limited in the present numerical simulation as discussed previously. Nevertheless, overall this result appears to support that the transition process of the pulsating detonation front may follow closely Feigenbaum's picture for a simple nonlinear model with fewer degrees of freedom.

3.4.4 Existence of chaos

It is shown from the bifurcation diagram that by increasing the activation energy, the system behaviour continues through a sequence of period-doublings. This infinite sequence of bifurcations may eventually lead to chaos, a concept that has been well established in nonlinear dynamics. Mathematically, chaos means the system contains an infinite number of unstable period orbits. A more physical definition is an aperiodic dynamics in a deterministic system demonstrating sensitive dependence on initial conditions (Kaplan & Glass 1995). For a chaotic system, a small deviation in the initial conditions will result in an exponentially growing departure in its specific temporal behavior. Equivalently, a small change in the pulsating structure at a given starting time would result after a short period of time in a complete different oscillatory pattern. There are several regions in the bifurcation diagram where highly aperiodic oscillations are found. These results can be further analyzed for the

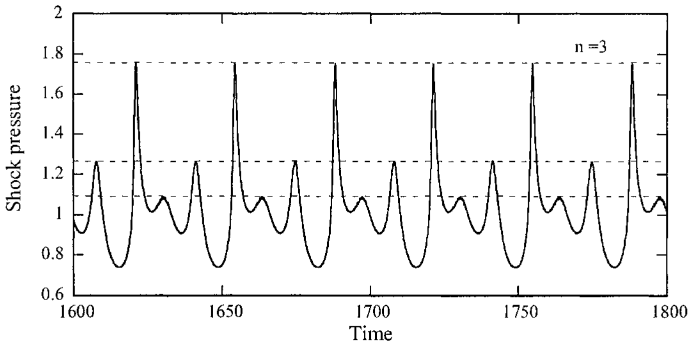

Figure 3.12. Unstable detonation for activation energy $E_a = 28.20$ with a period-three limit-cycle.

existence of deterministic chaos in the system.

First of all, a closer examination of the bifurcation diagram shows that there is a period-three limit-cycle around $E_a = 28.20$ and its leading shock pressure history is shown in figure 3.12. There is a well-known result in the nonlinear science literature saying that period-three implies chaos (Li & Yorke 1975). As discussed earlier, instability always grows through a sequence of bifurcations yielding even periods (period-two, period-four, etc.). The appearance of period-three suggests the solutions just to the left of this period-three window in the bifurcation parameter are chaotic.

Indeed, a more quantitative way to determine the existence of chaos is provided by the Lyapunov exponent (Eckmann & Ruelle 1985). It is a measure of sensitive dependence on initial conditions. It quantifies the exponential rate of divergence of initially neighbouring phase-space trajectories (figure 3.13) and estimates the degree of chaos in a system. For any time series in a dynamical system, the presence of a positive largest characteristic exponent indicates that the trajectories comprising an attractor diverge over a long time average, which is characteristic for chaotic behaviour. This divergence describes the rapid loss of the system's memory of its previous history as time evolves. There are several algorithms for estimating the

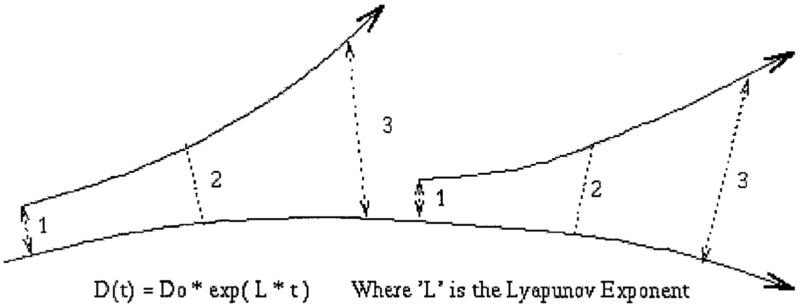

Figure 3.13. Time evolution and distance between initially neighbouring phase-space trajectories.

positive Lyapunov exponent directly from a time series (Wolf *et al.* 1985; Eckmann *et al.* 1986; Kantz 1994; etc.). The algorithm chosen in the present study is due to Rosenstein *et al.* (1993). It is tested carefully in their paper through several examples, including the effect of additive noise.

Following Rosenstein *et al.*'s approach, figure 3.14 shows some typical plots of natural log of divergence versus evolution time of initially close state-space trajectories for the case of $E_a = 28.17$ (just before the appearance of period-three oscillation) and for large activation energy $E_a = 30.00$. Different curves for each plot correspond to different embedded dimensions assumed for the system (Rosenstein *et al.* 1993). The linear region means the divergence of nearest neighbors is exponential, where the slope can be interpreted as a measure of the largest Lyapunov exponent. In both cases, a positive Lyapunov exponent is found, which indicates the presence of chaos in the system and that the system is sensitive to the uncertainty in the initial conditions. Note that the magnitude also provides a measure of degree of chaos, i.e. the rate of divergence. In a more general sense, the Lyapunov exponent also provides another way to characterize whether the systems are likely to be dynamically irregular (if positive) or not (otherwise).

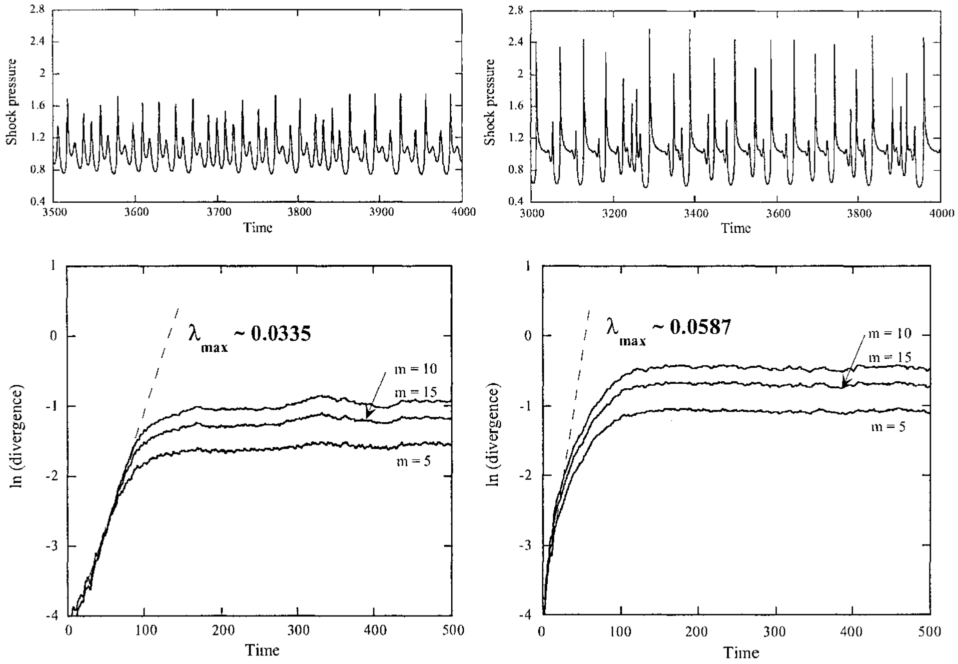

Figure 3.14. Calculation of largest Lyapunov exponent with different embedded dimensions m for the case of activation energies (a) $E_a = 28.17$; and (b) $E_a = 30.00$.

3.5 Discussion and summary

Numerical simulations of the one-dimensional pulsating detonation with global one-step chemistry elucidate how the detonation structure is strongly influenced by the chemical kinetics. It is shown that a wide instability spectrum can be achieved by varying the activation energy in the single-step kinetic model. Despite the unstable nature of the pulsating detonation, the existence of the rear information boundary is demonstrated. The limiting characteristic acts as a boundary to isolate the unsteady expansion from the rear and is responsible for the unstable detonation complex to remain as an unique autonomous system with self-excited oscillation.

Results from the nonlinear dynamic and chaos analysis, such as the Feigenbaum's period-doubling type break-up sequence as the activation energy increases, have indicated a strong similarity between the 1-D pulsating detonation and simple nonlinear mechanical systems. This suggests that it may be possible that the dynamics of the pulsating detonation front can be simply modeled by a nonlinear oscillator equation. The setting up of such equation can perhaps provide a useful analogy of the one-dimensional detonation with classical nonlinear mechanical system to gain further insight on how the oscillatory structure is influenced by different factors such as chemical kinetics. Such analogy has indeed been attempted previously by Zhang *et al.* (1998). From the integral conservation considerations of the detonation structure, they have derived the following oscillator equation (see Appendix A):

$$l_h I \ddot{F} + \frac{\rho_{cj} e_{cj}}{D} \dot{F} + \frac{l_h D}{2} \dot{I} = \frac{D_{cj} Q}{D} \Psi_1 \tag{3.2}$$

The validity of the above equation to model the instability pattern of the pulsating detonation is confirmed in this study. Equation 3.2 is integrated in which the coefficients for each term are obtained from the results of the numerical simulations. Figure 3.15 compares the solutions from the full direct numerical simulation as shown previously with those obtained from equation 3.2. Very good agreement is achieved and different oscillation modes of the front can indeed be recovered by the solution of the oscillator equation.

It is perhaps worthwhile to discuss some interesting aspects shown by Zhang *et al.* (1998) that are related to the present investigation. Firstly, it is possible to write equation 3.2 in a more analogous form of a classical nonlinear oscillator (see Appendix A):

$$\Phi^1\left(\dot{F}\right)\dddot{F} + \left(\frac{d\Phi^0\left(\dot{F}\right)}{d\dot{F}} + \frac{d\Phi^1\left(\dot{F}\right)}{d\dot{F}}\ddot{F} - \Psi^1\left(\dot{F}\right)\right)\ddot{F} + \rho_{cj} e_{cj} \dot{F} - \Psi^0\left(\dot{F}\right) = 0 \tag{3.3}$$

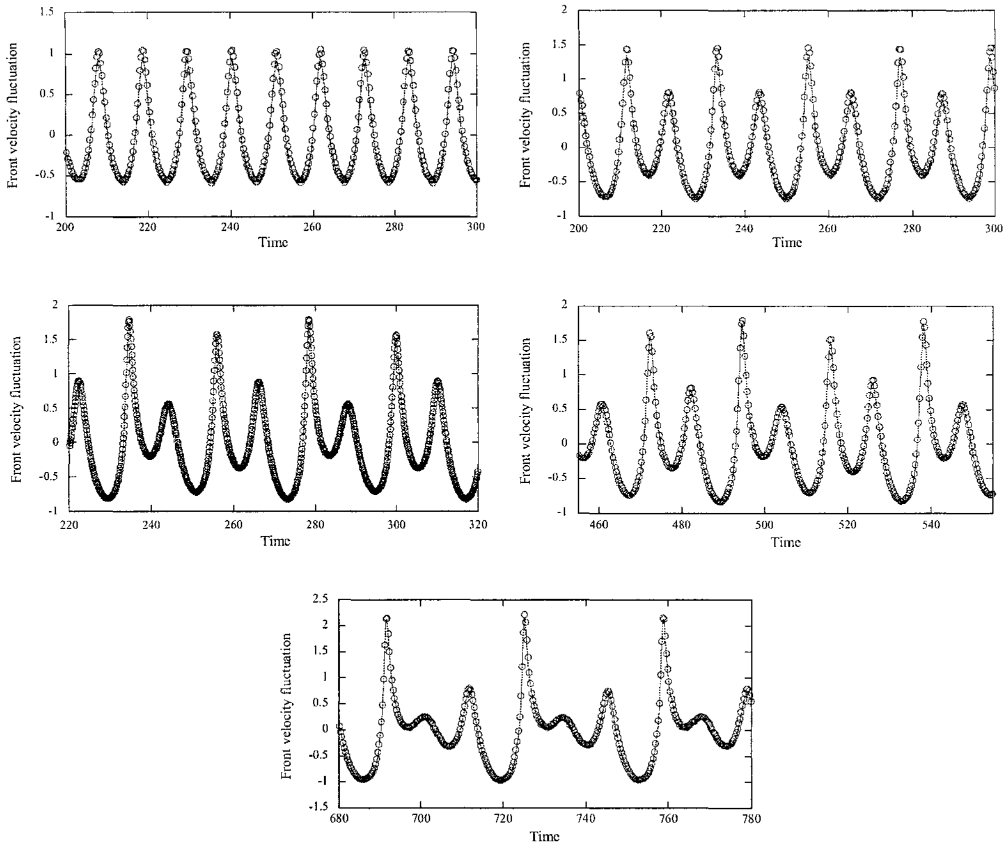

Figure 3.15. Comparison between the results obtained from the oscillator model (solid line) and direct numerical simulations (data points) for $E_a = 27.00$; $E_a = 27.40$; $E_a = 27.80$; $E_a = 27.82$; and $E_a = 28.20$.

In this form, the key components for the pulsating detonation analogous to the mass, spring and damper elements in a mechanical oscillator can be identified. From the point of view of the oscillator concept, the effect of chemical kinetics on the self-sustained pulsating detonation and the origin of different unstable temporal patterns can be discussed. The rate of heat release, which is governed by chemical kinetics, essentially affects the key components for the mechanism of the self-sustained oscillation, i.e. the self-exciting driving force represented by damping term

$\left(\frac{d\Phi^0(\dot{F})}{d\dot{F}} + \frac{d\Phi^1(\dot{F})}{d\dot{F}}\ddot{F} - \Psi^1\left(\dot{F}\right)\right)\ddot{F}$ and the restoring force $\left(\rho_{cj}e_{cj}\dot{F} - \Psi^0\left(\dot{F}\right)\right)$. An alternating damping controlled by these two terms is responsible for maintaining the oscillation as observed from the numerical results. Similar to the classical nonlinear dynamical system, the nonlinearity of the restoring force to the driving force embedded in the term $\Psi^0\left(\dot{F}\right)$ should provide the ingredient for the transition of the instability patterns.

Chemical kinetics also influences the amount of resonant excitation of oscillation as a result of the coupling between the self-excited driving force by the unsteady part of the chemical energy release and the front fluctuation, causing higher degree of the instability pattern. Resonant oscillation can be achieved when the fluctuations of the heat release rate and pressure are positively correlated (Rayleigh's criterion). In other word, it requires $\Psi(t)$ to be fully in phase with $\dot{F}$ so the product $\Psi(t) \cdot \dot{F} > 0$ holds over the entire oscillatory cycle. The product $\Psi(t) \cdot \dot{F}$ is essentially similar to the power input to the system and the integral of this product over a cycle describes the self-excited energy required for the oscillating motion of the shock front. From this argument, a generalized resonance-coupling criterion has been proposed by Zhang *et al.* (1998):

$$J^* = \frac{1}{\tau}\int_0^\tau \frac{\Psi(t)\,\dot{F}}{D_{cj}}dt > 0$$

where J^* has units of power and τJ^* gives the net excess (over the steady ZND value) of the excited energy. From the energy point of view, it is clear that more chemical energy release must be excited to the shock front in order to maintain higher instability mode of the detonation front. As shown in figure 3.16, the value of J^* remains zero below the neutral stability boundary limit (i.e. $E_a < 25.26$). As the value of activation energy increases away from the stability limit, the value of J^* also increases. The continuous increase of J^*due to different degrees of resonant coupling between the shock front fluctuation and heat release rate controlled by chemical

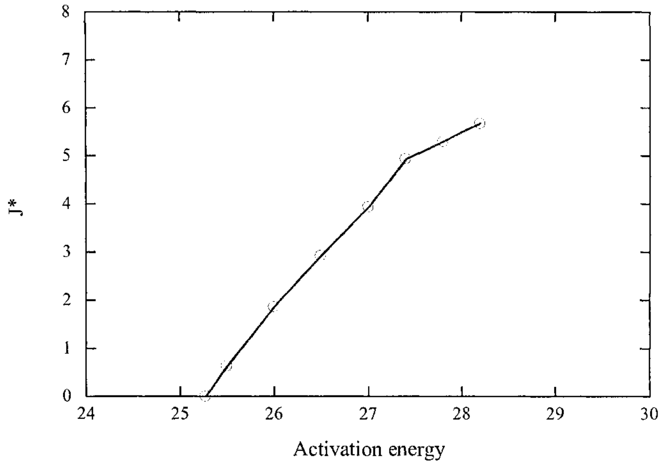

Figure 3.16. Integral value of the product of the unsteady chemical energy release and shock velocity fluctuation over a period τ for different values of activation energy.

kinetics results in the variety of instability patterns ranging from regular harmonic to irregular chaotic motion of the pulsating front.

In summary, the present results have fully established the remarkable resemblance of the pulsating detonation with classical oscillators. It is desirable to adopt other methodologies developed in nonlinear dynamics that are not considered here to shed lights on the dynamics of the pulsating detonation. The possible use of a nonlinear oscillator model to interpret the present numerical simulations can be emphasized as a new approach to study the detonation structure and different factors that influence its unstable behavior. From the framework of a nonlinear oscillator, the mechanism responsible for developing different irregular oscillatory pattern appears to be related to the resonant excitation of the heat release resulted from the change of chemical kinetics and the substantial effect of nonlinearity can in turn lead to the transition route of the instability to chaos as observed in classical dynamical systems.

Chapter 4

The effect of chain-branching kinetics

4.1 Introduction

In Chapter 3, the characteristics of the pulsating detonation structure such as its nonlinear dynamics and instability spectrum under the influence of chemical kinetics are described for a one-step kinetic model. However, a single Arrhenius reaction model cannot reproduce some important features of real detonations governed by chain-branching kinetics as pointed out in Chapter 1. In order to progress further in clarifying the role of chemical kinetics on the unsteady detonation structure, the dynamics of one-dimensional pulsating detonations with chain-branching kinetics will be investigated numerically in this chapter.

Although a complex set of chemical kinetic rate equations derived from elementary reactions could in principle be solved simultaneously with the reactive Euler equations within currently computational capabilities, direct interpretation of the large amount of detailed information generated by such numerical simulations becomes a difficult problem. Therefore, it may suffice to first use a simplified multi-step chemical kinetic model to mimic the chain-branching reactions instead and compare the previous results obtained using a one-step Arrhenius model.

The nonlinear dynamics of one-dimensional pulsating detonations have been recently studied, both asymptotically and numerically, using a two-step reaction model by Short (2001) and Short & Sharpe (2003). The two-step chemical kinetic description is a widely used model, which has been developed to retain the essential features described for chain-branching chemistry. The model consists of a temperature-sensitive induction stage, at the end of which the fuel is converted instantaneously into free radicals, followed by a main heat release (or chain-termination) stage. Similar two-step kinetic models are used for numerical simulations of unstable detonations in hydrogen-oxygen or liquid nitromethane (Taki & Fujiwara 1978; Guirguis *et al.* 1986; etc.). Different kinetic parameters in the two-step model can be determined by fitting data from constant volume explosion calculations computed using detailed chemical kinetic mechanisms and generally very good agreement can be obtained, especially for H_2-O_2-diluent mixtures (Clifford *et al.* 1998; Sichel *et al.* 2002; Sharpe & Short 2003). A main advantage of this two-step chain-branching kinetic model over the standard one-step Arrhenius kinetics is that the temperature-dependent induction and the main exothermic reaction zone are decoupled into two separate stages. Hence, it permits independent variation of the two important characteristic lengths of induction and main heat release layer.

Using the two-step model, Short & Sharpe (2003) found that the pulsating structure can be influenced by independently changing the main heat release reaction rate or equivalently, the length of the main heat release layer. The ZND detonation is stable when its structure is dominated by the chain-termination heat release zone. As the ratio of the induction length to the length of main heat release zone increases, the detonation becomes unstable and different oscillatory behavior can be observed. This has also been pointed out in the early studies by Short & Quirk (1997) and Ng & Lee (2003) using a more detailed version of three-step model where the chain-branching cross-over temperature T_B (the temperature at which the chain-termination reaction rate becomes of the same order as the chain-branching rate) is used as a bifurcation parameter to control the ratio of the chain-branching induction length to the length of the recombination zone. Short & Sharpe further suggests that a bifurcation boundary between stable and unstable ZND detonations may be found when the ratio of the length of the heat release layer to that of the induction zone layer is of the order $O(\varepsilon_I)$, where ε_I is the activation energy in the induction zone. If the ratio $\Delta_R/\Delta_I \lesssim O(\varepsilon_I)$, the ZND detonation is unstable.

The present study is an extension of the work by Short & Sharpe (2003). The purpose is to carry out a series of numerical computations and examine the long-term nonlinear dynamics of one-dimension pulsating detonation with a generic two-step reaction model and compare to the predictions from one-step model. Simulations are performed for a wide range of initial conditions and reaction parameters of the model. The aim of the parametric study is to identify numerically the neutral stability curve for one-dimensional detonations with chain-branched kinetics and introduce a well-defined quantitative parameter, which can be used to characterize the one-dimensional detonation stability. Two dimensional simulations are also performed to elucidate any relevance between the 1-D instability results with the unstable cellular detonation.

4.2 Two-step chain-branching kinetic model

As in Short & Sharpe (2003), a two-step reaction scheme is used in this study to mimic the essential dynamics of a chain-branching reaction. This model is coupled with the Euler equations (i.e., equations 2.32 - 2.35) to describe the detonation structure. The first step represents a thermally neutral induction zone or ignition process (thus the heat release of this step $Q_1 = 0$), with a temperature-sensitive Arrhenius form of the reaction rate given by:

$$\Omega_1 = H\left(1-\xi\right) \cdot K_I \exp\left[E_I\left(\frac{1}{T_s} - \frac{1}{T}\right)\right] \tag{4.1}$$

where $\beta_1 = \xi$ is the reaction progress variable in the induction period and $H(1-\xi)$ is a step function, i.e.:

$$H(1-\xi)\begin{cases} = 1 & \text{if} \quad \xi < 1 \\ = 0 & \text{if} \quad \xi \geq 1 \end{cases} \tag{4.2}$$

Here, the reference length scale x_{ref} is chosen such that the one-dimensional ZND induction length is unity, i.e. $K_I = -u'_{vn}$ where u'_{vn} is the particle velocity behind the shock front in the shock-fixed frame for the CJ detonation. The reference time scale is therefore set to the reference length scale divided by the initial sound speed of the reactant (i.e. $t_{ref} = x_{ref}/c_o$). At the end of induction period (i.e., $x = 1$), the second step begins to describe the rapid energy release after the branched-chain thermal explosion and the slow heat release in the radical recombination stage. The reaction rate equation for this step is given by:

$$\Omega_2 = -\left(1 - H(1-\xi)\right) \cdot \beta_2 K_R \exp\left(-E_R/T\right) \tag{4.3}$$

where β_2 and K_R denote the chain-recombination reaction progress variable and rate constant for the heat release process. Similar to previous studies, the reaction rate constant K_R is used as a parameter to control the ratio of the reaction time to the induction time. The present model differs slightly from that of Short & Sharpe (2003) only in the rate of the second step, which is chosen in Arrhenius form for generality. The local chemical energy that has been released at any instant during the reaction is equal to $q = \beta_2 Q$, where $Q = Q_2$ is the total chemical energy available in the mixture and released in the second reaction step. The Mach number of the Chapman-Jouguet detonation (CJ) corresponds to a chosen value of Q can be determined by:

$$M_{cj} = \frac{D}{c_o} = \left[\left(1 + \frac{\gamma^2 - 1}{\gamma} Q\right) + \sqrt{\left[\left(1 + \frac{\gamma^2 - 1}{\gamma} Q\right)^2 - 1 \right]} \right]^{1/2} \tag{4.4}$$

Consistent with previous non-dimensionalization, the energy release Q and activation energies $E_{I,R}$ have been scaled with RT_o. For ease of comparison in the following discussion, this study also introduces alternative scaling for the activation energies:

$$\varepsilon_I = \frac{E_I}{\delta}, \quad \varepsilon_R = \frac{E_R}{\delta} \quad \text{with} \quad \delta = \frac{\left[2\gamma M_{cj}^2 - (\gamma - 1)\right] \left[2 + (\gamma - 1) M_{cj}^2\right]}{(\gamma + 1)^2 M_{cj}^2} \tag{4.5}$$

where δ is the temperature jump across the leading shock. Therefore, ε is simply the reduced activation energy normalized by the temperature behind the leading shock of the CJ detonation. For typical hydrocarbon mixtures, the reduced activation energy of the induction stage ε_I is large because in the induction zone, energy is required to break the strong chemical bonds of the fuel and convert it into radicals. Typical values for ε_I usually ranges from 4 (for H_2-O_2 mixture) to 12 (for heavy hydrocarbon mixtures). In contrast, the second step involves only reactions between energetic free radicals. For typical chain-branching reactions, therefore, the induction stage generally has a larger activation energy compared to the second step. Hence, for the present study:

$$E_I >> E_R \quad or \quad \varepsilon_I >> \varepsilon_R \tag{4.6}$$

Typical steady ZND profiles are given in figure 4.1. From these profiles, it is shown that the two important length scales for detonation chemistry, namely the induction and heat release zone length, can be clearly recognized using the present two-step kinetic model. In principle, it is possible to derive a number of different steady profiles by varying different kinetic parameters available in this model. It also permits the independent variation of the two chemical length scales. As mentioned above, the reaction rate constant K_R is used as a bifurcation parameter. In figure

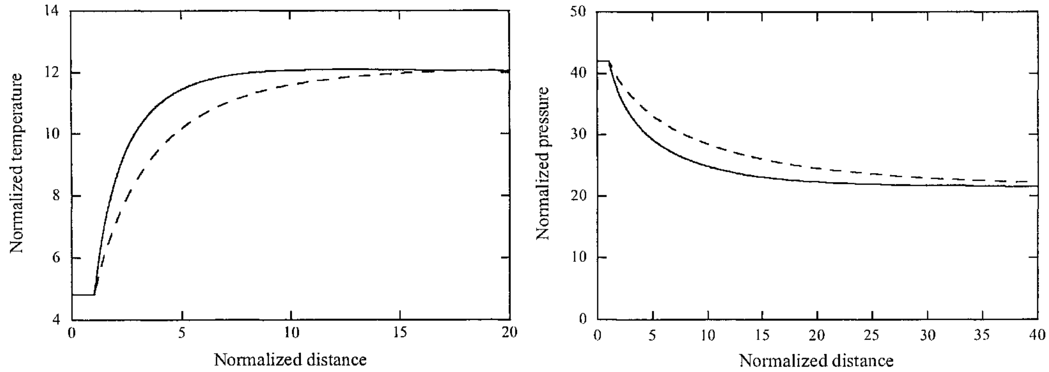

Figure 4.1. Steady ZND detonation profiles computed using the two-step chain-branching kinetic model for a mixture with $Q = 50$, $\gamma = 1.2$, $\varepsilon_I = 8$, $\varepsilon_R = 1$ and two reaction rate constants $K_R = 0.779$ (dashed lines); and $K_R = 1.558$ (solid lines).

4.1, it is shown again that increasing the reaction rate constant K_R should have an effect of shortening the heat release zone length of the detonation structure.

4.2.1 Stability parameter

One of the motivations for this study is to identify the quantitative parameter that controls the detonation stability driven by chain-branching kinetics as analogous to the activation energy as a stability parameter for the case of one-step Arrhenius kinetics. From the earlier work (Short 2001; Short & Sharpe 2003), it was found that the bifurcation boundary between stable and unstable detonations occurs when the ratio of the length of the heat release layer to that of the induction zone layer is $O(\varepsilon_I)$. However, an appropriate and useful definition of a quantitative parameter has not yet been justified. Based on these previous analyses, the following stability parameter to characterize the detonation stability is mathematically proposed:

$$\chi \equiv \varepsilon_I \frac{\Delta_I}{\Delta_R} = \varepsilon_I \Delta_I \frac{\dot{\sigma}_{\max}}{u'_{cj}} \tag{4.7}$$

where Δ_I and Δ_R denote the characteristic induction length and reaction length, respectively. ε_I is activation energy governing the sensitivity of the induction period as defined previously. It should be pointed out that a similar stability parameter can indeed be formulated from Short's stability analysis of the amplitude of oscillations in self-supported ZND detonations (Short 2001). Generally, the induction length is simply defined as the length of the thermally neutral period. However, there is no standard definition for reaction length. In this study, it is suggested that the characteristic reaction length can be defined using the thermicity parameter. For the present two-step chemical model of ideal gases with constant specific heat ratio, the thermicity is expressed as (Fickett & Davis 1979):

$$\dot{\sigma} = (\gamma - 1)\frac{Q}{c^2}\frac{d\beta_2}{dt} \tag{4.8}$$

The thermicity $\dot{\sigma}$ basically denotes the normalized chemical energy release rate and has a dimension of 1/time. Hence, the inverse of maximum thermicity $\dot{\sigma}_{\max}$ can be taken as a characteristic time scale for the heat release, which may provide an appropriate choice to define a characteristic reaction time. Using this characteristic reaction time, the reaction length can be estimated by:

$$\Delta_R = \frac{u'_{cj}}{\dot{\sigma}_{\max}} \tag{4.9}$$

where u'_{cj} is simply the particle velocity at the CJ plane in shock-fixed coordinates. Note that the above definition of different chemical kinetic parameters should be general enough such that it can be determined easily from any detailed chemical kinetic model.

4.3 One-dimensional detonation instability

To investigate the instability of the one-dimensional unsteady detonation, the one-dimensional reactive Euler equations with the present two-step chemical kinetic model are solved numerically using the second-order centered scheme described in Chapter 2. For all the one-dimensional simulations, an effective numerical resolution of 128 points per induction zone length of the steady ZND detonation is used to ensure the detailed features of the pulsating front are properly resolved. The computations are initialized by the steady solution of the ZND detonation.

4.3.1 Development of pulsating instability

The development of instability is first investigated near the stability boundary. For each set of chemical parameters (i.e. the heat release Q, specific heat ratio γ and activation energies ε_I and ε_R), simulations are performed to identify the stability limit below which the detonation propagation is stable by varying the value of the reaction rate constant K_R. Leading shock pressure history is recorded and used to determine stable or unstable detonations based on its decay or growth at the long time-evolution. For example, the pressure histories of the detonation front for $Q = 50$, $\gamma = 1.2$, $\varepsilon_I = 8$ and $\varepsilon_R = 1$ with different reaction rate constants K_R are displayed in figure 4.2. For $K_R = 0.887$ and $K_R = 0.967$, the initial perturbation due to the numerical startup errors damps with time and the propagating detonation eventually reaches a stable configuration after the long-term evolution. However, for case with $K_R = 1.021$, results show a slow amplification of a weakly pulsating instability, exhibiting a single mode low-frequency oscillation. Results indicate that the stability limit is found to be approximately around $K_R \approx 0.975$. As K_R is increased further, the instability grows quickly from the initial perturbation and the propagating detonation becomes unstable. These results agree well with the earlier work by Short & Sharpe (2003), showing that the increase in K_R resulting in a reduction in reaction length relative to the induction length can cause instability in the detonation propagation. To illustrate the grid convergence, table 4.1 shows the numerically determined value of the stability boundary for various numerical resolutions. The resolution study indicates that a resolution of 128 grids per induction length of the steady ZND detonation provides sufficient refinement to obtain a converged value of the stability boundary.

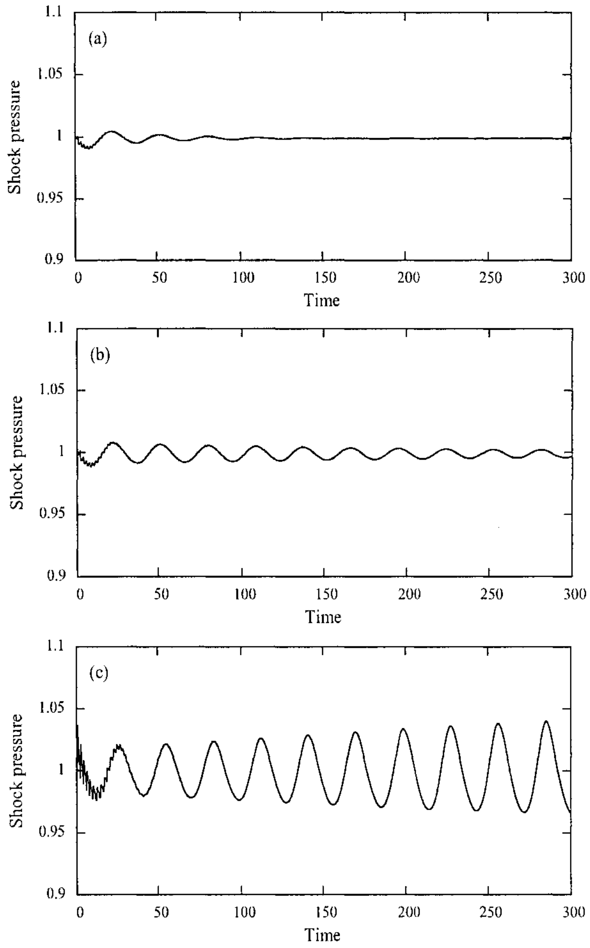

Figure 4.2. Leading shock pressure history for reaction rate constants close to the stability limit: (a) $K_R = 0.887$; (b) $K_R = 0.967$; and (c) $K_R = 1.021$.

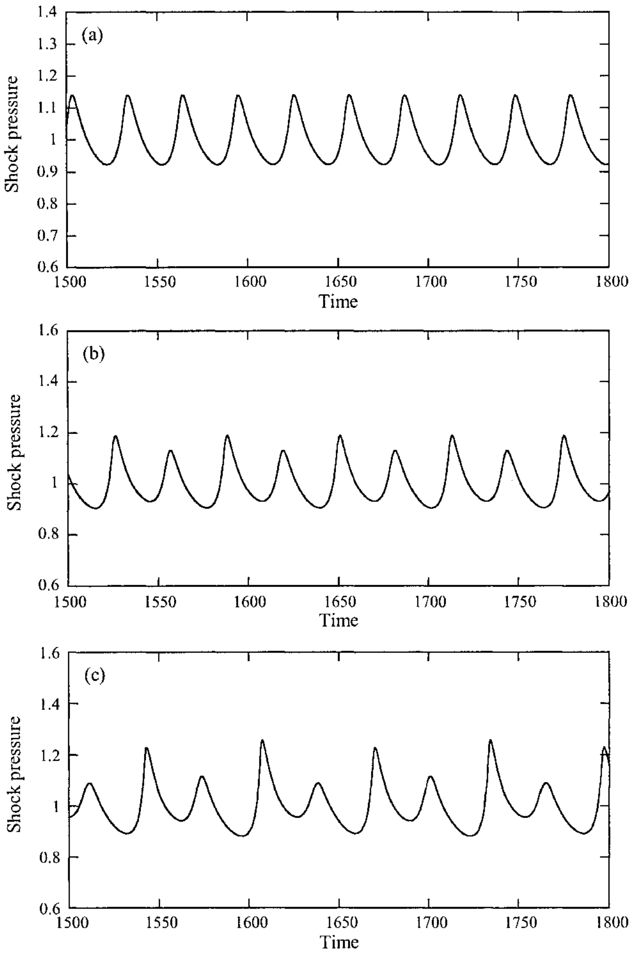

Figure 4.3. Leading shock pressure history exhibiting a period-doubling bifurcation for unstable detonations: (a) $K_R = 1.126$; (b) $K_R = 1.157$; and (c) $K_R = 1.189$

If the value of K_R increases from the neutral stability boundary, the propagating detonation undergoes a period-doubling bifurcation to a higher mode oscillation (figure 4.3). Similar to those results obtained using a single-step Arrhenius rate law in Chapter 3, development of the higher instability mode is done via a series of bifurcation processes and this period-doubling cascade eventually leads to chaos. A

Resolution	K_R
8	1.001
16	0.990
32	0.978
64	0.974
128	0.974
256	0.974

Table 4.1. Numerically determined stability boundary for different resolutions

bifurcation diagram can also be constructed here with chain-branching kinetics to illustrate the sequences of transitions, as given in figure 4.4. The bifurcation diagram is again generated by measuring the peak pressure amplitude of the oscillations for each value of reaction constant K_R. In this way, a bifurcation diagram would display the magnitude of one mode of oscillation as a single point as explained previously in Chapter 3. Following the same analyses, the ratio between the spacing of successive bifurcations, i.e., the Feigenbaum number:

$$\delta = \frac{\mu_i - \mu_{i-1}}{\mu_{i+1} - \mu_i} \tag{4.10}$$

is computed. To do so, the values of reaction rate constant K_R at which the bifurcation occurs are determined directly from the bifurcation diagram. These values of K_R as well as the computed Feigenbaum numbers are displayed in table 4.2. It is interested to note that the Feigenbaum numbers for the present bifurcation diagram also appear to be close to the universal value of 4.669, derived by Feigenbaum for a simple nonlinear model with fewer degrees of freedom. In summary, the bifurcation diagram indicates that the instability transition process of the pulsating detonation front driven by chain-branching kinetics also follows closely the generic pattern of Feigenbaum's period-doubling scenario (Feigenbaum 1983). The present result also agrees with that of Chapter 3 in which activation energy of single-step Arrhenius rate law was varied and a similar value of the Feigenbaum number was measured. Hence,

i	Reaction constant K_R	Oscillation mode	Feigenbaum number
0	0.975	1	–
1	1.144	2	–
2	1.183	4	4.33
3	1.191	8	4.88

Table 4.2. Values of bifurcation limits and Feigenbaum numbers obtained using the two-step chain-branching kinetic model.

the transition pattern for unstable pulsating detonations appears to be independent of the chemical kinetics used in the model. These universality properties may perhaps reinforce the fact that some simple model belonging to the Feigenbaum's system and other nonlinear dynamics concepts can be employed as a way to investigate the dynamics of one-dimensional pulsating detonations.

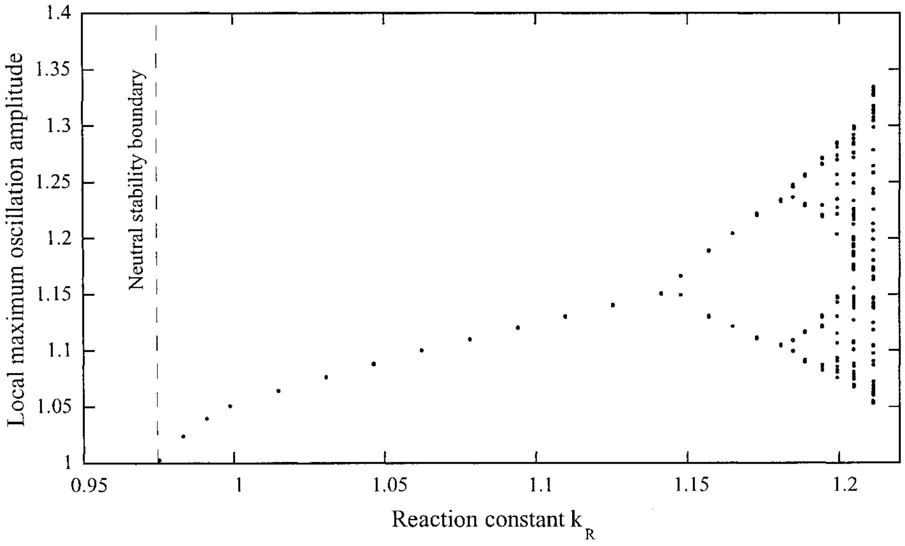

Figure 4.4. Bifurcation diagram for the two-step chian-branching kinetic model with varying K_R.

4.3.2 Neutral stability boundaries

More numerical computations are carried out in order to obtain a general neutral stability curve for various combustible mixture parameters. In the present study, calculations are performed for three specific heat ratios, $\gamma = 1.2$, 1.3 and 1.4. For each γ, the value of chemical heat release Q is varied to give a range of Mach numbers M_{cj} between 3.5 and 7.8. This study also considers a combination of parameters with three possible activation energies $\varepsilon_I = 4$, 6, 8 and two possible activation energies $\varepsilon_R = 0.5$, 1. The variation of these different parameters should be able to mimic the characteristics of any realistic chemical systems and can be easily obtained for various combustible mixtures. For each set of mixture parameters $(\gamma, Q, \varepsilon_I, \varepsilon_R)$, computations were performed in which the value of the reaction rate constant K_R was systematically varied to determine its critical value at which the detonation becomes unstable, as described in Chapter 3. The stability parameter χ associated with this critical reaction rate constant K_R is then computed, which corresponds to the value at the stability boundary.

Figure 4.5 summarizes all the computational results by constructing a plot in the χ - M_{cj} plane for different mixture parameters considered in this study as shown in the figure legend. Only the critical value of stability parameter χ, at which the detonation becomes unstable, is shown for a given set of parameters $(\gamma, Q, \varepsilon_I, \varepsilon_R)$. It is interesting to note that all the data points corresponding to different mixture conditions can be essentially collapsed to a single curve. Although there are still some differences among these data points, this can be readily explained by the fact that the value of the exothermic reaction zone length Δ_R, which is necessary to determine the stability parameter χ, is evaluated using a rather simple mathematical approximation as given by equation 4.9. Secondly, the difference in the data points can also be attributed to the incremental size of K_R used in the present computational study and the way it determines the stability boundary. Nevertheless, those discrepancies

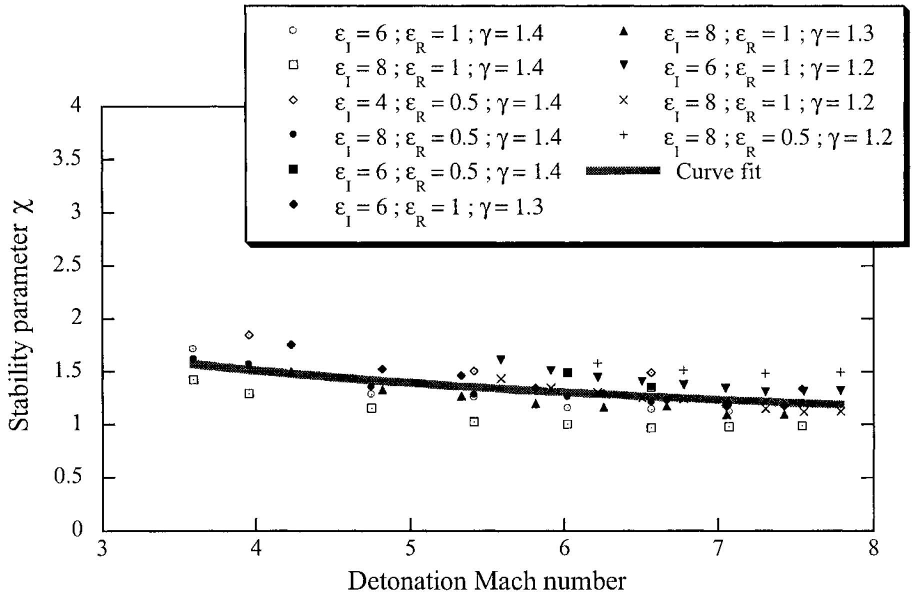

Figure 4.5. Neutral stability curve in χ - M_{cj} plane.

are not significant and this may suggest a universal curve to define the stability boundary for one-dimensional detonations.

4.4 Two-dimensional cellular structure of detonations

So far, the influence of the branched-chain chemistry on the one-dimensional, time-dependent dynamics of unsteady, planar detonations has been discussed. It would be of interest to examine the extent to which the results can be compared with multi-dimensional cellular detonations. Traditionally, the regularity of the cellular structure on soot foils has been used to classify the structure of detonation wave. Previous studies have suggested that the regularity of cell spacing and ZND detonation

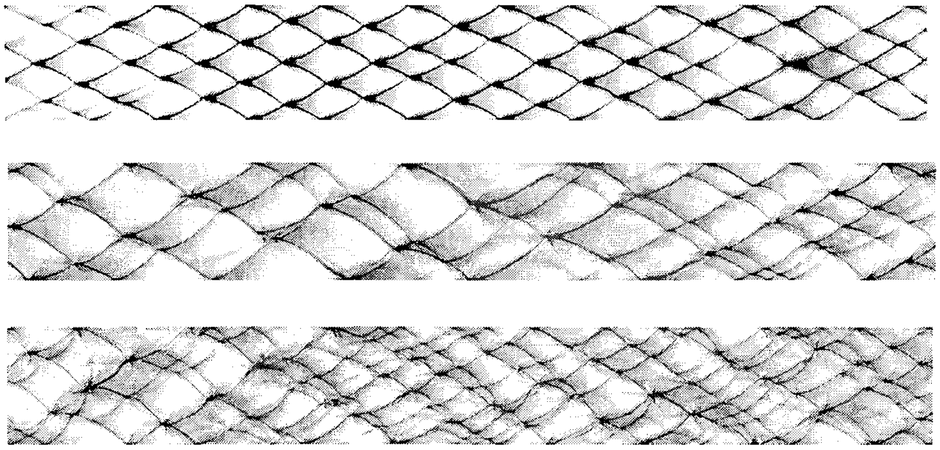

Figure 4.6. Numerical foils obtained from the simulations using the two-step chain-branching kinetic model for $K_R = 0.866$ (top); $K_R = 3.46$ (middle); and $K_R = 12.9$ (bottom).

stability appear to be intimately inter-related (Gamezo *et al.* 1999). Highly unstable systems are characterized by relatively strong and irregular transverse waves. Stable systems are characterized by relatively weak and regular transverse waves. This section thus concerns in the cellular structure of detonation wave driven by the two-step chain-branching model and looks at its relationship with the degree of instability of the one-dimensional pulsating structure.

To simulate the propagation of two-dimensional cellular detonation waves, solutions of the two-dimensional Euler equations coupled with the two-step kinetic model are approximated using again the high-resolution SLIC scheme described in Chapter 2. Similar to the one-dimensional case, this study first looks at the effect of the ratio of the reaction time to the induction time by using the reaction rate constant K_R as a bifurcation parameter. Other values of the initial conditions for the numerical experiments are given by $Q = 23.98$; $\varepsilon_I = 4$; $\varepsilon_R = 1$ and $\gamma = 1.333$, which approximately models the conditions for a H_2-O_2 mixture.

To examine the regularity of the cellular structure, figures 4.6 gives some numerical foils showing the time-integrated maximum pressure contour for three different values K_R. For low value of K_R, a fairly regular cell pattern is observed. By increasing the value of K_R, thus increasing the rate of heat release in the exothermic reaction layer, there is some evidence of bifurcation in the soot traces and the regularity of the cellular pattern becomes poor. For very large value of K_R, the cell behavior becomes highly irregular. Such irregularity can be explained by the presence of more than one dominant frequency of the transverse fluctuation as well as the excitation of higher harmonics, which manifest themselves as finer cell patterns superimposed on the dominant bands. From these numerical simulations, results thus show a transition structure for unstable cellular detonations, between regular regime to highly irregular pattern by increasing systematically the reaction rate constant K_R. These results are in good agreement with the one-dimensional pulsating detonation structure.

Recalled from the previous section on the one-dimensional pulsating detonation driven by the same two-step chain-branching kinetic model, that the effect of increasing K_R is to render the wave to become unstable. Here, similar observations are made for the two-dimensional case where the degree of cell regularity is also influenced by the increase of K_R. Hence, the dependence of the regularity of the cellular pattern thus follows with the stability analysis.

For the three cases studied above, one can evaluate the stability parameter χ associated with each reaction rate constant K_R. These 2-D results can then be mapped onto the χ - M_{cj} plane. By doing so, one can explain these different cases by identifying their associated location of parameter χ relative to the neutral stability curve, as shown in figure 4.7. From this figure, it is understood that below the neutral stability curve, the cellular structure should be very regular. On the other side far away from this stability boundary limit, the cellular pattern can be described as

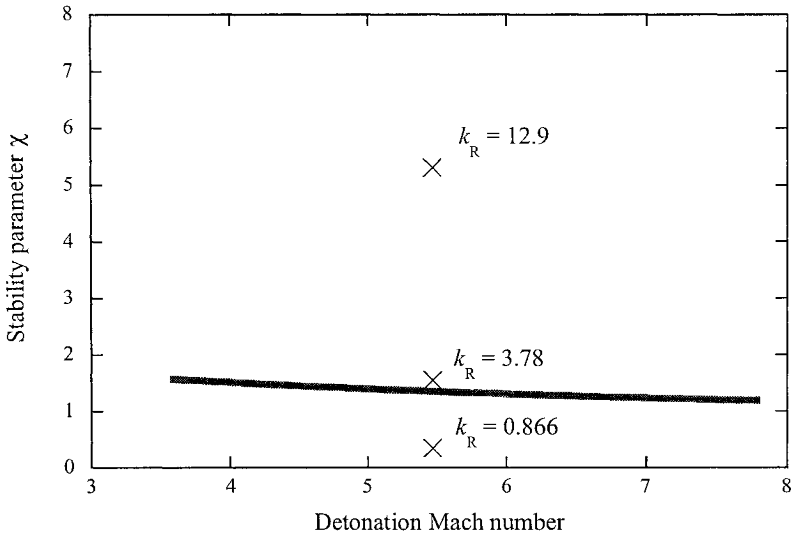

Figure 4.7. Characterization of the two-dimensional cellular structures shown in figure 4.6 using the χ - M_{cj} plane.

highly irregular or chaotic. It is of interest to note that not only the parameter χ can be related to the degree of instability of 1-D pulsating detonation structure, but it can also be considered as a fundamental parameter taking into account the essential chemical kinetic parameters to assess the degree of regularity of the cellular detonation waves.

4.5 Discussion on the stability parameter

Previous studies by other researchers (Short 2001; Short & Sharpe 2003) as well as the present analysis all support that χ is the relevant parameter governing stability. It may be worthwhile to point out that the derivation and physical meaning of this parameter were equivalently discussed by Soloukhin in a comment to Meyer and Oppenheim's work on the shock-induced ignition problem. In discussion of the experiments, Soloukhin and Oppenheim both noted that ignition behind a shock could either occur uniformly (the strong regime) or originate from several exothermic spots (the mild regime) (Voyevodsky & Soloukhin 1965; Meyer & Oppenheim 1971a; Vermeer *et al.* 1972). For the case of detonations, the mild regime can analogously correspond to unstable detonations where instability is caused by pockets of partly burned gas (He & Lee 1995; Sharpe & Falle 1999; etc.), while the strong regime is similar to stable detonations, where chemical reaction is insensitive to perturbations and all the fuel burns uniformly as in the ZND model. Hence the stability in the reaction zone of gaseous detonations may be comparably linked to the regime of ignition behind shock waves, as already noted by Takai *et al.* (1974).

One can indeed follow Oppenheim's work to formulate the requirement of stability in the reaction structure of a detonation (Radulescu 2003; Ng *et al.* 2005). It demands that neighboring particles, shocked initially at slightly different shock strengths, would release their chemical energy with similar delays, so that the power pulses can overlap, or be 'coherent' in time and space as to give rise to a single global gasdynamic effect free of instabilities (Meyer & Oppenheim 1971b; Oppenheim 1985; Lutz *et al.* 1988). First, to meet this requirement, the sensitivity of the chemical induction length (or equivalently time) to changes in shock temperature needs to be small. Otherwise, particles of gas being shocked at different temperatures due to perturbations in the flow will take significantly different times to burn and thus, can possibly lead to the formation of pockets of partly burnt fuel whose burnout at later time will eventually cause instability in the reaction zone (Sharpe & Falle 1999). For gaseous detonation waves, the induction length can be assumed to have the common Arrhenius from:

$$\Delta_I \propto \exp\left(\frac{E_I}{T_s}\right) \tag{4.11}$$

where T_s is the initial shocked gas temperature and E_I the global activation energy describing the sensitivity of the thermally neutral chemical induction process. The stability thus requires that

$$\left|\left(\frac{T_s}{\Delta_I}\right)\left(\frac{\partial \Delta_I}{\partial T_s}\right)\right| = \frac{E_I}{T_s} \equiv \varepsilon_I \tag{4.12}$$

be small, i.e., small activation energy ε_I. However, in addition to the effect of sensitivity in the induction process, the characteristic length scale for energy deposition Δ_R should also play an important role. Note that a relatively long period for energy release (broad power pulses) will still lead to quasi-simultaneous energy deposition and coherence in time and space even if the changes of induction length (or time) are important. Thus, similar to Soloukhin's comment on Meyer and Oppenheim's work (Meyer & Oppenheim 1971a), stability can be more properly described by the sensitivity to temperature fluctuations of the characteristic induction length relative to the characteristic exothermic reaction length. This concept can be illustrated schematically as shown in figure 4.8. Mathematically, one can then define based on this physical concept a stability parameter of the form as shown equivalently in the previous section, i.e.,

$$\chi \equiv \left|\left(\frac{T_s}{\Delta_R}\right)\left(\frac{\partial \Delta_I}{\partial T_s}\right)\right| = \varepsilon_I \frac{\Delta_I}{\Delta_R} = \varepsilon_I \Delta_I \frac{\dot{\sigma}_{\max}}{u'_{cj}} \tag{4.13}$$

where the length scale for the exothermic power pulse Δ_R is simply the inverse of the maximum value of thermicity $\dot{\sigma}_{\max}$ multiplied by the CJ particle velocity u'_{cj}, as defined previously. This non-dimensional parameter includes the essential terms that influence the characteristics of power pulses or energy release. For small values of χ, it is expected that power pulses originating from neighboring particles will overlap, thus leading to a coherent phenomenon in time and space (see figure 4.8a - 4.8c). In that case, small disturbance in the flow will not cause significant fluctuation of the energy release in the reaction zone structure, giving a stable or weakly unstable system. On the other hand, if this parameter is large, as can occur with conditions given in figure 4.8d, the power pulses will not be coherent and this can lead to various gasdynamic fluctuations in the reaction zone structure. This stability parameter therefore describes the scenario in which the incoherence in the energy release of the gas leads to gasdynamic instabilities in the reaction zone.

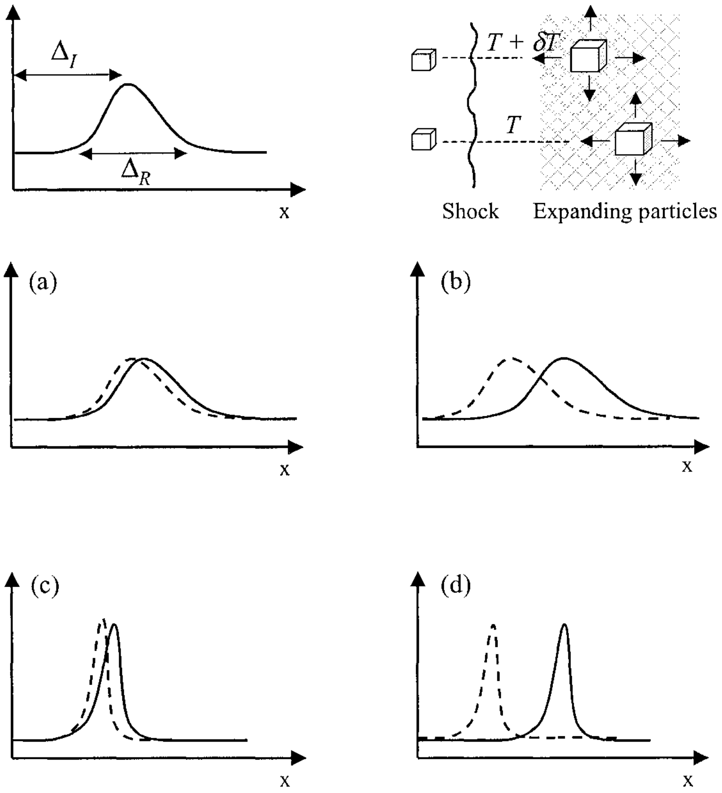

Figure 4.8. An illustration of the coherence concept between neighboring power pulses, given by the exothermicity profiles for two neigboring gas elements shocked at temperatures differing by δT. (a) small temperature senstivity, long exothermic reaction length; (b) large temperature sensitivity, long exothermic reaction length; (c) small temperature senstivity, short exothermic reaction length; and (d) large temperature senstivity, short exothermic reaction length. Only case (d) results in incoherence of power pulses and the development of instability. (Radulescu 2003; Ng *et al.* 2005).

4.6 Summary

The present investigation has performed a series of numerical computations of one-dimensional Chapman-Jouguet detonations driven by a two-step chain-branching kinetic mechanism. Use of this mechanism is intended to yield a better understanding of the stability and propagation of real detonations and to resolve the difficulties of using a one-step Arrhenius model for the chemical kinetic description. In this study, the results concur with previous studies of a similar kind that the shape of the reaction zone profile has a significant influence on the dynamic detonation structure. Detonations become unstable when the induction zone length dominates over the main reaction layer, which occurs when increasing the reaction rate constant K_R. Following the analysis of Chapter 3, the nonlinear dynamics for higher modes of instability is analyzed via the construction of a bifurcation diagram. It is shown that the route to higher instability follows also the Feigenbaum's bifurcation scenario.

Unlike prior detonation studies based on one-step Arrhenius kinetics where a global activation energy E_a is the sole parameter governing stability, the present study suggests a more general non-dimensional parameter, χ. It is defined as the degree of temperature sensitivity in the induction zone ε_I multiplied by the ratio of induction length Δ_I to the reaction length Δ_R, which is approximated by the inverse of the maximum thermicity $(1/\dot{\sigma}_{\max})$ multiplied by the CJ particle velocity u'_{cj}. The physical meaning of this parameter is pointed out to be equivalent to Meyer and Oppenheim's coherence concept. It states that stability can be achieved if the power pulses originating from neighboring particles will overlap or the reaction has a relatively long period for energy release, leading to a coherent phenomenon in time and space. On the other hand the incoherence in the power pulse or energy release, which is expected for large value of χ, leads to gasdynamic instabilities in the reaction zone. From the two-dimensional simulation, it appears that this parameter also provides some success in characterizing the regularity of cellular detonations.

Chapter 5

Numerical simulations with realistic chemical kinetics

5.1 Introduction

In this chapter, an investigation on the dynamic detonation structure using realistic chemistry of some common combustible mixtures is carried out. The focus is to generalize the previous results derived from the 2-step chain-branching kinetic model to a more complex chemistry system. With realistic detailed chemistry models, it is possible to compare numerical simulations with experimental observations. This chapter in particular will look at a specific phenomenon which has not been thoroughly explained, i.e. how argon dilution influences the structure of detonation waves.

It has been well illustrated by many studies that a variety of cellular detonation structures can be observed for different chemical compositions (Voitsekhovskii *et al.* 1966; Strehlow 1969; Libouton *et al.* 1975; etc.). Experimental observations indicate that combustible mixtures with large amount of argon dilution tend to produce remarkably regular cellular structure with only weak transverse waves. Earlier studies (e.g. Gamezo *et al.* 1999) and also the present investigation in Chapter 4 indicate that the cell regularity and the strength of the transverse waves are reflections of the degree of stability of the detonation structure, which is governed by the chemical reaction kinetics within the detonation front. For stable detonations, the transverse waves are weak and the cellular pattern is regular, whereas far from the stability limit, the transverse waves are strong and the detonation wave has a highly irregular cellular structure. Hence, a large amount of argon dilution tends to have equivalently a stabilizing effect on the detonation wave structure. However, the precise thermo-chemical role of argon dilutions in the detonation wave stability has not been demonstrated.

Previous investigations of the stability of ZND detonations were mostly performed for highly idealized chemistry models. For this reason, these studies only yielded qualitative information and did not permit any quantitative comparison with experiments. This study thus attempts to elucidate via numerical simulations the effect of argon dilution on the stability of detonations in a single representative mixture with realistic chemistry model, namely acetylene/oxygen mixtures. Since the regularity of cellular detonation structure and the 1-D detonation instability are inter-related, the stabilizing effect by heavy argon dilution is focused here by examining in details the changes in the structure of 1-D detonations, where the instability manifests itself in the form of nonlinear longitudinal pulsations as described in previous chapters. The one-dimensional treatment indeed permits highly resolved numerical simulations to be performed, which are necessary for describing the complex non-linear detonation phenomena and are difficult to achieve in multi-dimensional simulations.

To assess the role of argon dilution on the reaction zone structure, the corresponding steady-state ZND structure with detailed chemistry is examined closely. This chapter explains how the stability concept for detonation structure derived in

Chapter 4 based on the two-step chain-branching kinetic model can be extended to characterize the dynamics of detonation waves with any arbitrary realistic chemical reaction network. Results will elucidate how the detonation wave stability is linked with the experimental observation of the various degree of detonation cell regularity.

5.2 Reduced reaction mechanism for C_2H_2-O_2 detonations

It is obvious that the most comprehensive choice for a chemistry model that can produce accurate simulation of detonations with potentially excellent quantitative agreement with experimental results is the use of detailed chemical kinetic reaction mechanisms. To date, detailed reaction mechanisms for a large class of hydrocarbon combustion, especially for flames, have been developed and well validated with data from shock-tube experiments. In this case, the combustion process is described by an extensive list of elementary reactions among different chemical species with rate expressions given for each reaction. However, numerical studies employing detailed chemistry are computational expensive and often impractical because of its complexity of the elementary chemical kinetics. Beside the number of reaction steps involved, many of these reactions represent very rapid relaxation processes so that the differential equations representing the chemical reactions are typically very stiff, which require special integration techniques. Extremely high numerical resolution is also needed to properly resolve the fine temporal or length scales introduced by the detailed reaction mechanism. As a consequence, fully resolved numerical simulations are far from being routine.

With the advance in chemical kinetic modeling, several techniques have been devised to reduce the complexity of detailed chemical kinetic scheme (Peters 1991).

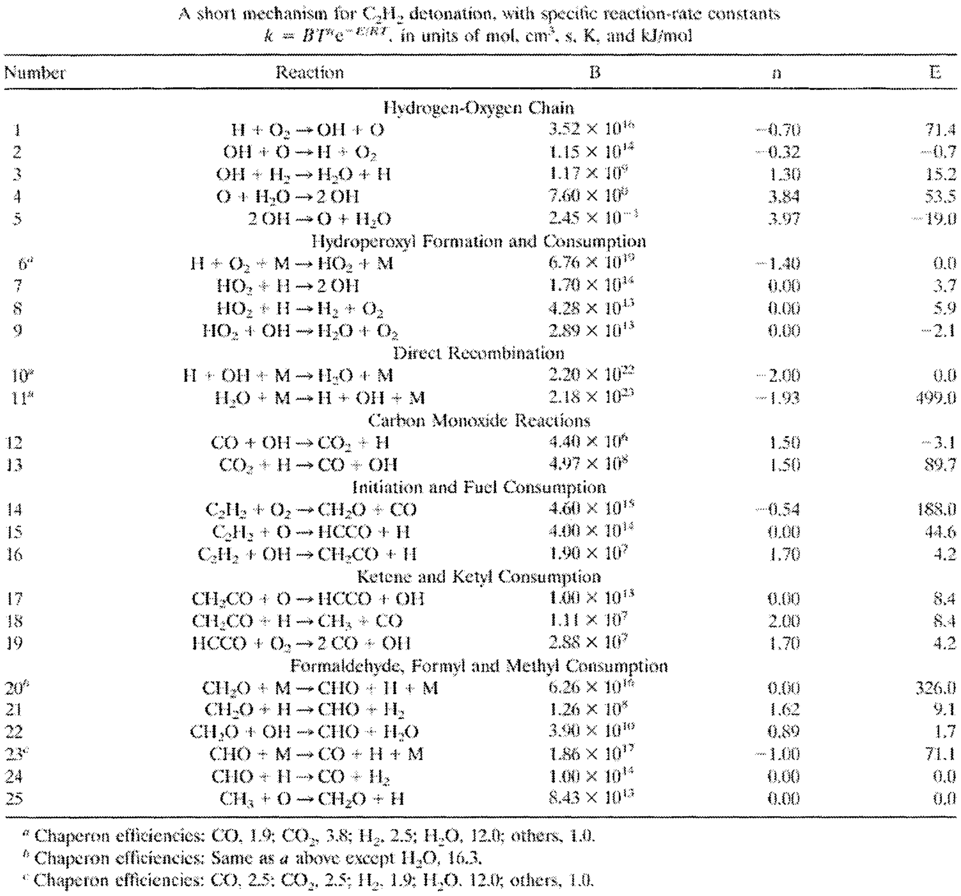

A short mechanism for C_2H_2 detonation, with specific reaction-rate constants $k = BT^n e^{-E/RT}$, in units of mol, cm^3, s, K, and kJ/mol

Number	Reaction	B	n	E
	Hydrogen-Oxygen Chain			
1	$H + O_2 \rightarrow OH + O$	3.52×10^{16}	−0.70	71.4
2	$OH + O \rightarrow H + O_2$	1.15×10^{14}	−0.32	−0.7
3	$OH + H_2 \rightarrow H_2O + H$	1.17×10^{9}	1.30	15.2
4	$O + H_2O \rightarrow 2\,OH$	7.60×10^{0}	3.84	53.5
5	$2\,OH \rightarrow O + H_2O$	2.45×10^{-3}	3.97	−19.0
	Hydroperoxyl Formation and Consumption			
6[a]	$H + O_2 + M \rightarrow HO_2 + M$	6.76×10^{19}	−1.40	0.0
7	$HO_2 + H \rightarrow 2\,OH$	1.70×10^{14}	0.00	3.7
8	$HO_2 + H \rightarrow H_2 + O_2$	4.28×10^{13}	0.00	5.9
9	$HO_2 + OH \rightarrow H_2O + O_2$	2.89×10^{13}	0.00	−2.1
	Direct Recombination			
10[a]	$H + OH + M \rightarrow H_2O + M$	2.20×10^{22}	−2.00	0.0
11[a]	$H_2O + M \rightarrow H + OH + M$	2.18×10^{23}	−1.93	499.0
	Carbon Monoxide Reactions			
12	$CO + OH \rightarrow CO_2 + H$	4.40×10^{6}	1.50	−3.1
13	$CO_2 + H \rightarrow CO + OH$	4.97×10^{8}	1.50	89.7
	Initiation and Fuel Consumption			
14	$C_2H_2 + O_2 \rightarrow CH_2O + CO$	4.60×10^{15}	−0.54	188.0
15	$C_2H_2 + O \rightarrow HCCO + H$	4.00×10^{14}	0.00	44.6
16	$C_2H_2 + OH \rightarrow CH_2CO + H$	1.90×10^{7}	1.70	4.2
	Ketene and Ketyl Consumption			
17	$CH_2CO + O \rightarrow HCCO + OH$	1.00×10^{13}	0.00	8.4
18	$CH_2CO + H \rightarrow CH_3 + CO$	1.11×10^{7}	2.00	8.4
19	$HCCO + O_2 \rightarrow 2\,CO + OH$	2.88×10^{7}	1.70	4.2
	Formaldehyde, Formyl and Methyl Consumption			
20[b]	$CH_2O + M \rightarrow CHO + H + M$	6.26×10^{16}	0.00	326.0
21	$CH_2O + H \rightarrow CHO + H_2$	1.26×10^{8}	1.62	9.1
22	$CH_2O + OH \rightarrow CHO + H_2O$	3.90×10^{10}	0.89	1.7
23[c]	$CHO + M \rightarrow CO + H + M$	1.86×10^{17}	−1.00	71.1
24	$CHO + H \rightarrow CO + H_2$	1.00×10^{14}	0.00	0.0
25	$CH_3 + O \rightarrow CH_2O + H$	8.43×10^{13}	0.00	0.0

[a] Chaperon efficiencies: CO, 1.9; CO_2, 3.8; H_2, 2.5; H_2O, 12.0; others, 1.0.

[b] Chaperon efficiencies: Same as *a* above except H_2O, 16.3.

[c] Chaperon efficiencies: CO, 2.5; CO_2, 2.5; H_2, 1.9; H_2O, 12.0; others, 1.0.

Table 5.1. A 25-step detailed mechanism for acetylene oxidation (Varatharajan & Williams 2001).

The idea is to remove the most rapid time scales and associated minor chemical species from the system without unacceptable loss of accuracy in the description of the slower processes. Reduced reaction mechanisms are thus developed from parent detailed reaction mechanisms, which are systematically reduced to much smaller mechanisms with fewer reaction steps and chemical species. The advantage of reduced kinetic mechanism is that much of the detailed chemical kinetic information can still be retained and that the numerical calculations are computationally much cheaper due to its simpler chemical kinetic description. Such reduced mechanisms that take the elementary chemistry into account offer a good compromise between the simplest one or two-steps and detailed chemical kinetic models that are available, and should be useful for studying detonation phenomena that have not been satisfactorily addressed previously.

A reduced seven-step chemical reaction mechanism, recently developed and validated specifically for acetylene-oxygen-diluent detonations, is employed to model the detonation chemistry. A detailed exposition of this chemical kinetic mechanism can be found in Varatharajan & Williams (2001) and only the main features are reproduced here. In essence, the seven-step mechanism was systematically derived from a more complex full mechanism by eliminating irrelevant reactions for the high temperatures prevailing in detonations and applying steady-state and partial equilibrium approximations to further simplify the kinetic description. The resulting mechanism has a chain-branching-thermal explosion character. The seven-step mechanism consists of four important steps during the induction process (I-IV) leading to ignition and three steps describing the exothermic stage following ignition during which radicals re-combine to form products (steps V-VII):

$$\begin{aligned}
\mathrm{C_2H_2+O_2} &\rightarrow \mathrm{CH_2O+CO} && \text{(I)}\\
\mathrm{CH_2O} &\rightarrow \mathrm{CO+2H} && \text{(II)}\\
\mathrm{C_2H_2+OH} &\rightarrow \mathrm{CH_2CO+H} && \text{(III)}\\
\mathrm{C_2H_2+2O_2} &\rightarrow \mathrm{2CO+2OH} && \text{(IV)}\\
\mathrm{2H+O_2} &\rightarrow \mathrm{H_2O+O} && \text{(V)}\\
\mathrm{CH_2CO+O+O_2} &\rightarrow \mathrm{2OH+2CO} && \text{(VI)}\\
\mathrm{CO+OH} &\rightarrow \mathrm{CO_2+H} && \text{(VII)}
\end{aligned}$$

The rates of each global reaction are derived in terms of the elementary rates of the detailed 25-step detailed mechanism for high-temperature kinetics (see table 5.1) and is given by:

$$\begin{aligned}
q_{I} &= -q_4 + q_5 - q_7 + q_{14} + q_{18} \\
q_{II} &= -q_4 + q_5 - q_7 + q_{20} + q_{21} + q_{22} \\
q_{III} &= -q_1 + q_2 + q_8 + q_9 + q_{10} - q_{11} + q_{15} + q_{16} + q_{21} + q_{22} + q_{24} \\
q_{IV} &= q_1 - q_2 + q_4 - q_5 + q_7 - q_8 - q_9 - q_{10} + q_{11} - q_{18} - q_{21} - q_{22} - q_{24} \\
q_{V} &= -q_4 + q_5 + q_8 + q_9 + q_{10} - q_{11} + q_{21} + q_{22} + q_{24} \\
q_{VI} &= -q_1 + q_2 + q_8 + q_9 + q_{10} - q_{11} + q_{15} + q_{17} + q_{18} + q_{21} + q_{22} + q_{24} \\
q_{VII} &= q_{12} - q_{13}
\end{aligned}$$

The concentrations of the five species (HCCO, CHO, HO_2, H_2 and CH_3) which are assumed to be steady-state (i.e. $\dot{\omega}_i = 0$) for the derivation of the reduced mechanism are expressed in terms of the concentration of the other species from the balance relations according to:

$$\begin{aligned}
[\mathrm{HCCO}] &= \frac{k_{15}\,[\mathrm{C_2H_2}]\,[\mathrm{O}] + k_{17}\,[\mathrm{CH_2CO}]\,[\mathrm{O}]}{k_{19}\,[\mathrm{O_2}]} \\
[\mathrm{CHO}] &= \frac{(k_{20}\,[\mathrm{M}] + k_{21}\,[\mathrm{H}])\,[\mathrm{CH_2O}] + k_{22}\,[\mathrm{CH_2O}]\,[\mathrm{OH}]}{k_{23}\,[\mathrm{M}] + k_{24}\,[\mathrm{H}]} \\
[\mathrm{HO_2}] &= \frac{k_6\,[\mathrm{H}]\,[\mathrm{O_2}]\,[\mathrm{M}]}{(k_7 + k_8)\,[\mathrm{H}] + k_9\,[\mathrm{OH}]} \\
[\mathrm{H_2}] &= \frac{(k_8\,[\mathrm{HO_2}] + k_{21}\,[\mathrm{CH_2O}] + k_{24}\,[\mathrm{CHO}])\,[\mathrm{H}]}{k_3\,[\mathrm{OH}]} \\
[\mathrm{CH_3}] &= \frac{k_{18}\,[\mathrm{CH_2CO}]\,[\mathrm{H}]}{k_{25}\,[\mathrm{O}]}
\end{aligned}$$

These concentrations of the steady-state species are required for some rates from the original 25-step detailed mechanism, which are in turn necessary to find the reduced rate of progress given above. Finally, the species net production rates in the reduced system are obtained from the stoichiometry of the reactions (I to VII) and their corresponding rates of progress are given by:

$$\begin{aligned}
\dot{\omega}_{\mathrm{C_2H_2}} &= -q_I - q_{III} - q_{IV} \\
\dot{\omega}_{\mathrm{O_2}} &= -q_I - 2 \cdot q_{IV} - q_V - q_{VI} \\
\dot{\omega}_{\mathrm{CH_2O}} &= q_I - q_{II} \\
\dot{\omega}_{\mathrm{CO}} &= q_I + q_{II} + 2 \cdot q_{IV} + 2 \cdot q_{VI} - q_{VII} \\
\dot{\omega}_{\mathrm{H}} &= 2 \cdot q_{II} + q_{III} - 2 \cdot q_V + q_{VII} \\
\dot{\omega}_{\mathrm{OH}} &= -q_{III} + 2 \cdot q_{IV} + 2 \cdot q_{VI} - q_{VII} \\
\dot{\omega}_{\mathrm{CH_2CO}} &= q_{III} - q_{VI} \\
\dot{\omega}_{\mathrm{O}} &= q_V - q_{VI} \\
\dot{\omega}_{\mathrm{H_2O}} &= q_V \\
\dot{\omega}_{\mathrm{CO_2}} &= q_{VII}
\end{aligned}$$

It is interesting to point out that the important steps are reactions (IV) and (V). Reaction (IV) is the main exothermic reaction in the induction zone, which proceeds mainly at the rate of the elementary chain branching reaction

$$\mathrm{H+O_2 \rightarrow OH+O} \tag{VIII}$$

Reaction (V) is chain-breaking and proceeds mainly at a fraction of the chain termination rate of the elementary reaction

$$\mathrm{H+O_2+M \rightarrow HO_2+M} \tag{IX}$$

This reaction is of increasing importance at low temperatures and contributes to the effective increase in the overall activation energy (thus ignition times) at low temperatures as due to the inhibition of the chain branching reaction (IV) producing the active OH radical. It should be noted that the competition between the same two reactions (VIII and IX) governs the second explosion limit in hydrogen-oxygen mixtures (Lewis & Von Elbe 1961), which was first suggested to be intimately linked to detonability by Belles (1959): below the chain-branching cross-over temperature, when the OH is not generated sufficiently fast, a chemical bottleneck occurs and detonations cannot be self-sustained.

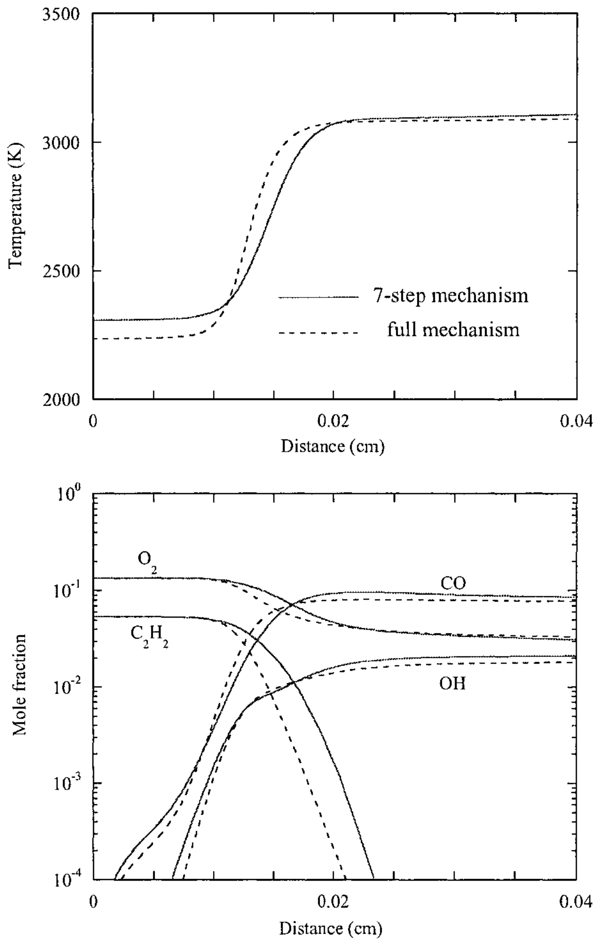

Figure 5.1. Comparison of the steady-state ZND structure obtained using the reduced seven-step mechanism and the 25-step detailed mechanism.

This reduced seven-step reaction mechanism is found to be very suitable for describing both the induction and exothermic re-combination part of the reactions and agreed very well with the full mechanism predictions for zero order isobaric explosions (Varatharajan & Williams 2001). For completeness, comparison of the ZND profiles obtained using the full and reduced mechanism for acetylene-oxygen-argon is presented. Figure 5.1 shows the ZND detonation structure obtained with the full or reduced mechanisms for $C_2H_2 + 2.5O_2 + 81\%Ar$ at $P_o = 41.7$ kPa. Clearly, the reduced mechanism reproduces very well both the induction zone length and the temperature history in the reaction zone. The figure also shows the evolutions of some key species (C_2H_2, O_2, OH and CO) in the reaction zone structure. Although the depletion rate of C_2H_2 is underestimated by the reduced mechanism, the global evolution of these key species is well reproduced by the reduced mechanism.

5.3 Analysis of the steady ZND structure

In an attempt to explain the effect of argon dilution that has been observed experimentally on the cellular detonation, the chemical reaction structure of the steady-state ZND model for varying degree of argon dilutions on the mixture is first analyzed. To obtain the steady ZND detonation structure, the one-dimensional steady ZND equations given in Chapter 2 coupled with the present seven-step reaction mechanism were integrated numerically using a computer code developed by Shepherd (1986). For meaningful comparison on the changes in the ZND structure with different argon dilutions, the simulations were conducted at an initial temperature $T_o = 298$K and at a constant density of fuel and oxidizer ($\rho_{\text{fuel+oxidizer}} = 9.69 \cdot 10^{-2}$ kg/m^3). The temperature profiles of the steady ZND detonation obtained for various argon dilutions are shown in figure 5.2.

It is clear that the energetic effect of argon dilution on detonation is to lower the total energy release of the mixture, which results in the decrease in detonation velocities and thus shock temperatures. However, addition of argon causes an increase

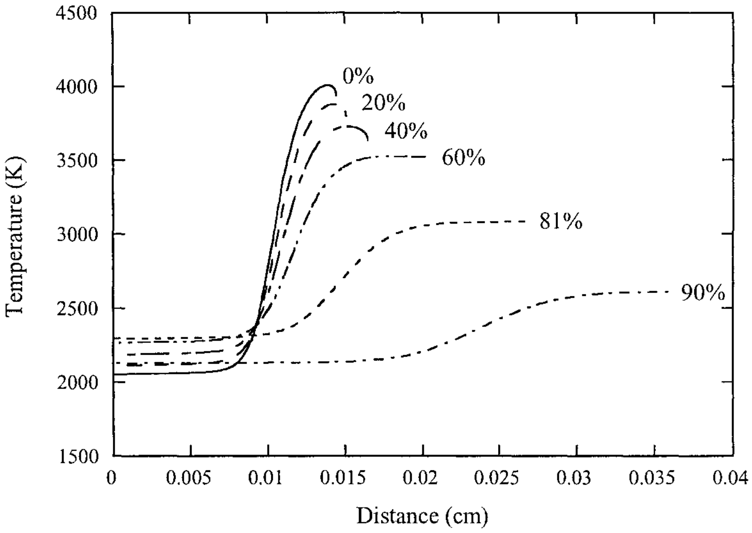

Figure 5.2. Steady ZND temperature profiles for stoichiometric acetylene-oxygen detonations with different argon dilutions at constant density of fuel and oxidizer ($\rho_{\text{fuel+oxidizer}} = 9.69{\cdot}10^{-2}$ kg/m^3) and T_o = 298K.

in the specific heat ratio of the mixture, leading to the opposite effect of increasing the shock temperature. The results indicate that these two competing effects are approximately balanced and therefore, the shock temperature T_s does not change significantly with argon dilution (i.e. with a slight increase in shock temperature of approximately 200K from a dilution of 0 to 81% Ar). Since the shock temperature remains almost constant, the influence of the inert diluent does not significantly affect the initiation rates. As shown in figure 5.2, where different ZND profiles are plotted for large variations of argon dilution, the length of thermally neutral induction length does not vary significantly. Another implication of the small changes in the shock temperature is that the global activation energy (E_a/RT_s), usually used in previous studies to describe the stability of gaseous detonations, does not vary significantly with argon dilution. Hence, it cannot account for the dramatic changes of stability observed experimentally. To calculate the global activation energy of an equivalent one-step reaction, numerical simulations at constant volume were performed. Its value can be obtained by performing constant-volume explosion calculations. Assuming that the induction time τ_i has an Arrhenius form, i.e.,

$$\tau_i = A\rho^n \exp\left(\frac{E_a}{RT}\right) \tag{5.1}$$

The activation temperature E_a/RT_s may be determined by

$$\varepsilon_I = \frac{E_a}{RT_s} = \frac{1}{T_s}\frac{\ln\tau_2 - \ln\tau_1}{\frac{1}{T_2} - \frac{1}{T_1}} \tag{5.2}$$

where two constant-volume explosion simulations are run with initial conditions (T_1, τ_1) and (T_2, τ_2). Conditions for states one and two are obtained by considering the effect of a change in the shock velocity by $\pm 1\% D_{cj}$ (Schultz & Shepherd 2000).

However, one can note from figure 5.2 the dramatic change in the reaction zone structure with increasing argon dilution, leading to an increase of the reaction zone length. The increase with argon dilution of the characteristic reaction zone during which the exothermic recombination processes occur can be explained by considering the changes in the elementary rates occurring at the end of the chain-branching steps and during the recombination steps of the oxidation scheme. As argon is added, the total heat release (per mole) decreases significantly, resulting in a lower temperature rise in the reaction zone. As a consequence of lower temperature in the reaction zone, the chemical reaction rates of the exothermic reactions are reduced, leading to an increase in the heat release characteristic times. Therefore, it appears from these ZND analyses that the main effect of argon dilution on the ZND structure is the lengthening of the reaction zone.

Mixture	P_o (kPa)	T_o (K)	P_{vn} (kPa)	T_{vn} (K)	l_{driver} (mm)
$C_2H_2 + 2.5O_2 +$ 90%Ar	100	298	2866	2146	2.2
$C_2H_2 + 2.5O_2 +$ 85%Ar	60	298	1919	2252	1.5
$C_2H_2 + 2.5O_2 +$ 81%Ar	41.7	298	1451	2308	1.5
$C_2H_2 + 2.5O_2 +$ 70%Ar	16.3	298	623	2259	2.0

Table 5.2. Different thermodynamic states of the quiescent and driver gas used in the computations

5.4 Numerical simulations

To further elucidate how the unsteady detonation structure and its stability change with increasing argon dilution, highly resolved numerical simulations of 1D detonations were performed. The numerical experiments were conducted for 90, 85, 81 and 70% argon dilution in stoichiometric acetylene-oxygen detonations. The initial thermodynamic states used in the numerical simulations were chosen such that the mixture sensitivity was approximately constant as determined experimentally. Different initial parameters are given in table 5.2. These initial conditions were also used in recent experiments by Radulescu (2003) and hence, the present numerical results permit direct comparison with experimental observations.

The computations were initialized by a region of length l_{driver} brought uniformly to the von Neumann state P_{vn} and T_{vn} of the corresponding steady ZND detonation. The length of the driver can be varied to monitor the decay rate of the initially overdriven detonation to unsupported CJ detonation. This method also allows one to monitor the dynamics of the detonation wave as it relaxed to the CJ velocity and reached an oscillating limit cycle. The state of initial quiescent gas and the state of the driver gas used in the present simulations are shown in table 5.2. One should note however that the final asymptotic behavior or the limit cycle reached should be independent of the computational technique used to initiate the detonation.

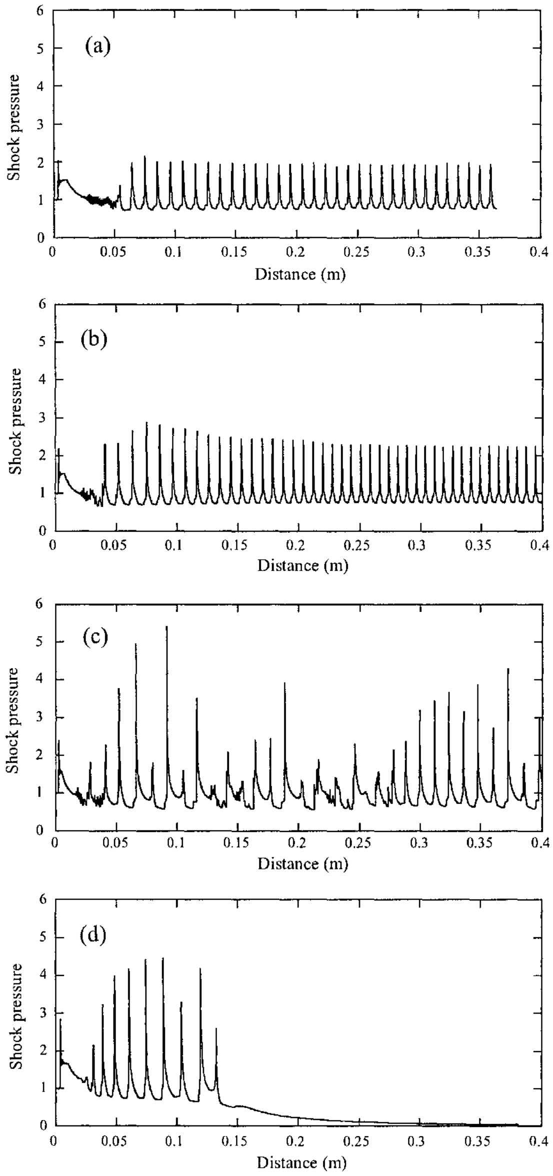

Figure 5.3. Leading shock pressure (normalized with steady-state von Neumann pressure P_{vn}) versus position for the propagation of planar detonation in stoichiometric acetylene-oxygen mixture with different degree of argon dilutions ($C_2H_2 + 2.5O_2 + \%Ar$): (a) 90%Ar at $P_o = 100$kPa and $T_o = 298$ K; (b) 85%Ar at $P_o = 60$kPa and $T_o = 298$ K; (c) 81%Ar at $P_o = 41.7$kPa and $T_o = 298$ K; (d) 70%Ar at $P_o = 16.3$kPa and $T_o = 298$ K.

The numerical results from the simulations are shown in figure 5.3 in the order of decreasing argon dilution. The overpressure ratio P/P_{vn} at the leading shock, where P_{vn} is the von Neumann shock pressure for a steady ZND detonation, is plotted with the position of the detonation front. For the case of 90% argon shown in figure 5.3a, as the initially overdriven detonation wave decays to the CJ velocity asymptotically, both a low-amplitude high-frequency and a low-frequency high-amplitude oscillation can be observed. After the initial transient, the high frequency mode soon dies out and the non-linear limit-cycle behavior is that of a single-frequency and relatively weak oscillations with a maximum value of amplitude around 2. As the amount of argon dilution is decreased to 85% (figure 5.3b), the similar phenomenon is observed, but the amplitude of the pulsations increases and reaches an overpressure amplitude of approximately 2.8. As the dilution is decreased further to 81%, the oscillations become more irregular, as displayed by the varying amplitude of the oscillations. In figure 5.3c, it is shown that the highest peaks of the oscillations are significantly larger than the previous cases, reaching a value of approximately 5 to 6. Although high frequency low amplitude oscillations are intermittently observed, the dominant frequency of oscillation is approximately constant.

For further decrease in argon dilutions, the initial degree of overdrive has to be augmented to permit an unambiguous observation of the phenomenon as the CJ conditions are approached. For 70% argon dilution shown in figure 5.3d, as the detonation wave decays from the initial overdriven state to the CJ average velocity, the frequency of oscillations increases and the amplitude of the pulsations grows. During the low velocity phase of the oscillation, the leading shock decays to lower sub-CJ velocities. When the leading shock decays below $\sim 0.7D_{cj}$, the detonation wave fails. Analysis of the reaction zone structure during the last cycle of the oscillation revealed that failure occurs due to the complete decoupling of the reaction zone from the leading shock front. This decoupling was found to occur when the temperature behind the leading front decays below ~1300 K. From figure 5.4 showing the ignition delay behind shocks with different strength in the constant volume approximation, one can see there is a rapid increase in the induction time below this critical Mach number or shock temperature value. This dramatic increase of ignition time is due to the chain-branching/chain-breaking competition which characterizes the oxidation of acetylene. This critical temperature is commonly referred to as the chain-branching cross-over temperature. Below this critical temperature, the generation of radicals from the chain-branching reaction is found to be too slow to maintain the coupling with the exothermic part of the reaction structure that is required to drive the wave. As a result, the reaction layer decouples from the shock and the detonation quenches. The detonation failure is thus due to this chemical "switch" effect. It is interesting to note that this failure scenario is in accord with the recent studies of Short *et al.* (1997, 1999). In their numerical simulations using a generalized three-step chain-branching reaction scheme, they also found that when the shock temperature decayed below the chain-branching cross-over temperature, the detonation would fail.

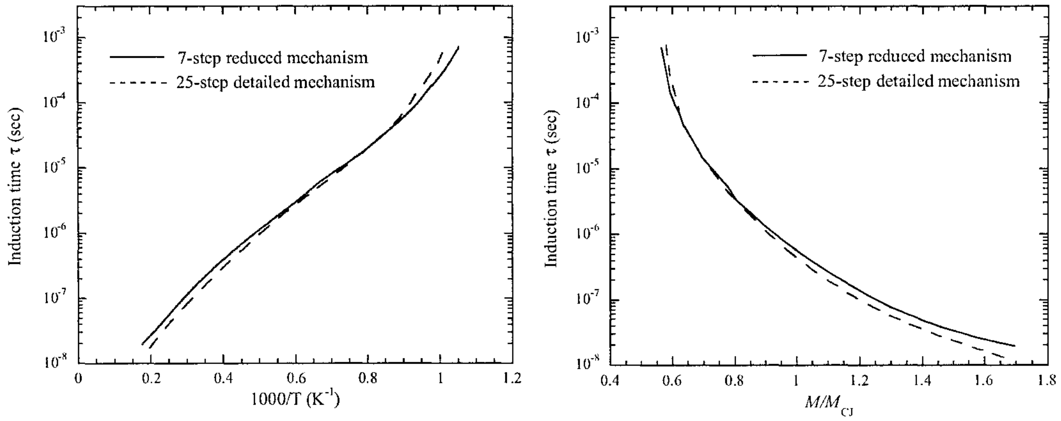

Figure 5.4. Ignition delay times for C_2H_2 + $2.5O_2$ + 70%Ar behind different shock strengths.

The present simulation results thus indicate that the amount of argon dilution controls the amplitude of the detonation pulsations. When these pulsations are

Mixture	P_o (kPa)	E_a/RT_s	Δ_I (cm)	Δ_R (cm)	χ
$C_2H_2 + 2.5O_2 + 90\%Ar$	100	5.07	1.92×10^{-2}	5.30×10^{-2}	1.83
$C_2H_2 + 2.5O_2 + 85\%Ar$	60	4.86	1.51×10^{-2}	3.41×10^{-2}	2.15
$C_2H_2 + 2.5O_2 + 81\%Ar$	41.7	4.77	1.52×10^{-2}	3.03×10^{-2}	2.39
$C_2H_2 + 2.5O_2 + 70\%Ar$	16	4.77	2.25×10^{-2}	3.32×10^{-2}	3.24

Table 5.3. Values of different detonation parameters.

too large, and the shock decays below a critical temperature, the rate of chain-branching reactions becomes slow and the one-dimensional detonation can no longer be self-sustained. The present results also indicate that the one-dimensional limit of acetylene-oxygen-argon detonations occurs at approximately 70% argon dilution.

5.5 Discussion

The present numerical investigation attempts to clarify the role of argon dilution in controlling the amplitude of the detonation wave pulsations in one dimension. The effect of argon dilution is often misleadingly attributed to the change in the global activation energy (E_a/RT_s) controlling the detonation wave stability as deduced from detonations involving only a single step reaction (e.g., Erpenbeck 1964; Lee & Stewart 1990). However, the present results demonstrate that the effect of argon dilution cannot simply be explained by the variation of the activation energy, since the global activation energy is essentially constant for different argon dilutions in acetylene-oxygen (see table 5.3). While the shock sensitivity of the induction time is constant, it is the effect of lengthening of the exothermic layer that results from the heavy argon dilution. This is due to the decrease of the exothermicity relative to the rate of induction reactions in the gas which can lead to the stabilizing effect of the detonation wave.

Following the previous analyses in Chapter 4, the loss of stability with decreasing argon dilution in acetylene-oxygen can perhaps be associated to the change of the parameter χ. Recalled that χ is defined as:

$$\chi \equiv \frac{E_I}{RT_s}\frac{\Delta_I}{\Delta_R} = \frac{E_I}{RT_s}\Delta_I\frac{\dot{\sigma}_{\max}}{u'_{cj}} \tag{5.3}$$

The activation energy $\varepsilon_I = E_I/RT_s$ in the induction process is already obtained from the constant-volume explosion calculations. Other parameters in the above definition can be obtained from the steady ZND analysis. The induction and reaction lengths were determined by solving the steady ZND structure of the detonation (figure 5.5). For the model with detailed chemistry, the induction length was defined quantitatively as the distance elapsed from the shock to the point where the fluid particle reaches its maximum rate of heat release, i.e., maximum thermicity $\dot{\sigma}_{\max}$. As discussed previously in Chapter 4, the characteristic length for the heat release was again taken as the inverse of the maximum rate of heat release multiplied by the CJ particle velocity, i.e. $u'_{cj}/\dot{\sigma}_{\max}$.

Table 5.3 shows the values of χ corresponding to the conditions in the numerical computations. The variation of the stability parameter χ by decreasing argon dilution follows the same trend as the loss of stability observed in the 1D numerical simulations. It is shown in figure 5.6 that the neutral stability curve obtained using the two-step kinetic model in Chapter 4 also provides a good assessment of the present numerical results. Hence, the parameter χ and the neutral stability curve together provide a quantitative measure of the degree of instability for one-dimensional pulsating detonations, irrespective to the chemical kinetic models.

As pointed out in Chapter 4, there is a strong dependence between the stability of ZND detonations with the regularity of the multi-dimensional cellular detonation structure. A sample experimental smoked foil obtained for 85% argon dilution is shown in figure 5.7. The result shows a very regular cellular pattern and the transverse waves are weak as indicated from the weak marking on the foil. It is also interesting to compare the cell length measured from the smoked foil for these highly

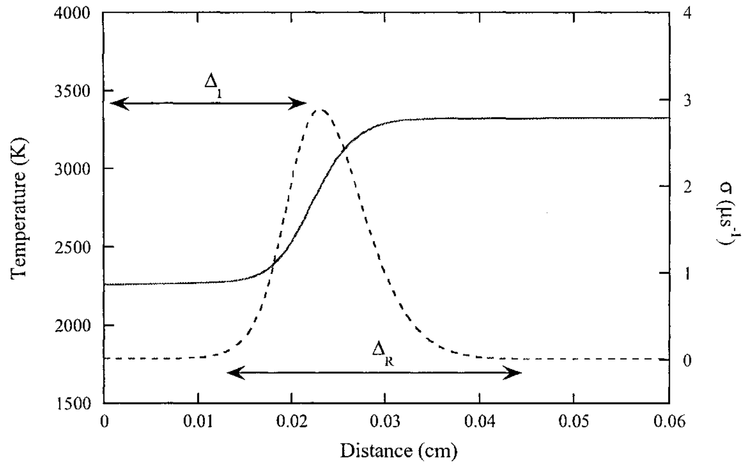

Figure 5.5. Temperature and thermicity profiles of the ZND structure for C_2H_2 + $2.5O_2$ + 70%Ar.

argon diluted cases with the oscillation period of the one-dimensional pulsating detonation obtained from numerical simulations. This comparison is given in table 5.4 and it shows very good agreement between the two. This good agreement may perhaps suggest that the regular cells observed experimentally in these highly diluted mixtures could essentially be a result of the one-dimensional instability mechanism only (Radulescu 2003).

In contrast, a completely different picture can be seen from the smoked foil obtained in the experiments with low argon diluted or undiluted acetylene-oxygen mixtures (see figure 1.4 in Chapter 1), which display much stronger transverse waves with higher cell irregularity. From the present numerical simulations, it is shown that below a critical argon dilution of approximately 70%, the large fluctuation in reaction rates due to the increasing instabilities causes the one-dimensional detonation to quench. The self-sustenance of 1-D detonation wave, which relies on the leading shock-ignition (i.e., the only propagation mechanism in one-dimensional case) is no longer possible. However, despite the inability of one-dimensional pulsating detona-

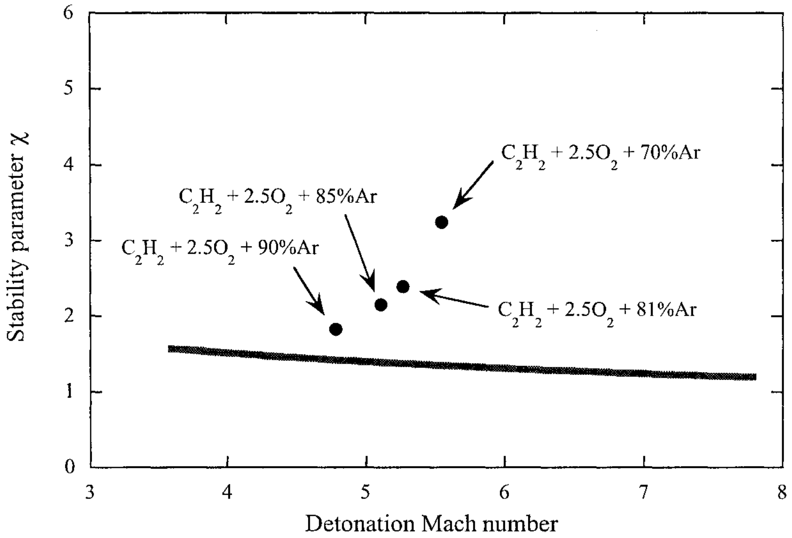

Figure 5.6. Characterization of the effect of argon dilution on the stoichiometric acetylene-oxygen detonation using the stability parameter χ and the neutral stability curve.

tions to propagate in low argon diluted acetylene-oxygen mixture, three-dimensional cellular detonations are commonly observed even for 0% argon dilution. In two or three-dimensional detonations, instabilities can give rise to multi-dimensional effects such as transverse wave interaction and turbulent mixing, etc., which may play a significant role in the detonation propagation mechanism. These can provide alternate means to cause auto-ignition and sustain the sufficiently high burning rates necessary for the self-sustenance of real detonation waves. Consequently, these strong multi-dimensional turbulence effects can also result in the highly irregular cellular detonation structure with strong transverse waves as observed experimentally.

It may also be worthwhile to discuss the recent experimental study carried out by Radulescu & Lee (2002) looking at the acetylene-oxygen-argon detonations propagating in porous wall tubes. The porous wall tubes are used to suppress multi-dimensional effects such as transverse waves. They have shown that there is a distinct switch-over in the failure mechanism at approximately 60±10%Ar dilution. Below

Mixture	1D pulsating length (mm)	Cellsize (mm)
$C_2H_2 + 2.5O_2 + 90\%Ar$	9	10.7
$C_2H_2 + 2.5O_2 + 85\%Ar$	7.5	8

Table 5.4. Comparison of experimental cell lengths with oscillation periods of the 1-D pulsating detonation.

this limit, transverse waves are found to play a dominant role for the detonation propagation. The detonation fails if these transverse waves are eliminated. Above this limit, the weak transverse wave structure is not significant and the detonation fails mainly by the global mass divergence mechanism and attenuation of the leading shock strength. This limit is indeed in good accord with the present numerical result. Both experimental and numerical findings indicate that the one-dimensional mode is not sufficient to maintain the detonation propagation below the critical limit of approximately 60±10%Ar dilution.

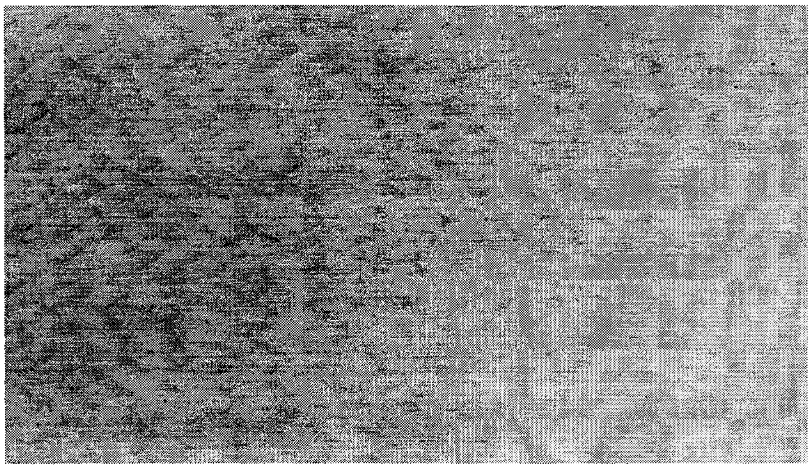

Figure 5.7. Experimental smoked foil record obtained for $C_2H_2 + 2.5O_2 + 85\%Ar$ (Courtesy of P. Pinard).

It is also interesting to compare the results for different combustible mixtures. Values for different detonation parameters of some common combustible mixtures are

Mixture	ε_I	$\Delta_I(cm)$	$\Delta_R(cm)$	χ	Cell regularity
$CH_4 + 2O_2$	11.84	0.102	2.30×10^{-2}	52.5	Highly Irregular
$C_3H_8 + 5O_2$	10.50	1.66×10^{-2}	1.05×10^{-2}	16.6	Highly Irregular
$C_2H_2 + 2.5O_2$	4.82	3.82×10^{-3}	3.57×10^{-3}	5.16	Irregular
$C_2H_2 + 2.5O_2 +$ 60%Ar	4.73	1.19×10^{-2}	1.57×10^{-2}	3.59	Regular
$C_2H_2 + 2.5O_2 +$ 85%Ar	4.83	5.42×10^{-2}	0.114	2.30	Regular
$2H_2 + O_2$	5.28	2.44×10^{-2}	5.72×10^{-2}	2.25	Regular
$2H_2 + O_2 +$ 25%Ar	4.91	2.18×10^{-2}	8.08×10^{-2}	1.33	Highly Regular
$2H_2 + O_2 +$ 40%Ar	4.68	2.32×10^{-2}	0.119	0.91	Highly Regular

Table 5.5. Values of different detonation parameters computed for mixtures at $T_o = 298$ K and $P_o = 0.2$ atm using Varatharajan & Williams 7-step reduced mechanism (2001) for C_2H_2–O_2; Oran *et al.* mechanism (1982) for H_2–O_2; and Konnov mechanism (2000) for others.

shown in table 5.5. Also tabulated is the qualitative assessment of the cell regularity as observed experimentally. The value of χ for each mixture is again mapped onto the neutral stability curve for comparison. Figure 5.8 clearly shows that for mixture like H_2-O_2 and C_2H_2-O_2 with argon dilution, their stability parameters lie slightly above the neutral stability boundary. One-dimensional unsteady simulations with detailed chemistry for these mixtures confirm that their propagation can be described by an one-dimensional pulsating mode and the periodic pattern is regular (figures 5.9 - 5.10). These mixtures are generally stable, which implies that they should have a higher regular cellular structure comprised of weak transverse waves and capable to maintain their propagation by the shock-induced ignition mechanism.

On the other hand, mixtures without argon dilution or those with hydrocarbon fuels such as methane or propane have a large value of χ. It becomes clear that why these mixtures are usually characterized by a highly irregular cellular structure.

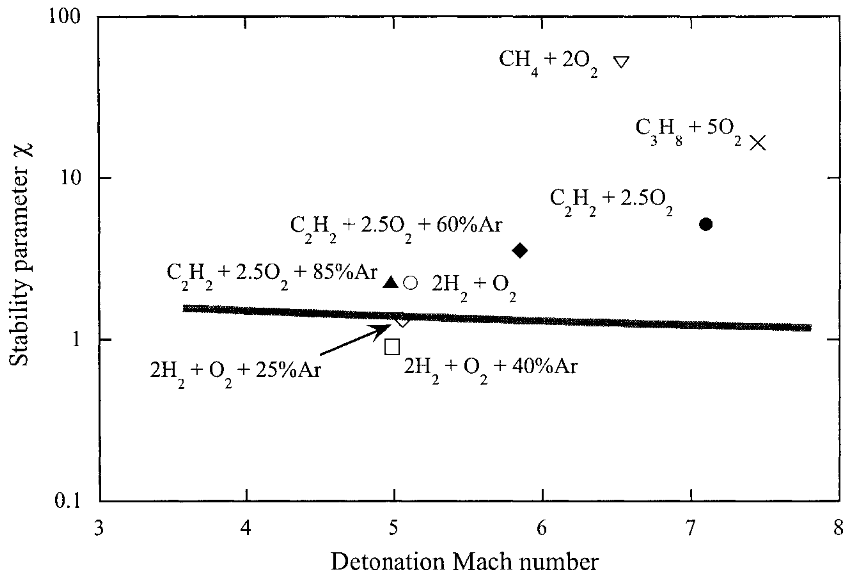

Figure 5.8. Characterization of the cellular structure of different combustible mixtures using the stability parameter χ and the neutral stability curve.

The incoherence in the power pulse or energy release originating from neighbouring particles, which is expected for large value of χ, leads to gasdynamic instabilities in the reaction zone. One-dimensional shock-ignition is no longer possible to maintain the self-propagation. Multi-dimensional effects such as transverse wave and other turbulent effects are essential for their propagation. These effects can thus cause significant irregularities in the detonation structure as discussed previously.

5.6 Summary

The present numerical investigation with realistic chemistry has obtained meaningful results on the structure and stability of real gaseous detonations, which can be readily compared with experiments. By extending the analysis shown in Chapter 4 to take

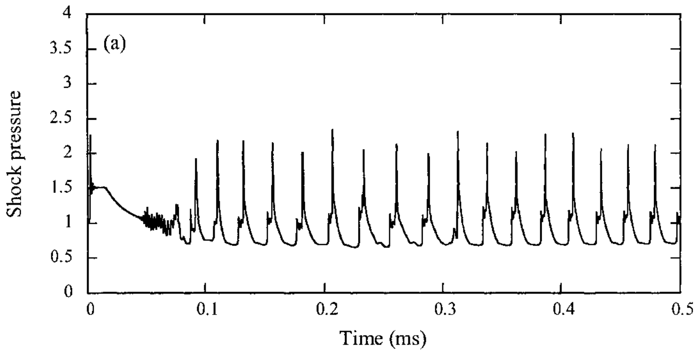

Figure 5.9. Leading shock pressure history for C_2H_2 + $2.5O_2$ + 85%Ar detonation at T_o = 298 K and P_o = 0.2 atm.

into account the realistic chemistry, the present study can also rationalize several experimental observations on the real reaction zone structure of detonation waves. The analysis has provided a better understanding of the stabilizing role played by high argon dilution on the detonation structure and its significance to the propagation mechanism of real cellular detonations. The stability parameter χ is shown to provide a good correlation in classifying the cell regularity. Together with the neutral stability curve, a good assessment of the degree of instability of the detonation wave can also be achieved.

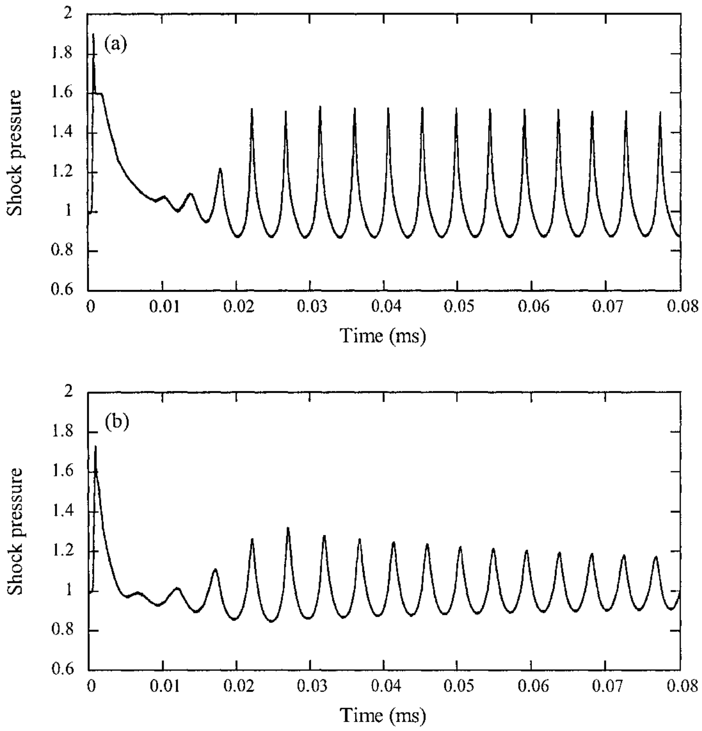

Figure 5.10. Leading shock pressure history for (a) $2H_2 + O_2 + 25\%Ar$ detonation; and (b) $2H_2 + O_2 + 40\%Ar$ detonation at $T_o = 298$ K and $P_o = 0.2$ atm.

Chapter 6

Detonation cell size prediction from chemical kinetics

6.1 Introduction

In this chapter, the relationship between chemical kinetics and experimentally measured cell sizes is examined quantitatively. The motivation is to establish a generalized correlation for the prediction of the characteristic detonation cell size from the calculated characteristic reaction length and other chemical kinetic properties. This is achieved by analyzing available experimental data from a large detonation database covering a wide variety of gaseous combustible mixtures at different initial conditions, together with the results that have been developed in early chapters.

The detonation cell size is commonly used to characterize sensitivity of an explosive mixture. Knowledge of the cell size permits other dynamic detonation parameters (i.e. critical initiation energy, detonability limit, critical tube diameter) to be estimated (Lee 1984). For this reason, there is a substantial amount of literature on the experimental measurement of cell sizes of different mixtures.

So far, no quantitative theory has been developed to predict the cell size. Yet, from pure dimensional analysis, it should be related to a characteristic reaction zone length of the detonation structure. Cell size appears to be an intrinsic property of the detonation and the reaction zone structure provides the only characteristic length scale of any relevance (Shepherd 1986). Therefore, the cell width must be proportional to some length determined by the reaction zone structure. As a first order approximation, the simplest length to choose is that determined by the idealized, steady-steady ZND model.

The first attempt to relate the calculated steady-state reaction zone length to the cell size for detonation is made by Schelkhin and Troshin (1965). A linear proportionality relationship between the cell size λ and the ZND chemical length scale Δ had been proposed, i.e. $\lambda = A \cdot \Delta$, where A is a constant proportionality factor. Since then, with the advance in the field of chemical kinetics, numerous attempts using this approach to relate experimentally measured cell sizes to characteristic chemical lengths from ZND calculation with detailed kinetic mechanism had been made, notably by Westbrook & Urtiew (1982); Moen *et al.* (1984); Shepherd (1986); Tieszen *et al.* (1986); etc. These results have shown to capture qualitatively the effects of mixture composition, temperature, and pressure on cell size, provided that a suitable choice is made of the factor A in the linear correlation. The factor A is generally determined by matching with one experimental data point for a particular combustible mixture (e.g. value at stoichiometric composition), and the relationship is then used to extend cell size prediction over any desired range of initial conditions. However, cell sizes predicted by this technique are usually valid only for mixtures with conditions that are similar to that of the matching point. The factor A is not universal and it significantly varies for different mixture compositions (especially off-stoichiometric and diluted mixture) and initial conditions. Hence, results for the predicted cell size can be several orders of magnitude different than the experimentally measured values.

In an attempt to improve this method for cell size prediction, Lee *et al.* (1982) and Shepherd (1986) proposed the ratio of cell size to induction length as a function of equivalent ratio for undiluted H_2-air mixture. The improved method appears to predict cell size within 50% for the same mixture diluted with CO_2 and H_2O. However, it is clear that this improvement is also limited and cannot be further generalized since even equilibrium detonation parameters are not universal function of equivalent ratio.

Additional computations by Shepherd (1986) on H_2-Air-diluent mixture indicate that the ratio A may perhaps be a function of both the sensitivity and the shape of the reaction zone. Recently, an attempt was carried out by Gavrikov *et al.* (2000) to seek a functional dependence of proportionality factor A on the various properties of the mixture and initial conditions. The ratio $A = \lambda/\Delta$ is assumed to be dependent on two stability parameters, the activation energy and a parameter that describes the relationship between the chemical energy and the critical internal energy of the mixture. However, an assumption is required that instead of computing the ZND reaction zone length based on the von Neumann state at D_{cj}, a higher value of the shock strength (averaged between the maximum of $1.6D_{cj}$ and D_{cj}) is used to take into account the multidimensional structure of real detonations. The new λ/Δ correlation appears to provide a better fit of the experimental data for hydrogen-air mixtures. However, the functional form of A is mathematically complicated and its general validity has yet to be determined.

Over the past decades, the detailed chemical kinetic schemes and their rate constants for high-temperature oxidation of most of the common fuels have been fairly well established. Hence, this permits the ZND reaction zone length to be accurately computed. A large body of experimental data is also available, and thus allows a quantitative comparison of cell size and reaction zone length over a wide range of mixture composition. In view of this availability, the present work carries out parametric reaction zone computations and attempts to correlate those results with experimental cell size data over a wide range of mixture compositions and initial conditions. In the same spirit as the work by Gavrikov *et al.* (2000), the objective of this study is to come up with an improved but simple correlation for detonation cell size with chemical reaction length by incorporating the stability parameter χ formulated in previous chapters of this thesis.

6.2 Experimental cell sizes data

To obtain a generalized correlation, the present study considers the widest possible range of experimental cell size data, starting with those for hydrogen-oxygen to other fuel-air mixtures at different initial compositions, temperatures and pressures. These cell size values were compiled in CalTech's detonation database (1997). Table 6.1 summarizes the mixtures considered for formulation of the empirical correlation.

A special remark should be made concerning the accuracy of the experimental results. Although a smoked foil record can easily be obtained experimentally, the interpretation of the foil in choosing the appropriate size for the detonation cells requires a certain degree of judgment and can be fairly subjective. This is due to the general irregularity in the cell pattern as well as the presence of substructure (representing higher harmonics) superimposed on the dominant cell pattern observed in most combustible mixtures. Only in special cases (e.g. H_2-O_2 highly diluted with argon) when the cell pattern is relatively regular and devoid of substructure can one identify the cell size easily. Nevertheless, in spite of the difficulties in the analysis of experimental smoked foil records, the cell size measurements obtained from different experiments are generally scattered within a factor of 2. Some values can be found to differ by a factor of 3, but this occurs only at the marginal cases where the detonations are near the single-head spin limit and may be influenced by the boundary condition.

Mixture	Initial condition	Variation	Reference
C_2H_2 / Air	$T = 293$ K; $P = 1$ atm	$\phi = 0.39 - 2.96$	Knystautas *et al.* (1984)
C_2H_2 / O_2	$T = 293$ K; $\phi = 1$	$P = 0.055 - 3.01$ atm	Manzhalei *et al.* (1974)
C_2H_4 / Air	$T = 293$ K; $P = 1$ atm	$\phi = 0.51 - 2.13$	Knystautas *et al.* (1984)
CH_4 / O_2	$T = 293$ K; $\phi = 1$	$P = 0.078 - 0.13$ atm	Knystautas *et al.* (1982)
		$P = 0.079 - 0.25$ atm	Laberge *et al.* (1993)
		$P = 0.37 - 6.08$ atm	Manzhalei *et al.* (1974)
CH_4 / Air	$T = 293$ K; $\phi = 1$	$P = 1$ atm	Moen *et al.* (1984)
CH_4 / O_2	$T = 298$ K; $P = 1.18$ atm	$\phi = 0.76 - 1.34$	Aminallah *et al.* (1993)
C_3H_8 / Air	$T = 293$ K; $P = 1$ atm	$\phi = 0.74 - 1.29$	Moen *et al.* (1984)
		$\phi = 0.61 - 1.66$	Knystautas *et al.* (1982)
C_2H_6 / Air	$T = 298$ K; $P = 0.92$ atm	$\phi = 1.03 - 1.29$	Moen *et al.* (1984)
C_2H_6 / Air	$T = 293$ K; $P = 1$ atm	$\phi = 0.79 - 1.27$	Knystautas *et al.* (1984)
		$\phi = 1.0$	Bull *et al.* (1982)
	$T = 298$ K; $P = 1$ atm	$\phi = 1.0$	Tieszen *et al.* (1991)
C_2H_6 / O_2	$T = 293$ K; $\phi = 1$	$P = 0.040 - 0.146$ atm	Knystautas *et al.* (1982)
H_2 / O_2 / 70%Ar	$T = 298$ K; $\phi = 1$	$P = 0.093 - 0.54$ atm	Barthel (1974)
H_2 / O_2 / 40%Ar	$T = 298$ K; $\phi = 1$	$P = 0.060 - 0.52$ atm	Barthel (1974)
H_2 / O_2	$T = 293$ K; $\phi = 1$	$P = 0.052 - 0.20$ atm	Knystautas *et al.* (1982)
		$P = 0.20 - 12.0$ atm	Manzhalei *et al.* (1974)
		$P = 0.281 - 0.977$ atm	Desbordes (1990)
H_2 / Air	$T = 300$ K; $P = 1$ atm	$\phi = 0.453 - 3.57$	Guirao *et al.* (1982)
		$\phi = 0.512 - 3.29$	Ciccarelli *et al.* (1994)
		$\phi = 0.5 - 1.0$	Stamps *et al.* (1991)
		$\phi = 0.369 - 5.51$	Tieszen *et al.* (1986)
H_2 / Air	$T = 500$ K; $P = 1$ atm	$\phi = 0.29 - 2.368$	Ciccarelli *et al.* (1997)
H_2 / Air	$T = 650$ K; $P = 1$ atm	$\phi = 0.19 - 2.397$	Ciccarelli *et al.* (1997)
H_2 / Air	$T = 373$ K; $P = 1$ atm	$\phi = 0.36 - 3.03$	Stamps *et al.* (1991)
H_2 / Air	$T = 300$ K; $\phi = 1$	$P = 0.0296 - 0.987$ atm	Bull *et al.* (1979)
		$P = 0.251 - 1.493$ atm	Stamps *et al.* (1991)
H_2 / Air	$T = 300$ K; $\phi = 0.5$	$P = 0.236 - 2.49$ atm	Stamps *et al.* (1991)

Table 6.1. A list of combustible mixtures at different variations used in the correlation.

6.3 Chemical kinetic calculations

Different definitions of the chemical reaction length scale were examined in the past (Shepherd 1986). Among these different definitions, the induction zone length, or the length corresponding to the distance between the leading shock and the location of the maximum rate of chemical energy release, is often used as the characteristic reaction zone for the correlation. The value of this length scale can be computed using the standard ZND model with a given chemical mechanism for various mixtures at different conditions. Two detailed chemical kinetic mechanisms were used in this study. For hydrogen mixtures, a recently updated comprehensive detailed mechanism is used (Li *et al.* 2004). It has been tested against a very wide range of experimental data, including laminar flame speed at normal or elevated temperature and pressure, shock tube ignition delay and other data from static and stirred reactors. The mechanism consists of 19 reversible elementary reactions based on the work of Mueller *et al.* (1999). It has been revised using recently published kinetic and thermodynamic information in literature. Among different updates, the most important revision is the reaction rate constant of the key chain-branching reaction $H + O_2 \rightarrow O + OH$ and the chain termination reaction $H + O_2 + M \rightarrow HO_2 + M$, which should have significant effects on the prediction of detonation parameters. For hydrocarbon mixture, the well-established Konnov's mechanism (2000) is considered which has been validated for detonation calculations by Schultz & Shepherd (2000).

6.4 Deficiency of the single constant proportionality relationship

To demonstrate the deficiency or non-universality of the linear correlation with constant coefficient of proportionality, the ratio of some experimentally measured cell width to the characteristic reaction zone width is shown in figure 6.1, grouped into few categories. It is shown that for a specific combustible mixture, for instance H_2-Air mixture shown in figure 6.1a, the ratio can vary over a range of about two orders of magnitude from 3 to 100, depending on the mixture composition. This large variation significantly exceeds the scatter of the experimental data measurement. It is also clear that A cannot be obtained as a function of the equivalent ratio alone. Both the initial conditions and mixture type may have significant influences on this ratio. It is thus not feasible to choose a constant parameter, which can universally estimate cell sizes with acceptable accuracy among different combustible mixtures.

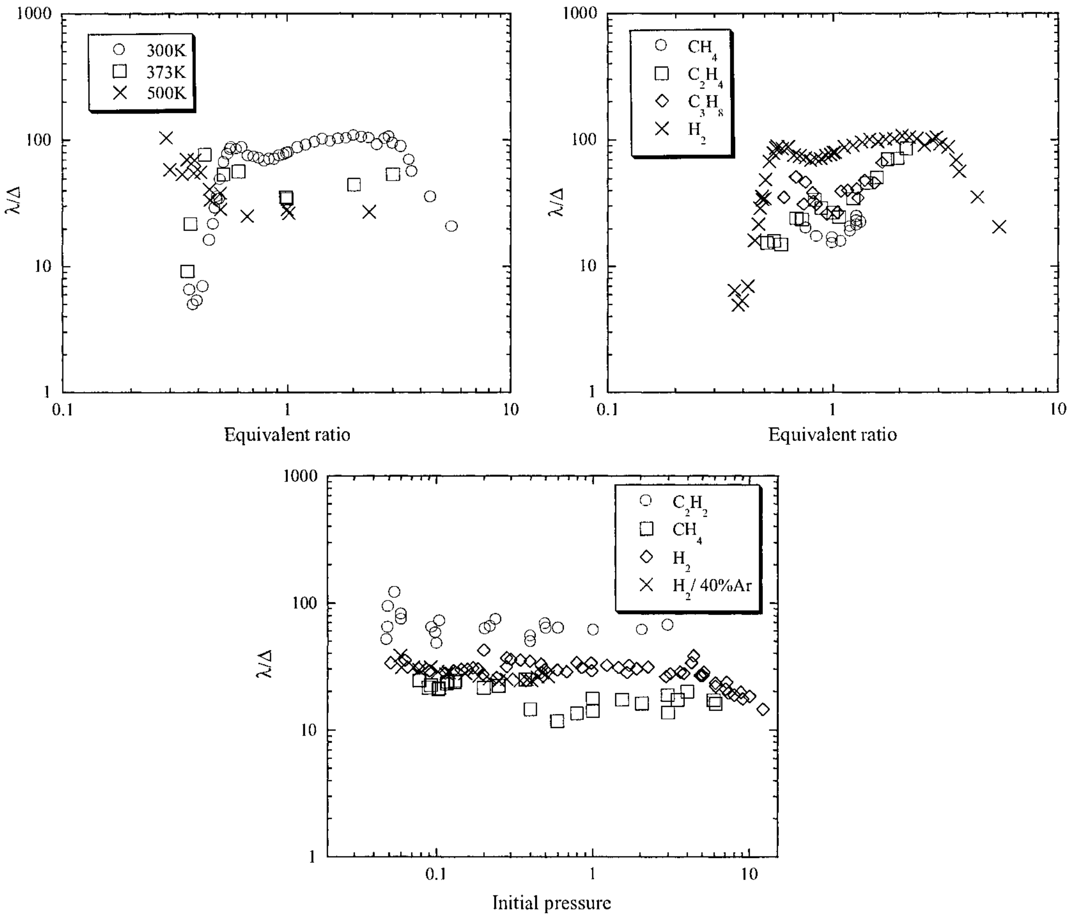

Figure 6.1. The ratio of experimental cell sizes to ZND induction lengths for various fuel mixtures at different initial conditions.

6.5 An improved correlation

The present study attempts to model the variation of the factor A and obtain an improved relationship to generalize the correlation between the cell sizes and the induction zone length computed from detailed chemical kinetic model. Taking into account the effect of detonation instability, the following relationship is purposed:

$$\lambda = A(\chi) \cdot \Delta_I = \sum_{k=0}^{N} \left(a_k \cdot \chi^{-k} + b_k \cdot \chi^k\right) \cdot \Delta_I \tag{6.1}$$

Since the function form is not known *a priori*, the relationship is written in term of a polynomial series of χ. Expanding the above relationship gives:

$$\begin{aligned} \lambda &= \left[(a_0 + b_0) + \frac{a_N}{\chi^N} + \ldots \frac{a_1}{\chi^1} + b_1 \cdot \chi^1 + \ldots b_N \cdot \chi^N\right] \cdot \Delta_I \\ &= \left[A_0 + \left(\frac{a_N}{\chi^N} + \ldots \frac{a_1}{\chi^1} + b_1 \cdot \chi^1 + \ldots b_N \cdot \chi^N\right)\right] \cdot \Delta_I \end{aligned} \tag{6.2}$$

where the instability term with χ can be regarded as a correction or perturbation to the original constant proportionality relationship. Therefore, the proposed correlation can retain the simplicity. The motivation behind this formulation is to address in the correlation both the sensitivity as well as the shape of the reaction structure, which have been previously realized to play an important role in the size of the detonation cell. Furthermore, the advantage of using the non-dimensional parameter χ derived in previous chapter as a parameter influencing the stability is that its definition already describes all the essential features and thus, the improved correlation can involve a minimum number of parameters to represent with a good accuracy a maximum number of experimental data.

For all the mixture data, the values of Δ_I and χ were calculated from chemical kinetics using the ZND model. To find all the coefficients in the proposed correlation, a multi-variable least square fitting is performed using Matlab. Values of these coefficients are given in table 6.2 for $N = 3$ in the expression.

In order to assess the validity of the present correlation, the percentage of deviation of the prediction from experimental values given by:

$$\% \text{ deviation} = \frac{\lambda_{\text{exp.}} - \lambda_{\text{prediction}}}{\lambda_{\text{exp.}}} \times 100\% \tag{6.3}$$

Coefficients	Values
A_0	30.465860763763
a_1	89.55438805808153
a_2	-130.792822369483
a_3	42.02450507117405
b_1	-0.02929128383850
b_2	$1.026325073064710\times10^{-5}$
b_3	$-1.031921244571857\times10^{-9}$

Table 6.2. Coefficients in the improved correlation with $N = 3$.

has been computed and plotted graphically. The mean deviation for all the data point is ±46.34%. Figure 6.2 shows that the correlation can predict most of the cell size values of different mixtures within 100%, i.e. by a factor of 2 of the experimental data point. Only for few points at which the error is given by a factor around 2.75. However, these points typically correspond to the limiting cases at which the cell size measurement is difficult to achieve experimentally. Despite of simplicity of the present correlation, the prediction is thus within the accuracy limits of the experimental data on cell widths and chemical kinetic models.

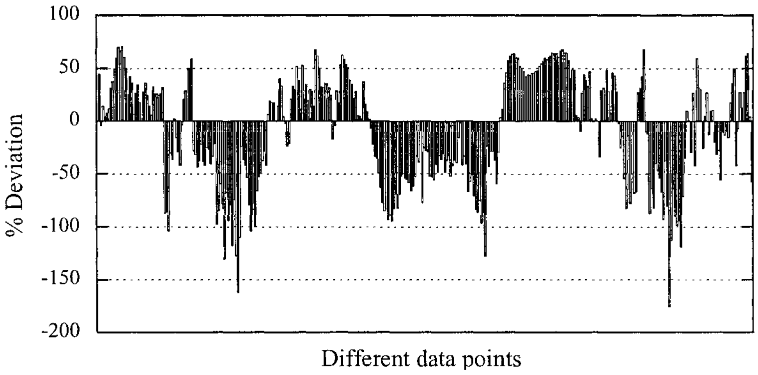

Figure 6.2. Percentage of deviation of calculated cell size values from experimental data. Data points from left to right correspond to the order of mixtures and initial conditions given in table 6.1.

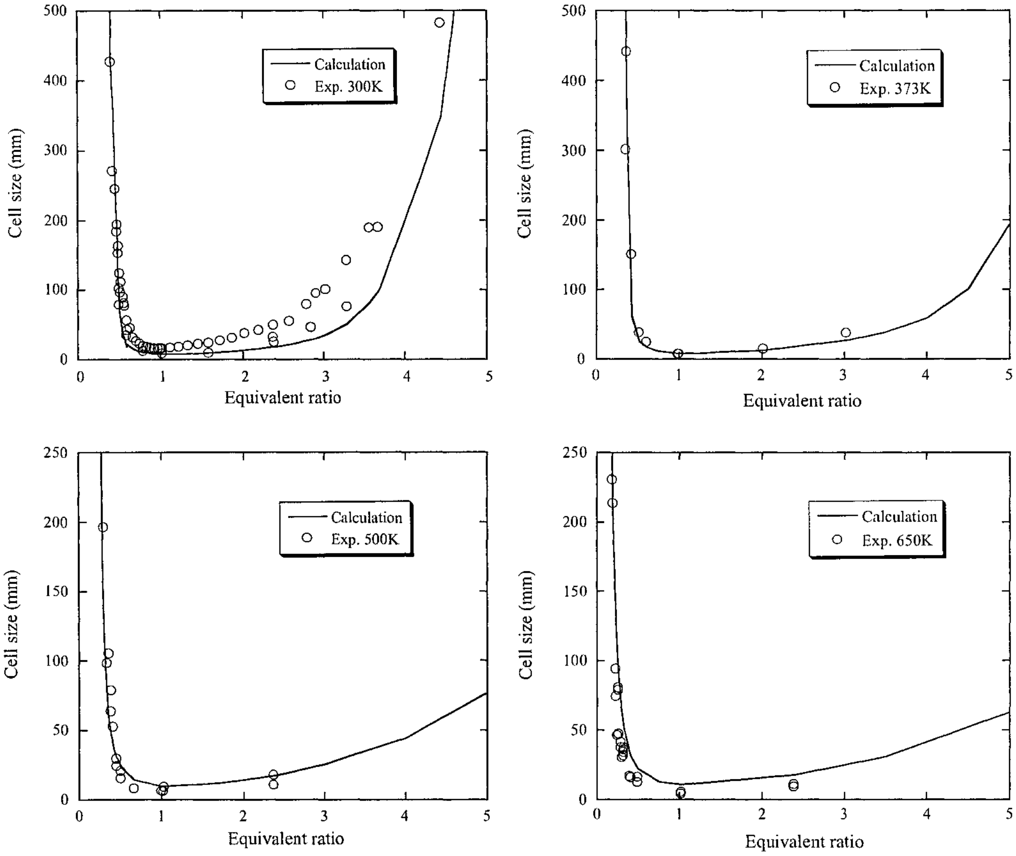

Figure 6.3. Comparison of cell size between experimental data and calculated values for hydrogen-air mixtures at different initial temperatures.

For a better representation of the improvement, figures 6.3-6.6 show a comparison of the predicted cell size with the original experimental data for different mixtures and initial conditions. For H_2-air mixtures, the correlation in general gives good estimates for the cell size as shown in figure 6.3 and 6.4. The improved correlation now provides a better approximation at both the lean and rich limits. This usually presented a problem for the standard correlation with constant coefficient of proportionality. Figure 6.3 and 6.4 also shows respectively that the effects of elevated temperature and pressure are described with good accuracy by the present correlation.

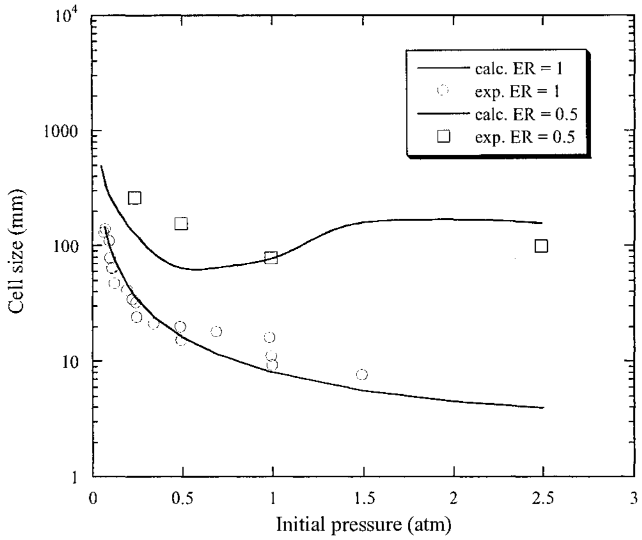

Figure 6.4. Comparison of cell size between experimental data and calculated values for hydrogen-air mixtures at different initial pressures.

To demonstrate the accuracy of the present correlation for different combustibles, figure 6.5 and 6.6 show comparisons of calculated cell sizes with experimental values for various fuel-air and fuel-oxygen mixtures. In general, one can see the prediction gives satisfactory agreement with experimental results. Except at high equivalent ratio, there is a rather large discrepancy compared to estimates at other conditions. One reason can be attributed to the inefficiency of the kinetic scheme to describe accurately the oxidation of high hydrocarbon mixture concentration.

The following set of results compares the predicted value and experimental data of cell size which were not included in the formulation of the improved correlation. Figure 6.7 shows such comparison for hydrogen-air mixtures diluted with CO_2. The present correlation not only predicts the general trend of U shape behavior in cell size variation with equivalent ratio, but it also provides reasonable estimates that are within the accuracy of the experimental data. The effect of argon dilution on the cell width for stoichiometric hydrogen-oxygen mixture is presented in figure 6.8.

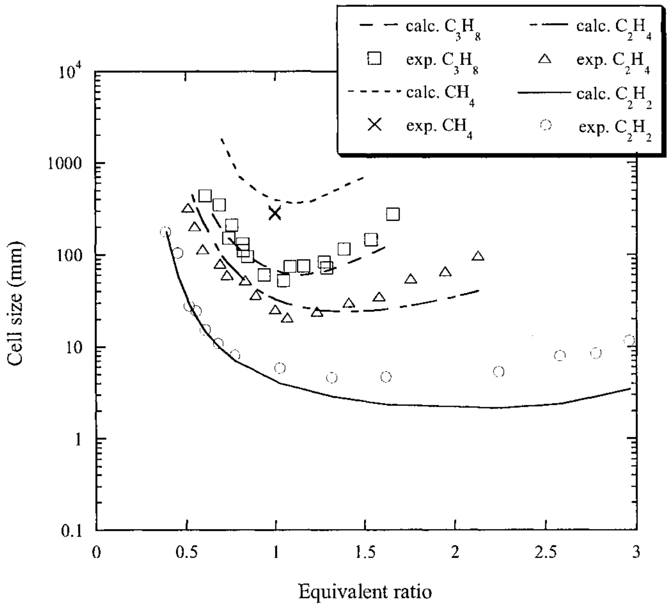

Figure 6.5. Comparison of cell size between experimental data and calculated values for various fuel-air mixtures at different equivalent ratios.

Similarly, it also appears that both the calculated and experimental values are in good agreement.

The last example compares results for hydrogen-air mixtures with steam dilution. Figure 6.9 once again shows that the model gives rather good estimates of the cell width including the effects of elevated temperature and initial pressure with different amounts of steam dilution.

6.6 Summary

In this work, an improved correlation is formulated, which provides a good estimate of the cell size value valid over a wide range of mixture composition and initial conditions. Probably even better results could have been obtained by introducing

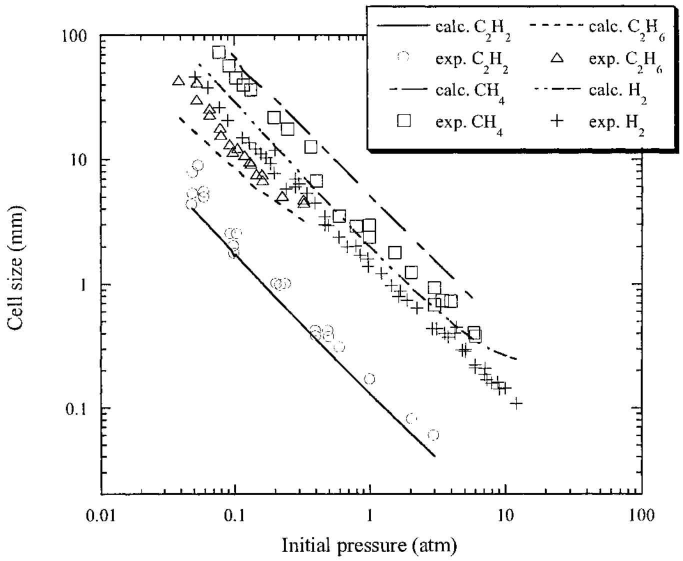

Figure 6.6. Comparison of cell size between experimental data and calculated values for various fuel-oxygen mixtures at different initial pressures.

further parameters or by using other functional expression to achieve better fits. The simplicity of this improved method to predict the cell size should be adequate for practical purpose such as industrial safety analyses, which generally requires only estimates concerned with detonability of gaseous mixtures.

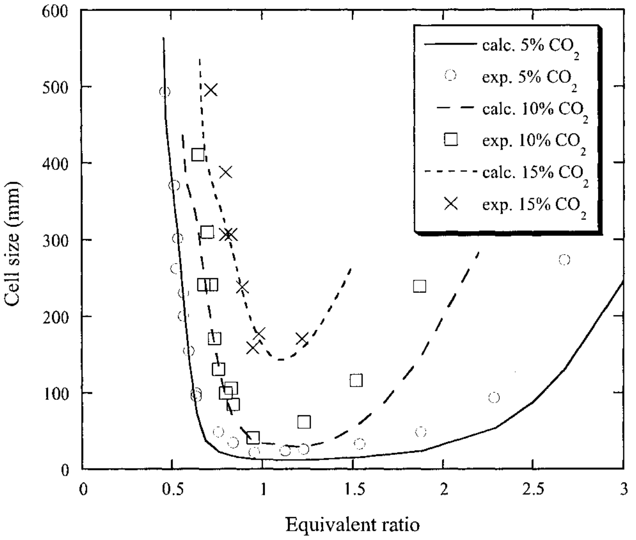

Figure 6.7. Comparison of cell size between experimental data and calculated values for hydrogen-air mixture diluted with CO_2 at different equivalent ratios.

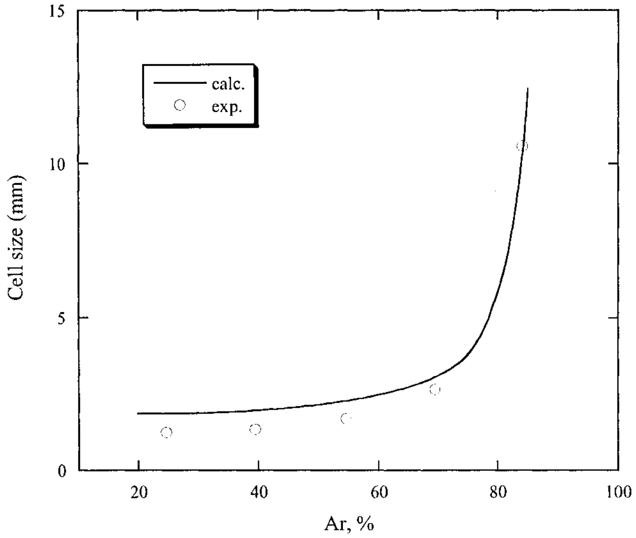

Figure 6.8. Comparison of cell size between experimental data and calculated values for hydrogen-oxygen mixture with different amounts of argon dilution.

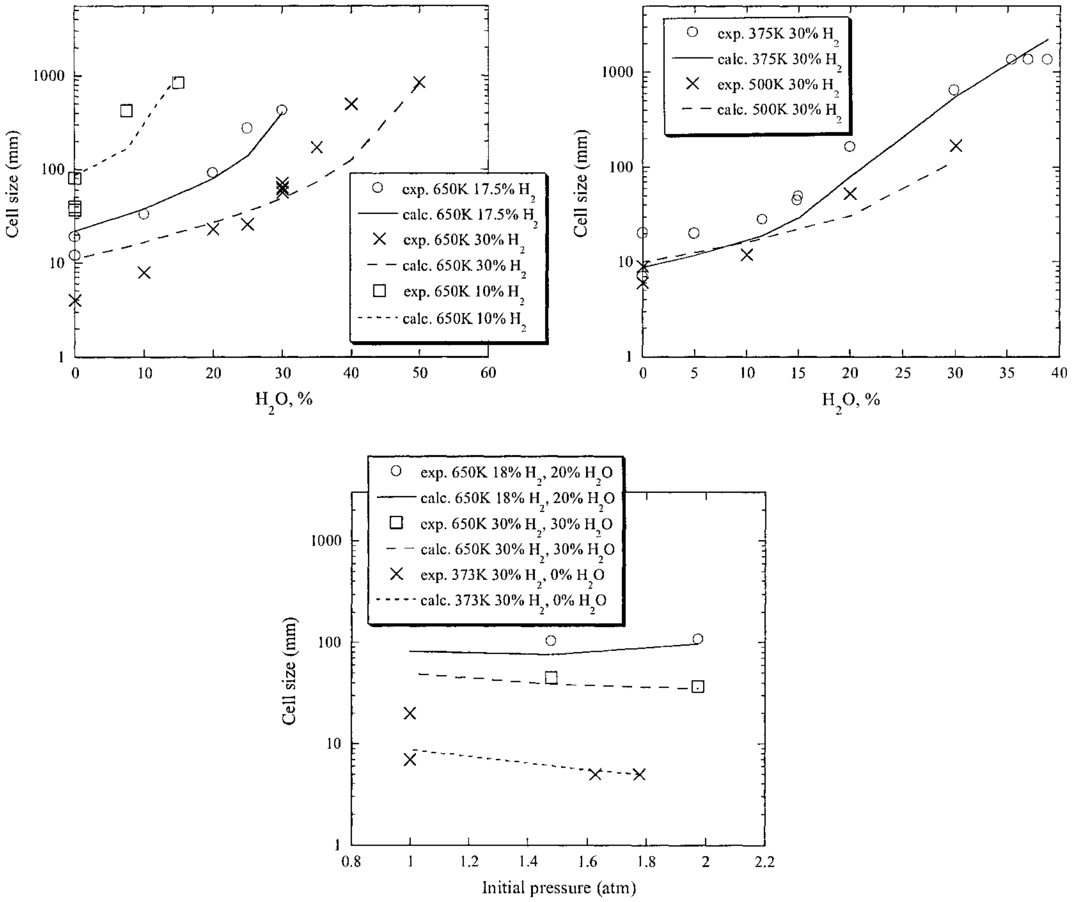

Figure 6.9. Comparison of cell size between experimental data and calculated values for hydrogen-air-steam mixture at different initial conditions.

Chapter 7

Head-on collision between a detonation and a shock wave

7.1 Introduction

It is demonstrated that chemical kinetics has a significant effect on the cellular detonation and its specific role on the dynamic structure has been discussed in previous chapters. However, there still remains questions regarding various chemical-gasdynamic processes and their mutual interaction within the unstable structure. Due to the complexity within the problem, where unsteady shock-shock and shock-vortex interactions are strongly coupled with chemical kinetics occurred in different scales, it is of great difficulty in conducting direct measurements to further explore such a multi-dimensional transient cellular structure. Apart from the cell size measurement using smoked foil, measurement of other significant length scales such as the hydrodynamic or effective thickness of the detonation is not yet successful. Alternatively, it becomes clear that more insight on the structure can be gained by studying its response to perturbation. In an effort to reveal some characteristic features within the reaction structure, previous attempts have been made on the study of detonation wave response to strong disturbances such as sudden area change, obstacles, density or concentration gradients, porous or acoustic absorbing walls, etc. (Lee 2001). Most of these external perturbations are generally applied at a local position and hence, results may not provide a meaningful conclusion to explain the multi-dimensional unsteady flow field in a average sense. Furthermore, these perturbation studies resulted in multi-dimensional phenomena are generally too complex to permit the problem to be modeled.

In this chapter, the frontal collision between a detonation and a weak shock wave is investigated. This problem has been recently posed in laboratory experiments (Terao *et al.* 2002). Indeed, it appears to offer a simple alternative means to explore the cellular structure through the transient response of the detonation after the head-on collision process. The weak planar shock can serve as a probe to provide a uniform one-dimensional perturbation to determine the average properties of the detonation structure in the direction of propagation. One hopes that such interaction will provide some characteristic length scale which can be easier to measure and can be related to other detonation parameters. The quantifiable perturbation by a weak shock also permits further analytical modeling as to complement the conclusions reached from experimental observations. However, before such technique can be applied to explore the unstable detonation structure and its dependence on the chemical kinetics, various aspects of this head-on collision problem need to be resolved beforehand.

Simple theoretical analysis of the head-on collision problem between a detonation and a shock wave has been carried recently by Ng *et al.* (2004) to establish the correct steady wave configuration. Details of this analysis can be found in Appendix C. The theoretical model simply assumes a steady one-dimensional geometry and treats the detonation wave as a gasdynamic discontinuity, i.e., chemical energy is released

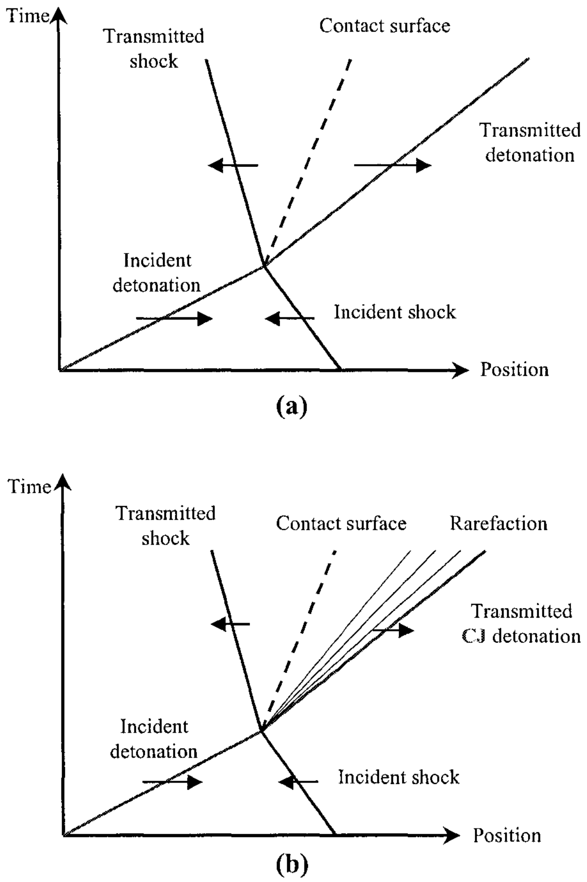

Figure 7.1. Schematic of the two possible one-dimensional wave configuration models for the collision between a detonation with a shock wave.

immediately behind the wave front. It has been shown that there exist multiple solutions to describe the steady wave configuration for the head-on collision problem within the context of this simple theoretical model . The different possible steady wave configurations are illustrated schematically in figure 7.1. The gasdynamic flow field depends on the type of the transmitted detonation and its different solutions are summarized in figure 7.2. Depending on the strength of the incident waves, the simple theoretical analysis has shown that the transmitted detonation can be either strong, or have multiple solutions being either weak or CJ solution followed by a rarefaction fan, which typically occurs in the region of interest of initial conditions (see Appendix C).

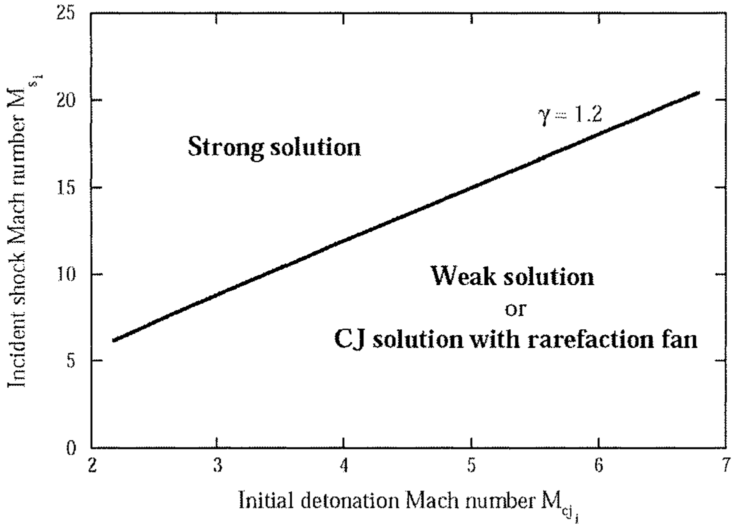

Figure 7.2. Summary of possible solutions for the transmitted detonation with varying incident detonation and incident shock strength based on different wave configurations.

However, the detonation structure and the influence of chemical kinetics are not considered in the above theoretical analysis using a simple model by assuming the detonation as a gasdynamic discontinuity. Knowing that even in the classical model for the detonation structure developed by Zel'dovich (1940), von Neumann (1942) and Döring (1943), the detonation wave structure consists of a leading shock coupled with a finite chemical reaction zone. Because of the presence of the finite reaction zone controlled by chemical kinetics, the steady wave configuration subsequent to the head-on collision will not be achieved 'instantaneously' as with shock waves. It should involve an early non-steady interaction between the shock and the chemical reaction zone behind the leading front of the detonation wave. A relaxation length is expected, which should be at least of the order of the detonation thickness or larger.

The relaxation process may perhaps play a role to determine which steady solution will result after the interaction.

In this study, the head-on collision problem between a detonation and a shock wave is investigated by taking into account the finite structure of the detonation wave. The main focus of this chapter is to describe how the detonation structure and its chemical kinetics respond to the unsteady interaction with the perturbation caused by the weak shock. In addition, by carrying out unsteady computations, the *a priori* assumption of the steady wave configuration can be relaxed. Thus, numerical results can also verify which steady-state solution of the interaction can be approached asymptotically. The significance of the numerical results can then be discussed by comparing with experimental observations.

7.2 Numerical simulation of the transient process

Unsteady numerical simulations are performed by solving the reactive Euler equations using the methodology presented in Chapter 2. In the present study, two chemistry models are used for the computations: single-step and two-step chain-branching kinetic model as described in previous chapters. Inspired from the paper by Oran & DeVore (1994) on the stability of imploding detonations, the motivation of using different kinetic models here is to observe whether using a more realistic chemistry model any new feature of the wave structure during the unsteady process can be observed. The governing equations are then solved numerically using the SLIC scheme with AMR as described in Chapter 2. For all the simulations, an effective numerical resolution of 256 points per corresponding characteristic chemical length of the model (i.e. half-reaction length for the one-step rate law or induction length for the chain-branching kinetic model) is used to ensure the detailed features of the wave front are properly resolved. The computation is initialized by placing a steady-state ZND detonation profile at the left end and a shock wave at the right end, both propagating in the opposite direction.

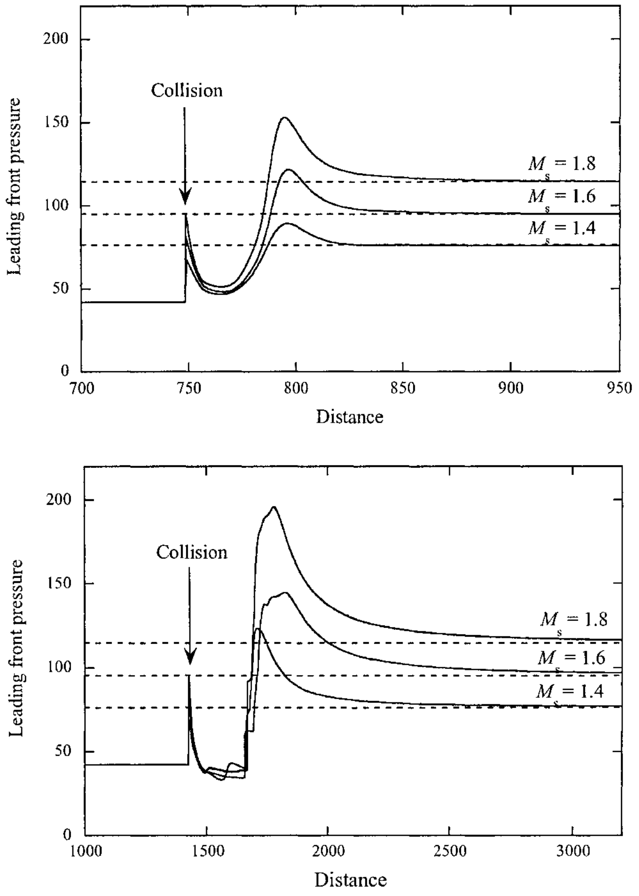

Figure 7.3. Pressure behind the leading front versus position for the detonation using (a) single-step Arrhenius and (b) chain-branching kinetic model. Dashed line represents the VN pressure based on the CJ solution from steady-state analysis for transmitted detonation.

The first series of computations are performed by choosing the chemical parameters such that the detonation is hydrodynamically stable. Figure 7.3 shows the von Neumann (VN) pressure versus front position plot, illustrating the response of the detonation after colliding with the planar shock of different strengths M_{s_i}. It is found that the global features of the phenomenon based on both chemistry models are very similar. In both cases, there exists a relaxation period until the flow field reaches steady-state again. When the incident CJ detonation collides with the shock, a higher pressure at the leading detonation front is obtained. However, that pressure is immediately followed by a decay. The reason is because since the transmitted shock continues to propagate into the finite chemical reaction zone of lower density following behind the leading front of the detonation, an expansion is reflected and causes the detonation to fail. The flow field cannot adjust itself immediately to account for the change caused by the collision and the early time after the interaction is highly transient. The leading front pressure of the transmitted reactive wave continues to decrease until its value close to the pressure behind the transmitted shock and a quasi-steady period can be observed. Due to the high temperature increase caused by the collision, the preheated reactive mixture can lead again the transition to detonation. The mechanism of transition is via the formation of localized explosions by small mixture pockets behind the front, which generate pressure waves and cause the acceleration of the leading front. The re-transition is very similar in nature to direct initiation (Ng & Lee 2003) or DDT (Lee 2001), which involves a sequence of amplification process of pressure waves propagating in an environment that is undergoing various stages of the induction process itself.

The detonation and shock trajectories for the case of $M_{s_i} = 1.6$ are given in figure 7.4. It is found that the results after the long-time development obtained from the numerical computations are well described by the second steady wave configuration shown in figure 7.1b. The transmitted detonation propagates at the CJ speed with respect to the shocked reactive mixture. The VN pressure based on the CJ detonation velocity determined from the steady-state analysis also agrees well with the numerical simulations after the long-term evolution. The transient analysis thus validates the use of the second steady wave configuration (see figure 7.1b and Appendix C) to provide analytically the gasdynamic flow field resulting from the interaction between a detonation and a shock.

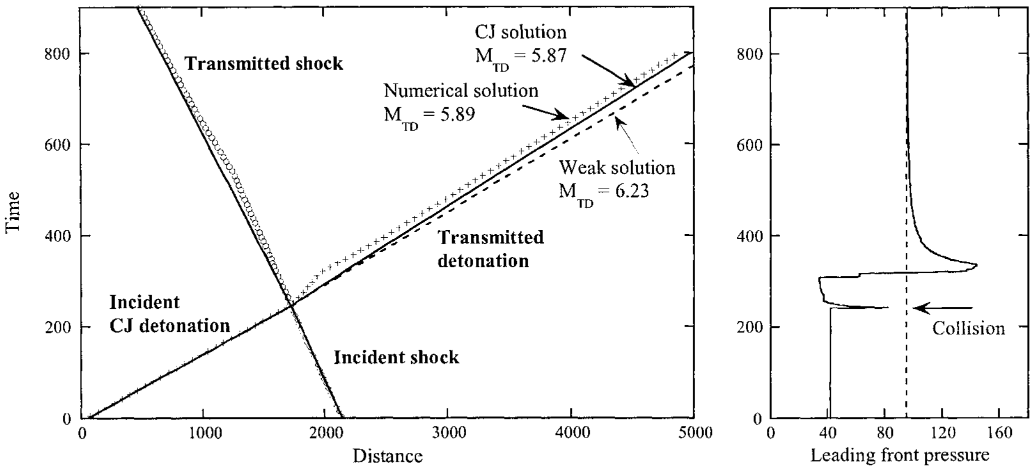

Figure 7.4. $x - t$ diagram showing different wave trajectories from numerical simulations (data points) and steady-state analysis using interaction model of figure 7.1a (dashed line) and figure 7.1b (solid line).

The study proceeds to look at the interaction between an unstable detonation with a planar shock wave. In the one-dimensional case, the unstable detonation is characterized by a nonlinear longitudinal pulsation of the leading front as shown in earlier chapters. Figure 7.5 shows the front pressure versus position plot of the detonation from simulations at different intervals of time. The subsequent phenomenon after collision is very similar to the stable case. However, due to the higher sensitivity of the chemical reaction, the relaxation length is longer compared to that of the stable case. Figure 7.5b indicates that the relaxation length is about 2 oscillation cycles of the incident pulsating detonation. Depending on the incident shock strength, it is also observed that the transmitted detonation wave can be stabilized after collision, characterized by a reduction in oscillation amplitude but with higher frequency (see figure 7.5c). This is due to the increase in thermodynamic state of the unburned mixture by the incident shock, also resulted in an increase of the post-shock temperature of the transmitted detonation. For the single-step Arrhenius model, the stability is governed by the parameter (E_a/RT_s). A higher value of the detonation post-shock temperature brings this parameter below the neutral stability limit curve (Lee & Stewart 1990). Equivalently for the chain-branching kinetic model, an increase in shock temperature makes the induction stage less sensitive to perturbations, which can render the wave to be more stable as discussed in previous chapter of this thesis.

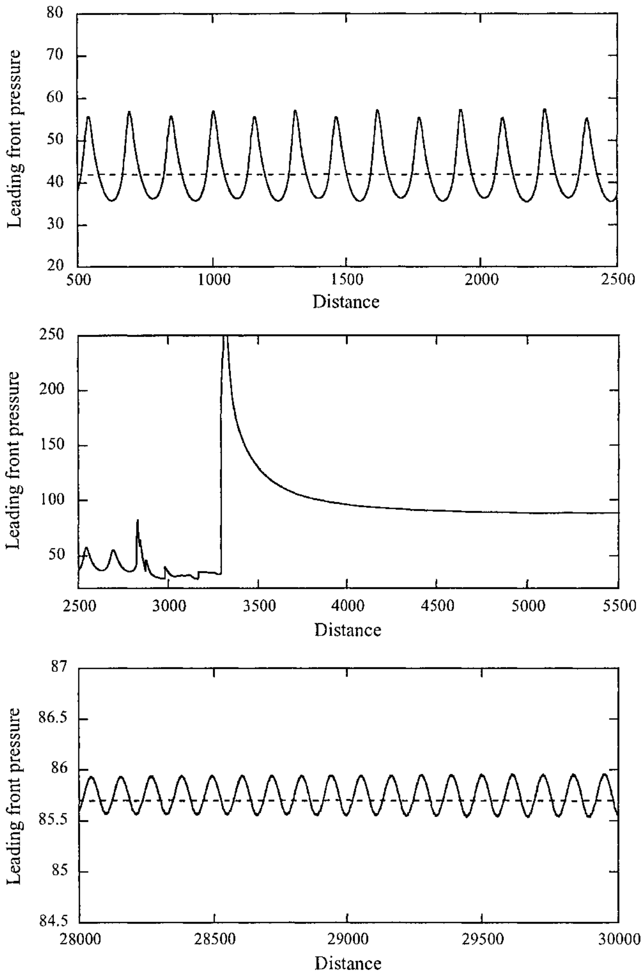

Figure 7.5. Leading front pressure versus position for the unstable detonation using the chain-branching kinetic model (a) before collision; (b) during relaxation process; and (c) after long-time evolution subsequent to the collision. Dashed line represents the VN pressure based on the CJ solution of steady-state analysis for both the incident and transmitted detonations.

7.3 Experimental investigation

In order to establish the significance of different characteristic features obtained from the 1-D numerical simulations on the dynamics of head-on collision phenomenon, the numerical results were compared with experimental observations. In the present study, experiment was carried out in a 6 m long steel tube with an inner diameter of 6 cm. A schematic of the experimental apparatus is shown in figure 7.6. The testing section of the tube was initially evacuated and then filled to the desired initial pressure. A stoichiometric combustible mixture of propane - oxygen was used, which was prepared beforehand in a separate vessel by the method of partial pressures. The high pressure (HP) driver chamber of the tube was used to generate the incident shock wave. A single thin Mylar diaphragm was inserted to separate the different gas in the driver and test section. Various diaphragm thickness was tested to sustain different pressure ratios across it. The shock was generated by filling up the HP section with air until the diaphragm ruptured. Consequently, shock waves having Mach number M_{s_i} from 1.2 - 2.0 were easily generated. Six PCB piezoelectric pressure transducers were mounted along the shock tube side walls for both recording pressure histories and arrival times of different waves. The first pressure transducer was also used as a triggering device for the ignition system to initiate the detonation. Its signal was first going through a delay generator used to adjust the location where collision between the detonation and the shock occurred.

A typical experimental result is displayed in figure 7.7, showing different trajectories resulted from the collision. The theoretical trajectories such as those of the incident detonation and incident shock, the transmitted detonation and transmitted shock (specifically computed from the second wave configuration which imposes the transmitted detonation to have a CJ solution) are sketched in for comparison. The input physical parameters used in the theoretical analysis modelling a stoichiometric propane - oxygen mixture and properties of the model system are summarized

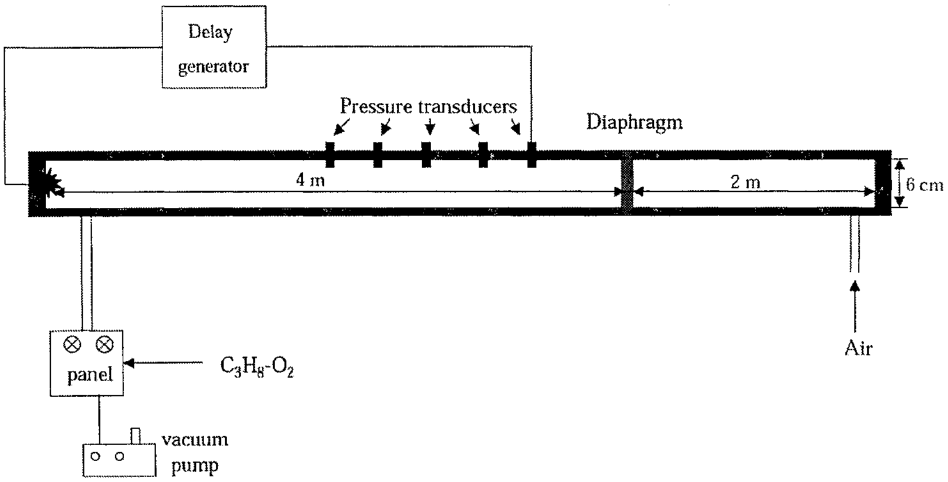

Figure 7.6. Schematic of the experimental apparatus.

in table 7.1. The model reproduces various quantities computed using STANJAN equilibrium code (Reynolds 1986).

From figure 7.7, the results indicate that the transmitted detonation subsequent to the collision matches well the calculated value based on the second wave configuration (figure 7.1b), which fixes the transmitted detonation to be a CJ wave. It should be pointed out that after the transmitted detonation passes $x = 3.2$ m, it slows down. This is due to the fact that there is a contact surface advected from the shock tube (indicated by a dashed line in the $x - t$ diagram), separating the air and the combustible mixture. Once the transmitted detonation passes this contact surface, it no longer propagates into a combustible mixture and therefore, it fails.

The experimental trajectory of the transmitted shock is also found to be close to the theoretical result, but propagates at a slightly higher velocity. This can be explained that there should be a Taylor wave following the incident detonation, which was ignored in the analytical model. It exists to slow down the particle velocity to match the boundary condition of the close ended wall. As the transmitted shock

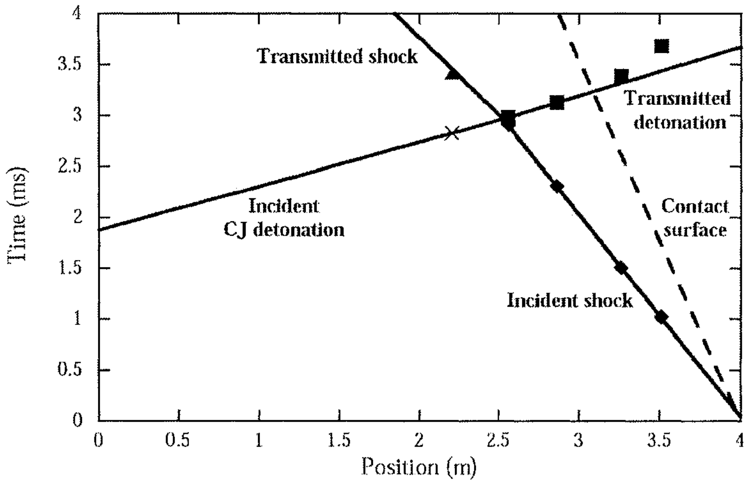

Figure 7.7. $x - t$ diagram showing the comparison between experimental data and theoretical results determined using the second wave configuration shown in figure 7.1b.

propagates into detonation products with continuous decreasing particle velocity, it speeds up in the laboratory frame.

In comparison, different values of wave velocities and pressures are displayed in table 7.2. For the transmitted detonation, there is only about 1.5% difference in velocity between the experimental result and the theoretical CJ solution. While there is larger difference in velocity (about 4.7%) if the experimental data is compared

Quantity	Value	Definition
T_o	298 K	Initial temperature
P_o	0.40 atm	Initial pressure
ρ_o	0.556 kg/m^3	Initial density
γ_r	1.29	Adiabatic (reactant)
γ_p	1.23	Adiabatic (product)
W	0.034 kg/mol	Molecular weight (reactant)
Q	70.50 RT_o/W	Chemical energy release

Table 7.1. Mixture properties used in the theoretical calculation.

Quantity	Experimental	Theoretical	% difference
Incident			
- CJ detonation velocity (m/s)	2321.9 m/s	2318.0 m/s	0.2 %
- shock velocity (m/s)	502.3 m/s	–	–
Transmitted:			
- detonation velocity (m/s)	2083.3 m/s	2052.0 m/s (CJ)	1.5 %
		2184.8 m/s (weak)	4.7 %
- detonation pressure (atm)	28.7 atm	29.9 atm (CJ)	4.0 %
		22.8 atm (weak)	25.9 %
- shock velocity (m/s)	738.7 m/s	629.5 m/s (CJ)	17.3 %

Table 7.2. Comparison between experimental data and theoretical results corresponding to the case shown in figure 7.7.

Incident shock	Transmitted detonation		
M_{s_i}	Experimental	Theoretical CJ	% difference
1.65	2083.3 m/s	2052.0 m/s	1.5 %
1.70	2043.1 m/s	2029.3 m/s	0.7 %
1.72	2041.1 m/s	2022.3 m/s	0.9 %
1.80	1986.1 m/s	1995.0 m/s	0.5 %

Table 7.3. Comparison between experimental and theoretical results based on the CJ solution for the transmitted detonation.

with the weak solution obtained from theoretical analysis. There is also a much larger difference in detonation pressure between the experimental result and the weak solution than that of the CJ solution from theoretical analysis. Similarly, results for the incident detonation collides head-on with different strengths of shock wave M_{s_i} can be found in table 7.3. This table again shows the good agreement between the experimental and theoretical results of a CJ transmitted detonation. Hence, all these results, both from numerical simulations taking into account the reaction structure and from real experiments, clearly suggest that the transmitted detonation is a CJ detonation and the second wave configuration (figure 7.1b) should be a valid one to interpret the phenomenon of head-on collision between a detonation and a shock.

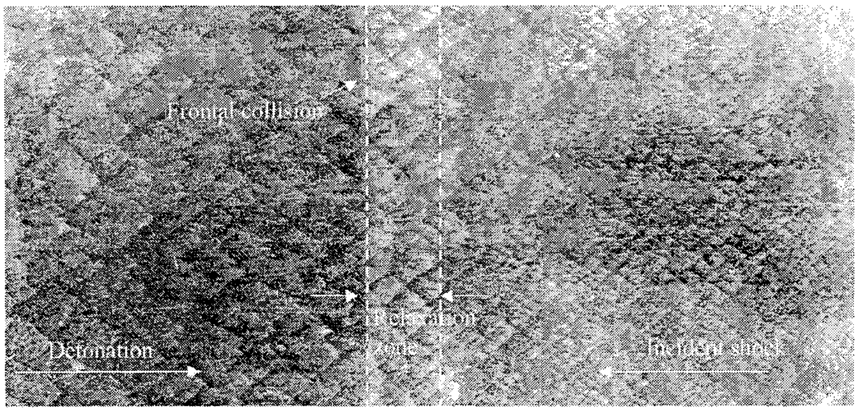

Figure 7.8. Smoked foil record showing the change in structure of the cellular detonation propagating from left to right at shock collision

Although the duality in possible steady wave configurations of the interaction has been resolved, the early non-steady interaction and the effect of chemical kinetics on the head-on collision cannot be fully analyzed from the pressure traces. Some evidences in regard with the relaxation process can perhaps be seen from the smoked foil. Figure 7.8 shows a typical smoked foil obtained from experiment. From this figure, the cellular pattern on the left side (darker region) corresponds to the cell size of the incident detonation propagating to the right. After colliding with the shock, the pattern evolves accordingly and one can see a finite region where transition takes place. It takes roughly 2 cell lengths of the unperturbed detonation to reach again the final steady cellular pattern. This can be referred to as the relaxation process after collision which is observed from the numerical simulations. Another important phenomenon that was observed from the experiment is the significant change in the final cellular structure of the detonation wave, where its pattern is much finer and more regular than that before the head-on collision. This is in accord with the numerical results which show the pulsating detonation, after colliding with a shock, has a smaller amplitude and higher frequency oscillation.

To confirm that the significant reduction in detonation cell size after the interaction is due primarily to thermodynamics (i.e., chemical kinetics) and not to gasdynamics (i.e., the incoming flow generated by the incident shock), some simple chemical kinetic calculations are carried out to see if the predicted cell size corresponding to the thermodynamics state generated by the incident shock agrees well with the experimental results. The prediction is obtained using the correlation developed in Chapter 6. Figure 7.9 plots the ratio between the cell size of the perturbed detonation λ with that of the original incident detonation λ_o versus different incident shock strengths M_{s_i} for initial conditions of stoichiometric propane - oxygen mixture at $P_o = 0.20$ atm and $T_o = 298$ K. For the case corresponding to the conditions used in figure 7.8, results from chemical kinetic calculations show that the cell size will be reduced approximately by a factor of 4, which is in good agreement with that found in this smoked foil from experiment.

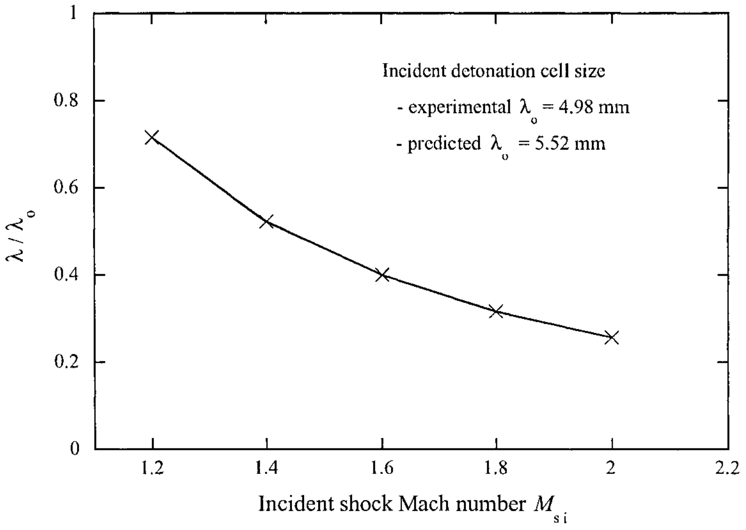

Figure 7.9. Cell size determined from chemical kinetic calculations using Konnov (2000) reaction mechanism.

7.4 Summary

Investigations have been carried out to study the unsteady dynamics of the head-on collision between a detonation and a planar shock wave with consideration of the detonation structure and chemical kinetics. Unsteady numerical simulation is performed to observe the early transient development subsequent to the head-on collision. Using both a single-step rate law as well as a chain-branching kinetic model for the ZND structure, the numerical results show that the early process involves a period of relaxation due to the effect of transient structure in the reaction zone of the detonation. A quasi-steady period and an overshoot for the transmitted detonation subsequent to the head-on collision can be observed (as in direct initiation process), followed by the asymptotic decay again to a CJ detonation as predicted theoretically. Due to the increase in initial thermodynamic state of the reactive mixture caused by the incident shock, the transmitted detonation can become more stable. The numerical results appear also to be in good qualitative agreement with the experimental tendencies by looking at the development of cellular pattern and its regularity for the detonation propagation. The multiplicity of possible steady wave configurations of the interaction is also resolved. It is found that good quantitative agreement was observed between different wave trajectories measured from the experiment and analytical predictions using a simple model imposing the transmitted detonation as a CJ solution followed by a rarefaction fan.

Chapter 8

Conclusions

8.1 Concluding remarks

Detonation waves propagate by means of strong interactions between gasdynamics and chemical reactions. A broad spectrum of dynamics has been reported for which the detonation structure is very sensitive to the chemical kinetics within the reaction zone behind the propagating front. The present study attempted to answer some of the critical issues related to this phenomenon including: how does the chemical kinetics change the dynamic structure of detonations and what are the key chemical kinetic parameters leading to various characteristic features of detonation fronts? These questions have been addressed through an investigation of detonation structure by high-resolution numerical simulations. The chemical models have ranged from simplified single-step reaction kinetics to complex models with detailed chemical reaction schemes.

Analysis of the one-dimensional pulsating detonation with simplified global chemistry model provided some insight on how the dynamic structure is manifested and affected by chemical kinetics. Despite its unstable nature, the dynamic structure of a detonation remains in essence as a self-contained autonomous system. The existence of the limiting characteristic, confirmed by simulation, is an important concept in the study of detonation dynamics as discussed recently also by Kasimov & Stewart (2004) and Radulescu & Lee (2005). It allows the detonation structure to be isolated from any unsteady flow disturbance from the back boundary and maintain its unique propagation.

Within the detonation structure the prominent effect played by the chemical kinetic is clear. As a result of the change in some chemical kinetic parameter, the propagation of the detonation front can go from harmonic oscillations near the stability boundary to highly nonlinear and eventually to chaotic oscillations via a sequence of period-doubling cascade. One important conclusion of this study discusses the strong similarity of these nonlinear properties with those found in a simple dynamical system. Cast in this light, the detonation structure can be viewed as an example of a wide class of phenomenon in classical nonlinear dynamical systems. The present study suggests that recent advance in nonlinear field theories may offer a new direction to the study of detonation structure and different factors that influence it.

One of the major objectives of the present study was to identify the key chemical kinetic factors that influence the dynamic structure of a detonation. This was addressed by using a more detailed chemical kinetic model. Numerical simulations have shown that the shape of the reaction zone profile is as crucial as the temperature sensitivity of the reactions. Since the reaction zone profile cannot be expressed independently by a simple activation energy, it becomes clear that the single-step Arrhenius model, which has been used in most of the earlier theoretical and numerical studies, may not offer a complete chemical kinetic description for characterizing the dynamics of real detonations and predicting quantitative properties. The essential elements of the chemical kinetics are basically the temperature sensitivity, induction zone and chemical energy release zone length. From a physical point of view, the role of these parameters provides the scenario that incoherence in the exothermicity can lead to gasdynamic instabilities in the reaction zone resulted in different behaviors of the detonation front. As a result of the above conclusion, an appropriate non-dimensional stability parameter χ was introduced in this study. It is defined as the activation energy for the induction process ε_I multiplied by the ratio of the induction length Δ_I to the reaction length Δ_R. The reaction length Δ_R is estimated by the inverse of the maximum thermicity $(1/\dot{\sigma}_{\max})$ multiplied by the Chapman-Jouguet particle velocity u'_{cj}. The definition that has been introduced for this parameter holds for essentially arbitrary kinetic models of gaseous mixtures and can be easily obtained from the ZND analysis.

Although most of the analyses in this research are derived from the simplest one-dimensional configuration, they can still provide useful information related to the dynamic structure of real detonations. Indeed, comparisons of the one-dimensional numerical results with 2-D simulations and experimental data demonstrate that the regularity of cellular detonation structure and the 1-D detonation instability are inter-related. The use of stability parameter and neutral stability curve to assess and characterize the regularity of cellular detonations was also justified through some illustrations. For instance, the cell regularity and the strength of the transverse waves for mixtures with different amounts of argon dilution can be attributed to the degree of stability of the detonation structure. It is also interesting to note from the 1-D simulation that with argon dilution less than approximately 70%, a one-dimensional time-dependent detonation cannot self-propagate, resulting from the quenching of chemical reactions due to large temperature fluctuations. This limit agrees well with the experimental value at which transverse waves are necessary for the propagation of detonations and at which the loss of regularity in the cellular pattern occurs. This limit implies that a one-dimensional shock-induced ignition mechanism in an unstable detonation is insufficient to account for the propagation mechanism of multi-dimensional detonations observed experimentally. The effect of going to higher dimensions and the presence of transverse waves begin to play the dominant role. These results perhaps provide some explanations why a real detonation wave must display such a complicated structure with an ensemble of interacting transverse shock waves in order to sustain its propagation.

The final aspect of this research is how all these different findings discussed so far contribute toward the determination of an appropriate length scale for the detonation wave, such that different dynamic parameters can be estimated. A practical application that can be obtained from the above conclusion is the extension of classical detonation model for cell size prediction. It is clear from the research of the past decade that the linear correlation of the cell size with a chemical length scale is insufficient and that a stability parameter characterizing the cell regularity must be included. The parameter χ appears to be an intrinsic detonation property of different mixtures and provides a quantitative measure of the stability. In this work, an improved correlation has been derived by incorporating this parameter to take into consideration the instability effect for cell size prediction from chemical kinetics. The improved correlation provides a better approximation to the experimental cell size than the standard single-parameter constant relationship with induction length. The model retains the simplicity for predicting the detonation cell size in a straightforward manner from the ZND analysis, making the present correlation useful as a reliable tool for engineering estimates.

However, the use of such empirical correlation should not be overestimated. It is no doubt that the correlation is not derived from a scientific but rather an empirical approach. For instance, correlation with the reaction zone width computed from the ZND model takes no account of the multidimensional structure of the wave. The highly nonlinear interactions between fluid dynamics and chemistry that are actually occurring at the cellular detonation front are simply being ignored. Although attempt has been made here to include a stability parameter to account for these effects, but a much more rigorous theory is still no doubt necessary.

In fact, recent advances in detonation theory begin to challenge the sound basis of the cell size as a fundamental parameter for unstable multidimensional cellular detonations. Experimentally, it is rather challenging or even impossible to estimate one characteristic cell size from a typical smoked foil pattern. The smoked foil records usually reveal a spectrum of cell sizes and deducing a single representative cell dimension requires one's own judgment and experience, thus making the characteristic cell size somehow arbitrary. Without a definitive unique value for λ, the various criteria based on it are also approximate and can only serve as a guideline.

Such irregularity in the cell pattern can be originated from the turbulence effects inside the reaction zones. Turbulent fluctuations cause the presence of multimoded substructures, which make determination of the cell widths difficult. Because of the non-uniqueness of cell width for common ordinary fuel-air detonations, future developments in detonation theory should perhaps be toward the derivation of an appropriate thickness of cellular detonation as a characteristic length scale by taking into consideration details of the different chemical-gasdynamic processes and turbulent fluctuations involving in the unstable detonation structure.

The final part of this thesis investigates the problem of head-on collision problem between a detonation and a planar shock wave. The motivation was to achieve a better description on the coupling between gasdynamics and chemical reaction processes inside the unsteady detonation structure by looking at the response of the detonation subject to a weak shock perturbation. The significance of the finite reaction zone and chemical kinetics on the dynamics of this unsteady interaction has been first described through numerical simulations. It appears that there are few interesting results that future research should pursue in detail. The numerical results from the one-dimensional simulation show that a relaxation process consisting of a quasi-steady period and an overshoot for the transmitted detonation subsequent to the head-on collisions can be observed, followed by the asymptotic decay to a CJ detonation as predicted theoretically. For unstable pulsating detonations, it is found that due to the increase in the thermodynamic state of the reactive mixture caused by the shock resulting in a change of chemical kinetics, the transmitted pulsating detonation can become more stable with smaller amplitude and period oscillation. These observations appear to be in good agreement with experimental tendencies by looking at the development of cellular pattern and its regularity for the detonation propagation. Further investigation should be carried out in future to explore, even just within the one-dimensional context, the gasdynamics during the relaxation process, which should provide some insight in regards with the attenuation and amplification processes inside the incident detonation structure. In addition, the relaxation length appears to be a measurable length scale which may be useful to characterize the detonation structure. Experimentally, the smoked foil pattern can provide a ready means of obtaining a measure of the relaxation length of the interaction. The appearance of finer cells is equivalent to the re-initiation process shown in the one-dimensional numerical simulation, which should indicate the end of the relaxation process. Attempts can perhaps be made to relate this relaxation length to other detonation parameters such as the detonation thickness.

In conclusion, the present study demonstrates some interesting nonlinear dynamic features of the detonation waves originating from the change in chemical kinetics in the reaction zone. This study also reveals the importance of using realistic chemistry in future studies of the detonation structure and proposes a simple technique for future experimental investigation. Together with well-established chemical kinetic mechanisms, some representative parameter or length scale that characterizes the reaction zone and a good database of experimental data for a wide range of initial and boundary conditions, detonation models can be developed to achieve the capability of predicting various detonation dynamic parameters.

8.2 Contributions to knowledge

This work contributes to the understanding of the dynamic structure of detonation waves from the point of view of chemical reaction kinetics. The present investigation elucidates through numerical analyses different aspects of the self-organized dynamic structure arising from the chemical kinetic effect within the reaction zone of detonation waves. With the inclusion of a more realistic chemistry model, the present study clarified important chemical kinetic factors influencing dynamics of the detonation structure. It permitted one to rationalize several experimental observations on the real structure of cellular detonation waves. In particular, results have implications for establishing the characterization of cell regularity with chemical kinetic parameters, elucidating the propagation mechanism and for predicting the detonation sensitivity and its thickness for a given combustible mixture.

References

[1] Abouseif, G. E. & Toong, T. Y. (1982) Theory of unstable detonations. *Combust. Flame* **45**, 67-94

[2] Alpert, R. L. & Toong, T. Y. (1972) Periodicity in exothermic hypersonic flows about blunt projectiles. *Astro. Acta.* **17**, 539-560

[3] Aminallah, M., Brossard, J. & Vasiliev, A. (1993) Cylindrical detonations in methane-oxygen-nitrogen mixtures. *Prog. Astronaut. Aeronaut.* **153**, 203-228

[4] Anile, A. M., Nikiforakis, N. & Pidatella, R. M. (2000) Assessment of a high resolution centered scheme for the solution of hydrodynamical semiconductor equations. *SIAM J. Sci. Comput.* **22**, 1533-1548

[5] Barthel, H. O. (1974) Predicted spacings in hydrogen-oxygen-argon detonations. *Phys. Fluids* **17**(8), 1547-1553

[6] Belles, F. E. (1959) Detonability and chemical kinetics: Prediction of limits of detonability of hydrogen. *Proc. Combust. Inst.* **7**, 745-751

[7] Berger, M. J. & Colella, P. (1989) Local adaptive mesh refinement for shock hydrodynamics. *J. Comput. Phys.* **82**, 64-84

[8] Berger, M. J. & LeVeque, R. J. (1998) Adaptive mesh refinement using wave-propagation algorithms for hyperbolic systems. *SIAM J. Numer. Anal.* **35**, 2298-2316

[9] Berger, M. J. & Oliger, J. (1984) Adaptive mesh refinement for hyperbolic partial differential equations. *J. Comput. Phys.* **53**, 484-512

[10] Bourlioux, A. & Majda, A. J. (1992) Theoretical and numerical structure for unstable two-dimensional detonations. *Combust. Flame* **90**, 211-229

[11] Bourlioux, A., Majda, A. J., & Roytburd, V. (1991) Theoretical and numerical structure for unstable one-dimensional detonations. *SIAM J. Appl. Math.* **51,** 303-343

[12] Bull, D. C., Elsworth, J. E., Shuff, P. J. & Metcalfe, E. (1982) Detonation cell structures in fuel/air mixtures. *Combust. Flame* **45**, 7-22

[13] Chue, R. S. (1993) *High Speed Deflagration and its Transition to Detonation.* PhD Thesis, McGill University, Montréal, Canada

[14] Ciccarelli, G., Ginsberg, T., Boccio, J., Economos, C., Sato, K. & Kinoshita, M. (1994) Detonation cell size measurements and predictions in hydrogen-air-steam mixtures at elevated temperatures. *Combust. Flame* **99**, 212-220

[15] Ciccarelli, G., Ginsberg, T., Boccio, J., Finfrock, C., Gerlach, L., Tagawa, H. & Malliakos, A. (1997) Detonation cell size measurements in high-temperature hydrogen-air-steam mixtures at the BNL high-temperature combustion facility. *Brookhaven National Laboratory Technical Report* BNL-NUREG-52482

[16] Clifford, L. J., Milne, A. M., Turanyi, T. & Boulton, D. (1998) An induction parameter model for shock-induced hydrogen combustion simulations. *Combust. Flame* **113**, 106-118

[17] Courant, R. & Friedrichs, K. O. (1946) *Supersonic Flow and Shock Waves.* Springer-Verlag, New York

[18] Deiterding, R. (2000) Simulation of a shock tube experiment with non-equilibrium chemistry. *Technical Report, Brandenburgische Technische Universität Cottbus.* NMWR-00-3

[19] Denisov, Y. N. & Troshin, Y. K. (1959) Pulsating and spinning detonation of gaseous mixtures in tubes. *Dokl. Akad. Nauk SSSR* **125**, 110-113

[20] Desbordes, D. (1990) Aspects stationnaires et transitoires de la detonation dans les gaz: relation avec la structure cellulaire du front. PhD thesis, Universite de Poitiers

[21] Dionne, J. P. (2000) *Numerical Study of the Propagation of Non-Ideal Detonations.* PhD Thesis, McGill University, Montréal, Canada

[22] Dold, J. W. & Kapila, A. K. (1991) Comparison between shock initiations of detonation using thermally-sensitive and chain-branching chemical models. *Combust. Flame* **85**, 185-194

[23] Döring, W. (1943) On detonation processes in gases. *Ann. Phys.* **43**, 421-436

[24] Eckmann, J. P. (1981) Roads to turbulence in dissipative dynamical systems. *Rev. Mod. Phys.* **53**, 643-654

[25] Eckmann, J. P. & Ruelle, D. (1985) Ergodic theory of chaos and strange attractors. *Rev. Mod. Phys.* **57,** 617-656

[26] Eckmann, J. P., Kamphorst, S. O., Ruelle, D. & Ciliberto, S. (1986) Lyapunov exponents from time series. *Phys. Rev. A* **34**(6), 4971-4979

[27] Erpenbeck, J. J. (1962) Stability of steady-state equilibrium detonations. *Phys. Fluids* **5**, 604-614

[28] Erpenbeck, J. J. (1964) Stability of idealized one-reaction detonations. *Phys. Fluids* **7,** 684-696

[29] Erpenbeck, J. J. (1967) Nonlinear theory of unstable one-dimensional detonations. *Phys. Fluids* **10**, 274-288

[30] Feigenbaum, M. J. (1978) Quantitative universality for a class of nonlinear transformations. *J. Stat. Phys.* **19**(1), 25-52

[31] Feigenbaum, M. J. (1983) Universal behavior in nonlinear systems. *Physica D* **7,** 16-39

[32] Feigenbaum, M. J. (1983) Low dimensional dynamics and the period doubling scenario. *Lecture notes in physics* **179,** 131-148

[33] Fickett, W. & Davis, W. C. (1979) *Detonation.* Berkeley, CA: University of California Press

[34] Fickett, W. & Wood, W. W. (1966) Flow calculations for pulsating one-dimensional detonations. *Phys. Fluids* **9**, 903-916

[35] Frank, W. J. (1957) Interaction of a shock wave with a wire screen. *Univ. Toronto Inst. Aerophysics UTIA Technical Notes* **13**

[36] Fujiwara, T. & Reddy, K. V. (1989) Propagation mechanism of detonation-Three-dimensional phenomena. *Memoirs of the Faculty of Engineering,* Nagoya University **41**, 1-18

[37] Gamezo, V. N., Desbordes, D. & Oran, E. S. (1999) Formation and evolution of two-dimensional cellular detonations. *Combust. Flame* **116**,154-165

[38] Gavrikov, A. I., Efimenko, A. A. & Dorofeev, S. B. (2000) A model for detonation cell size prediction from chemical kinetics. *Combust. Flame* **120**, 19-33

[39] Guirao, C. M., Knystautas, R. & Lee, J. H. S. (1989) A summary of hydrogen-air detonation experiments. *Sandia National Laboratories Report* SAND87-7128

[40] Guirao, C. M., Knystautas, R., Lee, J. H. S., Benedick, W. & Berman, M. (1982) Hydrogen-air detonations. *Proc. Combust. Inst.* **19**, 583-590

[41] Guirguis, R., Oran, E. S. & Kailasanath, K. (1986) The effect of energy release on the regularity of detonation cells in liquid nitromethane. *Proc. Combust. Inst.* **21**, 1639-1668

[42] Hao, B. L. (1984) *Chaos, An Introduction and Reprints Volume.* World Scientific Publishing Co., Singapore, 1-576

[43] He, L. & Lee, J. H. S. (1995) The dynamical limit of one-dimensional detonations. *Phys. Fluids* **7**(5), 1151-1158

[44] Helzel, C. (2000) *Numerical Approximation of Conservation Laws with Stiff Source Term for the Modelling of Detonation Waves.* Thesis, Otto-von-Guericke Universität Magdeburg

[45] Hern, S. D. (1999) *Numerical Relativity and Inhomogeneous Cosmologies.* PhD thesis, University of Cambridge, UK

[46] Hwang, P., Fedkiw, R. P., Merriman, B., Aslam, T. D., Karagozian, A. R. & Osher, S. J. (2000) Numerical resolution of pulsating detonation waves. *Combust. Theory Modelling* **4**, 217-240

[47] Im, K. S., Yu, S. T., Kim, C. K., Chang, S. C. & Jorgenson, P. C. E. (2002) Application of the CE/SE method to detonation with realistic finite-rate chemistry. *AIAA Paper 2002-1020, the 40th AIAA Aerospace Sciences Meeting & Exhibit, Reno, NV, Jan. 14-17, 2002*

[48] Kaneshige, M. & Shepherd, J. E. (1997) Detonation database. *GALCIT Technical Report FM97* (web page at *http://www.galcit.caltech.edu/detn_db/html/db.html*)

[49] Kantz, H. (1994) A robust method to estimate the maximal Lyapunov exponent of a time series. *Phys. Lett. A* **185**, 77-87

[50] Kapila, A. K., Schwendeman, D. W., Quirk, J. J. & Hawa, T. (2002) Mechanisims of detonation formation due to a temperature gradient. *Combust. Theory. Model.* **6**, 553-594

[51] Kaplan, D. & Glass, L. (1995) *Understanding Nonlinear Dynamics.* Springer, New York

[52] Kasimov, A. R. (2004) *Theory of Instability and Nonlinear Evolution of Self-Sustained Detonation Waves.* PhD thesis, University of Illinois at Urbana-Champaign, Urbana, Illinois

[53] Kasimov, A. R. & Stewart, D. S. (2004) On the dynamics of self-sustained one-dimensional detonations: a numerical study in the shock-attached frame. *Phys. Fluids* **16**(10), 3566-3578

[54] Kee, R. J., Rupley, F. M. & Miller, J. A. (1989) Chemkin-II: a Fortran chemical kinetics package for the analysis of gas-phase chemical kinetics. *Sandia National Laboratories Report* SAND89-8009

[55] Knystautas, R., Lee, J. H. & Guirao, C. M. (1982) The critical tube diameter for detonation failure in hydrocarbon-air mixtures. *Combust. Flame* **48**, 63-83

[56] Knystautas, R., Guirao, C. M., Lee, J. H. & Sulmistras, A. (1984) Measurement of cell size in hydrocarbon-air mixtures and predictions of critical tube diameter, critical initiation energy, and detonability limits. *Prog. Astronaut. Aeronaut.* **94**, 23-37

[57] Konnov, A. A. (2000) Detailed reaction mechanism for small hydrocarbons combustion. Release 0.5 (*http://homepages.vub.ac.be/~akonnov/*)

[58] Laberge, S., Knystautas, R. & Lee, J. H. S. (1993) Propagation and extinction of detonation waves in tube bundles. *Prog. Astronaut. Aeronaut.* **153**, 381-396

[59] Lee, J. H. S. (1972) Gasdynamics of detonations. *Astro. Acta* **17**, 455–466

[60] Lee, J. H. S. (1984) Dynamic parameters of gaseous detonations. *Ann. Rev. Fluids Mech.* **16**, 311-336

[61] Lee, J. H. (1996) On the critical tube diameter. *Dynamics of Exothermicity* (Bowen, J.R. Ed.), Gordon and Breech Publishers, Netherlands, 321-336

[62] Lee, J. H. S. (2001) Detonation waves in gaseous explosives. *Handbook of Shock Waves Vol. III*, (Ben-Dor, G., Igra, O. & Elperin T. Ed.), Academic Press, 309–415.

[63] Lee, J. H. S., Soloukhin, R. I. & Oppenheim, A. K. (1969) Current views on gaseous detonations. *Astro. Acta.* **14**, 565-584

[64] Lee, J. H. S., Knystautas, R. M., Guirao, C., Benedick, W. B. & Shepherd, J. E. (1982) Hydrogen-Air detonations. *Sandia National Laboratories Report* SAND82-2456

[65] Lee, H. I. & Stewart, D. S. (1990) Calculation of linear detonation instability: one-dimensional instability of planar detonations. *J. Fluid Mech.* **216**, 103-132

[66] Lewis, B. & von Elbe, G. (1951) *Combustion, Flames, and Explosions of Gases.* Academic Press, New York

[67] Li, J., Zhao, Z. W., Kazakov, A. & Dryer, F. L. (2004) An updated comprehensive kinetic model of hydrogen combustion. *Int. J. Chem. Kinet.* **36**, 566-575

[68] Li, T. Y. & Yorke, J. A. (1975) Period three implies chaos. *Amer. Math. Monthly* **82,** 985-992

[69] Libouton, J. C., Dormal, M. & Van Tiggelen, P. J. (1975) The role of chemical kinetics on structure of detonation waves. *Proc. Combust. Inst.* **15**, 79-86

[70] Lutz, A. E., Kee, R. J., Miller, J. A., Dwyer, H. A. & Oppenheim, A. K. (1988) Dynamic effects of autoignition centers for hydrogen and C1,2-hydrocarbon fuels. *Proc. Combust. Inst.* **22,** 1683-1693

[71] May, R. M. (1973) *Stability and Complexity in Model Ecosystems.* Princeton University Press

[72] May, R. M. (1976) Simple mathematical models with very complicated dynamics. *Nature* **261**, 459-467

[73] Manzhalei, V. I. (1977) Fine structure of the leading front of a gaseous detonation. *Fizika Gorenija i Vzryva* **13** (3), 470-472

[74] Manzhalei, V. I., Mitrofanov, V. V. & Subbotin, V. A. (1974) Measurement of inhomogeneities of a detonation front in gas mixtures at elevated pressures. *Combust. Explos. Shock Waves* **10**(1), 89-95

[75] Mazaheri, B. K. (1997) *Mechanism of the Onset of Detonation in Blast Initiation.* PhD thesis, McGill University, Montreal, Canada

[76] McVey, J. B. & Toong, T. Y. (1971) Mechanisms of instabilities of exothermic hypersonic blunt-body flows. *Combust. Sci. Tech.* **3**, 63-76

[77] Meyer, J. W. & Oppenheim, A. K. (1971a) Coherence theory of the strong ignition limit. *Combust. Flame* **17**, 65-68

[78] Meyer, J. W. & Oppenheim, A. K. (1971b) On the shock-induced ignition of explosive gases. *Proc. Combust. Inst.* **13,** 1153-1164

[79] Moen, I. O., Sulmistras, A., Thomas, G. O., Bjerketvedt, D. & Thibault, P. A. (1986) Influence of cellular regularity on the behavior of gaseous detonations. *Prog. Astronaut. Aeronaut.* **106**, 220-243

[80] Moen, I. O., Funk, J. W., Ward, S. A., Rude, G. M. & Thibault, P. A. (1984) Detonation length scales for fuel-air explosives. *Prog. Astronaut. Aeronaut.* **94,** 55-79

[81] Moen, I. O., Ward, S. A., Thibault, P. A., Lee, J. H. S., Knystautas, R., Dean, T. & Westbrook, C.K. (1984), The influence of diluents and inhibitors on detonations. *Proc. Combust. Inst.* **20**, 1717-1726

[82] Mueller, M. A., Yetter, R. A. & Dryer, F. L. (1999) Flow reactor studies and kinetic modeling of the H_2/O_2 reaction. *Int. J. Chem. Kinet.* **31**, 113-125

[83] Nessyahu, H. & Tadmor, E. (1990) Non-oscillatory central differencing for hyperbolic conservation laws. *J. Comput. Phys.* **87**, 408-463

[84] Ng, H. D. & Lee, J. H. S. (2003) Direct initiation of detonation with a multistep reaction scheme. *J. Fluid Mech.* **476**, 179-211

[85] Ng, H. D., Nikiforakis, N. & Lee, J. H. S. (2004) Head-on collision of a detonation with a planar shock wave. *Proc. 24th Int. Sym. Shock Waves*, Vol. 2, 745-750, Beijing, China

[86] Ng, H. D., Radulescu, M. I., Higgins, A. J., Nikiforakis, N. & Lee, J. H. S. (2005) Numerical Investigation of the instability for one-dimensional Chapman-Jouguet detonations with chain-branching kinetics. *Combust. Theory. Model.* (In press)

[87] Ng, H. D., Higgins, A. J., Kiyanda, C. B., Radulescu, M. I., Lee, J. H. S., Bates, K. R. & Nikiforakis, N. (2005) Nonlinear dynamics and chaos analysis of one-dimensional pulsating detonations. *Combust. Theory. Model.* **9**, 159-170

[88] Oppenheim, A. K. (1985) Dynamic features of combustion. *Phil. Trans R. Soc. A* **315,** 471-508

[89] Oppenheim, A. K., Urtiew, P. A. & Stern, R. A. (1959) Peculiarity of shock impingement on area convergence. *Phys. Fluids* **2**(4), 427–431

[90] Oran, E. S. & Boris, J. P. (1987) *Numerical Simulation of Reactive Flow.* Elsevier Science Ltd.

[91] Oran, E. S. & DeVore, C. R. (1994) The stability of imploding detonations: results of numerical simulations. *Phys. Fluids* **6**(1), 369–380

[92] Oran, E. S., Young, T. R., Boris, J. P. & Cohen, A. (1982) Weak and strong ignition. I. Numerical simulation of shock tube experiments. *Combust. Flame* **48**, 135-148

[93] Papalexandris, M. V., Leonard, A. & Dimotakis, P. E. (1997) Unsplit schemes for hyperbolic conservation laws with source terms in one space dimension. *J. Comput. Phys.* **134,** 31-61

[94] Peters, N. (1991) Reducing mechanisms. *Lecture Notes in Physics* **384**, 48-67

[95] Plewa, T. (1999) Adaptive mesh refinement for structured grids. (web page at *http://www.camk.edu.pl/~tomek/AMRA/amr.html*)

[96] Quirk, J. J. (1994) Godunov-type schemes applied to detonation flows. *Combustion in High-Speed Flows* (Buckmaster, J. *et al.* Ed.), Dordrecht: Kluwer, 575-596

[97] Radulescu, M. I. (2003) *The Propagation and Failure Mechanism of Gaseous Detonations: Experiments in Porous-Walled Tubes.* PhD thesis, McGill University, Montreal, Canada

[98] Radulescu, M. I. & Lee, J. H. S. (2002) The failure mechanism of gaseous detonations - Experiments in porous wall tubes. *Combust. Flame* **131**, 29-46

[99] Radulescu, M. I. & Lee, J. H. S. (2005) On the hydrodynamic thickness of cellular detonations. Submitted to *Combust. Expl. Shock Waves*

[100] Radulescu, M. I., Ng, H. D., Lee, J. H. S. & Varatharajan, B. (2002) The effect of argon dilution on the stability of acetylene-oxygen detonations. *Proc. Combust. Inst.* **29,** 2825-2831

[101] Reynolds, W. C. (1986) *The Element Potential Method for Chemical Equilibrium Analysis: Implementation in the Interactive Program STANJAN.* (3rd Ed.) Mechanical Engineering Department, Stanford University

[102] Rosenstein, M. T., Collins, J. J. & De Luca, C. J. (1993) A practical method for calculating largest Lyapunov exponents from small data sets. *Physica D* **65**, 117-134

[103] Sánchez, A. L., Carretero, M., Clavin, P. & Williams, F. A. (2001) One-dimensional overdriven detonations with branched-chain kinetics. *Phys. Fluids* **13**, 776-792

[104] Schultz, E. & Shepherd, J. E. (2000) Validation of detailed reaction mechanisms for detonation simulation. *GALCIT Technical Report FM99-5*

[105] Sharpe, G. J. (1997) Linear stability of idealized detonations. *Proc. R. Soc. Lond. A* **453**, 2603-2625

[106] Sharpe, G. J. (2000) Numerical simulations of pulsating detonations: I. Nonlinear stability of steady detonations. *Combust. Theory. Model.* **4**, 557-574

[107] Sharpe, G. J. (2001) Transverse waves in numerical simulations of cellular detonations. *J. Fluid Mech.* **447**, 31-51

[108] Sharpe, G. J. (2002) Shock-induced ignition for a two-step chain-branching kinetics model. *Phys. Fluids* **14**, 4372-4388

[109] Sharpe, G. J. & Falle, S. A. E. G. (1999) One-dimensional numerical simulations of idealized detonations. *Proc. R. Soc. Lond. A* **455**, 1203-1214

[110] Sharpe, G. J. & Falle, S. A. E. G. (2000) One-dimensional nonlinear stability of pathological detonations. *J. Fluid Mech.* **414**, 339-366

[111] Sharpe, G. J. & Short, M. (2003) Detonation ignition from a temperature gradient for a two-step chain-branching kinetics model. *J. Fluid Mech.* **476**, 267-292

[112] Shchelkin, K. I. & Troshin, Y. K. (1965) *Gasdynamics of Combustion.* Mono Book Co., Baltimore

[113] Shepherd, J. E. (1986) Chemical kinetics of hydrogen-air-diluent mixtures. *Prog. Astro. Aeronaut.* **106**, 263-293

[114] Shepherd, J. E., Moen, I. O., Murray, S. B. & Thibault, P. A. (1986) Analyses of the cellular structure of detonations. *Proc. Combust. Inst.* **21**, 1649-1658

[115] Short, M. (2001) A nonlinear evolution equation for pulsating Chapman-Jouguet detonations with chain-branching kinetics. *J. Fluid Mech.* **430**, 381-400

[116] Short, M. & Dold, J. W. (1996) Linear stability of a detonation wave with a model three-step chain-branching reaction. *Math. Comput. Model.* **24**, 115-123

[117] Short, M. & Quirk, J. J. (1997) On the nonlinear stability and detonability limit of a detonation wave for a model three-step chain-branching reaction. *J. Fluid Mech.* **339**, 89-119

[118] Short, M. & Sharpe, G. J. (2003) Pulsating instability of detonations with a two-step chain-branching reaction model: theory and numerics. *Combust. Theory. Model.* **7**, 401-416

[119] Short, M., Kapila, A. K. & Quirk, J. J. (1999) The chemical-gas dynamic mechanisms of pulsating detonation wave instability. *Phil. Trans. R. Soc. Lond. A* **357**, 3621-3637

[120] Sichel, M., Tonello, N. A., Oran, E. S. & Jones, D. A. (2002) A two-step kinetics model for numerical simulation of explosions and detonations in H_2-O_2 mixtures. *Proc. R. Soc. Lond.* A **458**, 49-82

[121] Soloukhin, R. I. (1969) Nonstationary phenomena in gaseous detonation. *Proc. Combust. Inst.* **12**, 799-807

[122] Stamps, D. W. & Tieszen, S. R. (1991) The influence of initial pressure and temperature on hydrogen-air-diluent detonations. *Combust. Flame* **83**, 353-364

[123] Stamps, D. W., Benedick, W. B. & Tieszen, S. R. (1991) Hydrogen-air-diluent detonation study for nuclear reactor safety analyses. *Sandia National Laboratories Report* SAND89-2398

[124] Strang, G. (1964) Accurate partial difference methods. II. Non-linear problems. *Numer. Math.* **6**, 37-64

[125] Strehlow, R. A. (1969) The nature of transverse waves in detonations, *Astro. Acta.* **5**, 539-548

[126] Strehlow, R. A., Liangminas, R., Watson, R. H. & Eyman, J. R. (1967) Transverse wave structure in detonations. *Proc. Combust. Inst.* **11**, 683-692

[127] Taki, S. & Fujiwara, T. (1978) Numerical analysis of two-dimensional non-steady detonations. *AIAA J.* **16**, 73-77

[128] Takai, R., Yoneda, K. & Hikita, T. (1974) Study of detonation wave structure. *Proc. Combust. Inst.* **15**, 69-78

[129] Taylor G. I. (1950) The dynamics of the combustion products behind plane and spherical detonation fronts in explosives. *Proc. R. Soc. Lond. A* **200**, 235-247

[130] Terao, K., Yoshida, T., Kishi, K. & Ishii, K. (2002) Interaction between shock and detonation waves. *Proc. 18th Int. Colloquium on the Dynamics of Explosions and Reactive Systems*, Seattle, USA

[131] Tieszen, S. R., Stamps, D. W., Westbrook, C. K. & Pitz, W. J. (1991) Gaseous hydrocarbon - air detonations. *Combust. Flame* **84**, 376-390

[132] Tieszen, S. R., Sherman, M. P., Benedick, W. B. & Berman, M. (1987) Detonability of H_2-air-diluent mixtures. *Sandia National Laboratories Report* SAND85-1263

[133] Tieszen, S. R., Sherman, M. P., Benedick, W. B., Shepherd, J. E., Knystautas, R. & Lee, J. H. S. (1986) Detonation cell size measurements in hydrogen-air-steam mixtures. *Prog. Astronaut. Aeronaut.* **106**, 205-219

[134] Toro, E. F. (1997) *Riemann Solvers and Numerical Methods for Fluids Dynamics.* 1st Edition, Springer-Verlag

[135] Toro, E. F. (2003) Multi-stage predictor-corrector fluxes for hyperbolic equations. *Isaac Newton Institute for Mathematical Sciences Preprint Series* NI03037-NPA, University of Cambridge, UK

[136] Toro, E. F. & Billett, S. J. (2000) Centred TVD schemes for hyperbolic conservation laws. *IMA J. Numer. Anal.* **20**, 47-79

[137] Ul'yanitskii, V. Y. (1981) Role of flashing and transverse wave collisions in the evolution of a multifrontal detonation wave structure in gases. *Fizika Goreniya Vzryva* **17**, 227

[138] Vandermeiren, M. & Van Tiggelen, P. J. (1984) Cellular structure in detonation of acetylene-oxygen mixture. *Prog. Astronaut. Aeronaut.* **94**, 104-117

[139] Varatharajan, B. & Williams, F. A. (2001) Chemical-kinetic descriptions of high-temperature ignition and detonation of acetylene-oxygen-diluent systems. *Combust. Flame* **124**, 624-645

[140] Vermeer, D. J., Meyer, J. W. & Oppenheim, A. K. (1972) Auto-ignition of hydrocarbons behind reflected shock waves. *Combust. Flame* **18**, 327-336

[141] Voitsekhovskii, B. V., Mitrofanov, V. V. & Topchian, M. E. (1958) Optical studies of transverse detonation waves. *Izv. Sibirsk. Otd. Acad. Nauk SSSR* **9**, 44

[142] Voitsekhovskii, B. V., Mitrofanov, V. V. & Topchian, M. E. (1966) The structure of a detonation front in gases. *Rep. FTD-MT-64-527*, Foreign Technology Division, Wright-Patterson A.F.B., Ohio

[143] von Neumann, J. (1942) Theory of detonation wave. *John von Neumann, collected works. Vol. 6.* New York: Macmillan

[144] Voyevodsky, V. V. & Soloukhin, R. I. (1965) On the mechanism and explosion limits of hydrogen-oxygen chain self-ignition in shock waves. *Proc. Combust. Inst.* **10**, 279-283

[145] Westbrook, C. K. & Urtiew, P. A. (1982) Chemical-kinetic prediction of critical parameters in gaseous detonations. *Proc. Combust. Inst.* **19**, 615-623

[146] White, D. R. (1961) Turbulent structure of gaseous detonation. *Phys. Fluids* **4**, 465-480

[147] Wolf, A., Swift, J. B., Swinney, L. H. & Vastano, J. A. (1985) Determining Lyapunov exponent from a time series. *Physica D* **16**, 285-317

[148] Zaidel, R. M. (1961) Stability of detonation waves in gas. Mixtures. *Dokl. Akad. Nauk SSSR* **136**, 1142–1145

[149] Zel'dovich, Y. B. (1940) On the theory of the propagation of detonation in gaseous systems. *Zh. Eksp. Teor. Fiz.* **10**, 542-568

[150] Zhang, F., Chue, R. S., Lee, J. H. S. & Klein, R. (1998) A nonlinear oscillator concept for one-dimensional pulsating detonations. *Shock Waves* **8**, 351-359

Appendices

Appendix A

Derivation of the nonlinear oscillator model for 1D detonations

In this appendix, the nonlinear oscillator model proposed by Zhang *et al.* (1998) will be derived from the basic conservation laws of gasdynamics. The formulation considers a control volume shown in figure A.1. It moves with the detonation complex and is bounded by the leading shock front and a rear boundary. A suitable choice for that rear boundary can be defined by the limiting characteristic and its location can be estimated from the numerical simulation. The distance between the leading shock and the limiting characteristic is referred to as the hydrodynamic thickness $\tilde{l}_h$. Nevertheless, the exact location of this rear boundary is not required for the formulation of the oscillator equation and it is sufficient to assume such rear boundary exists.

Assume that the time-averaged velocity of the detonation front is in good agreement with the steady-state CJ values $\tilde{D}_{cj}$. i.e.

$$\tilde{D}_{cj} = \frac{1}{\tilde{\tau}} \int_{0}^{\tilde{\tau}} \tilde{D}\left(\tilde{t}\right) d\tilde{t} \tag{A.1}$$

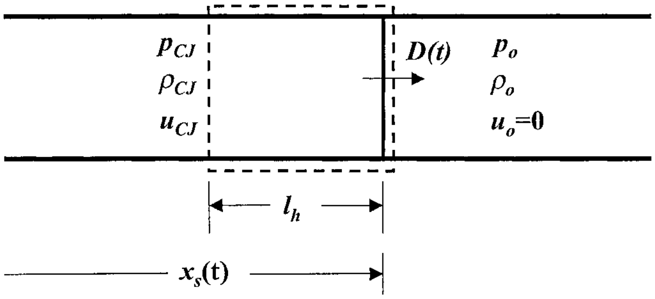

Figure A.1. Control volume for the formulation of the nonlinear oscillator model

Therefore, the instantaneous shock front location $\tilde{x}_s$ can be given by:

$$\tilde{x}_s = \tilde{D}_{cj} \cdot \tilde{t} + \tilde{F}\left(\tilde{t}\right) \tag{A.2}$$

where $\tilde{F}(t)$ denotes the displacement of the shock front from its mean trajectory and satisfies:

$$\frac{1}{\tilde{\tau}} \int\limits_0^{\tilde{\tau}} \tilde{F}\left(\tilde{t}\right) d\tilde{t} = 0 \tag{A.3}$$

Differentiating equation A.2 gives the shock velocity as:

$$\dot{\tilde{x}}_s(t) = \tilde{D}_{cj} + \dot{\tilde{F}}(t) \tag{A.4}$$

where $\dot{\tilde{F}}(t)$ is the fluctuating velocity with respect to its time-averaged part, $\tilde{D}_{cj}$. The fluctuation of the shock trajectory $\tilde{F}(t)$ is first chosen as the dependent variable in the oscillator equation to be formulated.

In a shock-attached coordinate, the conservation equations of mass, momentum and energy for the control volume shown in figure A.1 can be written as:

$$
\begin{aligned}
&\frac{d}{d\tilde{t}}\int_0^{\tilde{l}_h} \tilde{\rho}\, d\tilde{x} + \tilde{\rho}_{cj}\left(\tilde{D} - \tilde{u}_{cj}\right) - \tilde{\rho}_o \tilde{D} = 0 \\
&\frac{d}{d\tilde{t}}\int_0^{\tilde{l}_h} \tilde{\rho}\left(\tilde{D} - \tilde{u}\right) d\tilde{x} + \tilde{\rho}_{cj}\left(\tilde{D} - \tilde{u}_{cj}\right)^2 - \tilde{\rho}_o \tilde{D}^2 = -\tilde{p}_{cj} + \tilde{p}_o + \int_0^{\tilde{l}_h} \tilde{\rho}\frac{d\tilde{D}}{d\tilde{t}} d\tilde{x} \\
&\frac{d}{d\tilde{t}}\int_0^{\tilde{l}_h} \tilde{\rho}\left[\tilde{e}_i + \frac{\left(\tilde{D} - \tilde{u}\right)^2}{2}\right] d\tilde{x} + \tilde{\rho}_{cj}\left(\tilde{D} - \tilde{u}_{cj}\right)\left[\tilde{e}_{i,cj} + \frac{\left(\tilde{D} - \tilde{u}_{cj}\right)^2}{2} + \frac{\tilde{p}_{cj}}{\tilde{\rho}_{cj}}\right] \\
&\qquad - \tilde{\rho}_o \tilde{D}\left(\tilde{e}_{i,o} + \frac{\tilde{D}^2}{2} + \frac{\tilde{p}_o}{\tilde{\rho}_o}\right) = \tilde{Q}\int_0^{\tilde{l}_h} \tilde{\rho}\tilde{\Omega}\, d\tilde{x} + \int_0^{\tilde{l}_h} \tilde{\rho}\frac{d\tilde{D}}{d\tilde{t}}\left(\tilde{D} - \tilde{u}\right) d\tilde{x}
\end{aligned}
\tag{A.5}
$$

where $\tilde{\rho}$, $\tilde{u}$, $\tilde{p}$ and $\tilde{e}_i$ are the density, particle velocity in lab frame, pressure and the specific internal energy, respectively. $\tilde{Q}$ and $\tilde{\Omega}$ represent the amount of heat release and the reaction rate. The subscript "o" refers to the quiescent state and the subscript "CJ" denotes the Chapman-Jouguet equilibrium state. By combining with the continuity and momentum equations, the energy equation can be re-arranged as follows:

$$
\frac{d}{d\tilde{t}}\int_0^{l_h} \tilde{\rho}\tilde{e}\, d\tilde{x} + \tilde{\rho}_{cj}\tilde{e}_{cj}\left(\tilde{D} - \tilde{u}_{cj}\right) - \tilde{\rho}_o \tilde{e}_o \tilde{D} - \tilde{p}_{cj}\tilde{u}_{cj} = \tilde{Q}\int_0^{\tilde{l}_h} \tilde{\rho}\tilde{\Omega}\, d\tilde{x} \tag{A.6}
$$

where the variable $\tilde{e}$ is the specific total energy as a sum of both the internal and kinetic energy, $\tilde{e} = \tilde{e}_i + \frac{\tilde{u}^2}{2}$.

For a steady ZND detonation where $\tilde{D}(\tilde{t}) = \tilde{D}_{cj}$, the unsteady integral term is canceled and equation A.6 reduces to

$$
\tilde{\rho}_{cj}\tilde{e}_{cj}\left(\tilde{D}_{cj} - \tilde{u}_{cj}\right) - \tilde{\rho}_o \tilde{e}_o \tilde{D}_{cj} - \tilde{p}_{cj}\tilde{u}_{cj} = \tilde{Q}\int_0^{\tilde{l}_h} \tilde{\rho}^o \tilde{\Omega}^o d\tilde{x} \tag{A.7}
$$

where superscript "o" refers to the steady ZND solution. The integral term on the above equation is given by

$$\int_0^{\tilde{l}_h} \tilde{\rho}^{o}\tilde{\Omega}^{o} d\tilde{x} = \tilde{\rho}_o \tilde{D}_{cj} \tag{A.8}$$

which simply states that the rate of reactant depletion inside the control volume is equal to the unburned mass flux entering the control volume for the steady ZND wave. If the steady state equation A.7 is subtracted from equation A.6, one obtains

$$\frac{d}{d\tilde{t}}\int_0^{l_h} \tilde{\rho}\tilde{e} d\tilde{x} + \tilde{\rho}_{cj}\tilde{e}_{cj}\dot{\tilde{F}} = \tilde{Q}\int_0^{\tilde{l}_h} \tilde{\rho}\tilde{\Omega} d\tilde{x} - \tilde{Q}\tilde{\rho}_o\tilde{D}_{cj} \tag{A.9}$$

where the term $\tilde{\rho}_o\tilde{e}_o\dot{\tilde{F}}$ has been neglected since $\tilde{\rho}_o\tilde{e}_o/\tilde{\rho}_{cj}\tilde{e}_{cj}$ is of the order $1/M_{cj}^2 << 1$.

Consistent with the normalization used in this investigation, the dimensional flow variables have been made non-dimensional and equation A.9 becomes:

$$\frac{d}{dt}\int_0^{l_h} \rho e dx + \rho_{cj}e_{cj}\dot{F} = Q\int_0^{l_h} \rho\Omega dx - QD_{cj} \tag{A.10}$$

It may also be useful to express both the reaction rate and total energy in the following non-dimensional volume-averaged quantities:

$$\Psi = \int_0^1 \frac{\rho\Omega}{D_{cj}l_h^{-1}} d\zeta \tag{A.11}$$

$$I = \int_0^1 \frac{\rho e}{D^2/2} d\zeta \tag{A.12}$$

where $\zeta = x/l_h$. Using these definitions, equation A.10 can be rewritten as:

$$l_h I\ddot{F} + \frac{\rho_{cj}e_{cj}}{D}\dot{F} + \frac{l_h D}{2}\dot{I} = \frac{D_{cj}Q}{D}\Psi_1 \tag{A.13}$$

where $\ddot{F}$ and $\dot{F}$ are the non-dimensional shock acceleration and the fluctuation of the shock velocity with respect to the steady ZND wave. $\Psi_1 = \Psi - 1$ is the fluctuation of the dimensionless mean rate of the reaction depletion within the control volume. $\dot{I}$ denotes the rate of the fluctuation of the non-dimensional total specific energy inside the control volume since:

$$\begin{aligned}\dot{I} = \frac{d}{dt}\left(I - I^o\right) &= \frac{d}{dt}\left(\int_0^1 \frac{\rho e}{D^2/2} d\zeta - \int_0^1 \frac{\rho^o e^o}{D_{cj}^2/2} d\zeta\right) \\ &= \frac{d}{dt}\int_0^1 \frac{\rho e}{D^2/2} d\zeta \qquad \text{(A.14)}\end{aligned}$$

Equation A.13 essentially gives a balance relation of the rate of energy fluctuation for the control volume. The first term on the left hand side denotes the energy fluctuation rate associated with the shock velocity oscillation. The second term corresponds to the unsteady exit condition at the rear boundary. The third term represents the rate of the energy fluctuation within the control volume itself, and the term on the right hand side denotes the fluctuation of the chemical energy release rate inside the control volume. Note that equation A.13 has the form of a second order nonlinear differential equation in terms of the variable F similar to that describing a nonlinear oscillator.

It is perhaps possible to rewrite equation A.13 in a more analogous form of a nonlinear oscillator (Zhang *et al.* 1998). Assuming that the shock speed is slowly varying compared to the time scale l_h/D_{cj} (i.e., $l_h/D_{cj} << \tau$), the integrands for a mass element can be expressed, to leading order, in terms of the shock speed at time t',

$$D_{cj} + \dot{F}\left(t'\right) = D_{cj} + \dot{F}\left(t\right) - \left(t - t'\right)\ddot{F}\left(t\right) + O\left[\left(t - t'\right)\right] \qquad \text{(A.15)}$$

In this situation, at any time, the structure of the detonation looks like that of a stationary wave traveling at speed $D_{cj} + \dot{F}\left(t\right)$, but with corrections due to the wave acceleration $\ddot{F}(t)$. Without carrying out the details here of the necessary integrations, the following asymptotic results should be expected,

$$\frac{d}{dt}\int_0^{l_h} \rho e dx = \Phi(t) = \Phi^0\left(\dot{F}(t)\right) + \Phi^1\left(\dot{F}(t)\right)\ddot{F}(t) + \ldots \qquad (A.16)$$

$$Q\int_0^{l_h} \rho\Omega dx - QD_{cj} = \Psi(t) = \Psi^0\left(\dot{F}(t)\right) + \Psi^1\left(\dot{F}(t)\right)\ddot{F}(t) + \ldots \qquad (A.17)$$

where the higher order corrections of the asymptotic expansions are neglected. The quantities Φ^0 and Ψ^0 are respectively the energy and the rate of heat release inside the control volume for a stationary wave traveling at speed $D_{cj} + \dot{F}(t)$. Φ^1 and Ψ^1 correspond to the coefficients of the temporal change of the energy and the rate of heat release caused by the wave acceleration, respectively. Substituting the above expansion into equation A.10 gives the following equation:

$$\Phi^1\left(\dot{F}\right)\dddot{F} + \left(\rho_{cj}e_{cj}\dot{F} - \Psi^0\left(\dot{F}\right)\right) + \left(\frac{d\Phi^0\left(\dot{F}\right)}{d\dot{F}} + \frac{d\Phi^1\left(\dot{F}\right)}{d\dot{F}}\ddot{F} - \Psi^1\left(\dot{F}\right)\right)\ddot{F} = 0 \qquad (A.18)$$

The above equation is in essence the balance relation of the rate of the energy fluctuation recast in a form of a second-order differential equation with respect to $\dot{F}(t)$. Comparing equation A.18 with the classical nonlinear oscillator equation, i.e.

$$m\ddot{x} + kx = \mu f(x, \dot{x})$$

The analogy is clear. It can be seen that the first term $\Phi^1\left(\dot{F}\right)\dddot{F}$ can indeed represent the inertia force (i.e. $m\ddot{x}$), the second term $\left(\rho_{cj}e_{cj}\dot{F} - \Psi^0\left(\dot{F}\right)\right)$ is similar to the spring or restoring force (i.e. kx) in which $\Psi^0\left(\dot{F}\right)$ provides a possible "nonlinear restoring force" responsible for different nonlinear instabilities. The final term $\left(\frac{d\Phi^0(\dot{F})}{d\dot{F}} + \frac{d\Phi^1(\dot{F})}{d\dot{F}}\ddot{F} - \Psi^1\left(\dot{F}\right)\right)\ddot{F}$ represents the self-excited driving force (i.e. $\mu f(x, \dot{x})$) that provides the damping responsible for the oscillatory behavior.

Appendix B

Derivation of the ZND equations with detailed chemistry

In this appendix, the ZND equations with detailed chemistry will be formulated. The derivation begins with the one-dimensional steady Euler conservation equations written in terms of a reference frame attached to the shock:

$$\begin{aligned}
\frac{d}{dx'}\left(\rho u'\right) &= 0 && \text{(B.1)}\\
\frac{d}{dx'}\left(\rho u'^2 + p\right) &= 0 && \text{(B.2)}\\
\frac{d}{dx'}\left[\left(\rho E + p\right) u'\right] &= 0 && \text{(B.3)}\\
\frac{d}{dx'}\left(\rho u' Y_i\right) &= \dot{\omega}_i W_i \qquad (i = 1, \ldots, N_s) && \text{(B.4)}
\end{aligned}$$

where x' and u' is the relative distance and particle velocity in the shock-attached coordinate (i.e. $u' = D - u$ where D is the steady detonation velocity); E is the total energy per unit mass which includes both the internal and kinetics energies. To be more convenient, it is written in the following form in terms of the mixture enthalpy

h per unit mass:

$$E = h - \frac{p}{\rho} + \frac{u'^2}{2} \tag{B.5}$$

For an ideal gas, the above expression can also be written as:

$$E = h - R_s T + \frac{u'^2}{2} \tag{B.6}$$

where R_s is the specific gas constant (i.e. $R_s = R\sum_{i=1}^{N_s} \frac{Y_i}{W_i}$). To solve for the ZND equations, the above equation is first differentiated with respective to distance x'. This yields:

$$\frac{dE}{dx'} = \frac{d}{dx'}\sum_{i=1}^{N_s} Y_i h_i - R_s \frac{dT}{dx'} - T\sum_{i=1}^{N_s} \frac{\partial R_s}{\partial Y_i}\frac{dY_i}{dx'} + u'\frac{du'}{dx'} \tag{B.7}$$

After expanding the derivatives using the chain rule and some re-arrangement, it can be expressed as:

$$\frac{dE}{dx'} = \frac{dT}{dx'}\left\{\sum_{i=1}^{N_s} Y_i \frac{dh_i}{dT} - R_s\right\} + \sum_{i=1}^{N_s}\left[\frac{dY_i}{dt'}\left\{\frac{h_i}{u'} - \frac{T}{u'}\frac{\partial R_s}{\partial Y_i}\right\}\right] + u'\frac{du'}{dx'} \tag{B.8}$$

By differentiating the ideal gas equation of state, the derivative $\frac{dT}{dx'}$ can be written as:

$$\begin{aligned} \frac{dT}{dx'} &= \frac{\partial T}{\partial p}\frac{dp}{dx'} + \frac{\partial T}{\partial \rho}\frac{d\rho}{dx'} + \frac{\partial T}{\partial R_s}\frac{dR_s}{dx'} \\ &= \frac{1}{\rho R_s}\frac{dp}{dx'} - \frac{p}{\rho^2 R_s}\frac{d\rho}{dx'} - \frac{p}{\rho u' R_s^2}\sum_{i=1}^{N_s}\frac{\partial R_s}{\partial Y_i}\frac{dY_i}{dt'} \end{aligned} \tag{B.9}$$

It may now be useful to rewrite the conservation equations B1 - B3 in a more appropriate format, i.e.:

$$u'\frac{d\rho}{dx'} = -\rho\frac{du}{dx'} \tag{B.10}$$

$$\frac{dp}{dx'} = -2\rho u'\frac{du'}{dx'} - u'^2\frac{d\rho}{dx'} \tag{B.11}$$

$$\frac{du'}{dx'}(\rho E + p) + u'\left[E\frac{d\rho}{dx'} + \rho\frac{dE}{dx'} + \frac{dp}{dx'}\right] = 0 \tag{B.12}$$

The above system can now be combined with the expression for dE/dx' and dT/dx' given by equations B.8 and B.9. After a number of algebraic manipulation, an expression involving only du'/dx' is obtained:

$$\frac{du'}{dx'} = \frac{1}{u'}\left[\sum_{i=1}^{N_s}\frac{dY_i}{dt'}\left\{\frac{R_s h_i}{\sum_{j}^{N_s} Y_j \frac{dh_j}{dT}} - T\frac{\partial R_s}{\partial Y_i}\right\}\right] \cdot \left[u' - \frac{R_s T}{u'} - \frac{u' R_s}{\sum_{j}^{N_s} Y_j \frac{dh_j}{dT}}\right]^{-1} \tag{B.13}$$

This equation for du'/dx' can be further simplified by introducing the following thermodynamics relationships:

$$C_p = \sum_{i=1}^{N_s} Y_i \frac{dh_i}{dT} \tag{B.14}$$

$$C_p - C_v = R \tag{B.15}$$

$$\gamma = \frac{C_p}{C_v} \tag{B.16}$$

$$c_f = \sqrt{\frac{\gamma p}{\rho}} = \sqrt{\gamma R_s T} \tag{B.17}$$

$$\frac{1}{R_s} = \frac{1}{R\sum_{i=1}^{N_s}\frac{Y_i}{W}} = \frac{W}{R} \quad ; \quad \frac{\partial R_s}{\partial Y_i} = R\sum_{i=1}^{N_s}\frac{1}{W_i} \tag{B.18}$$

where W is the mean molecular weight; C_p and C_v denote the heat capacity at constant pressure and constant volume, respectively; γ is the specific heat ratio and c_f is the frozen sound speed at fixed composition. Combining these expressions with equation B.13 gives:

$$\frac{du'}{dt'} = \frac{du'}{dx'}\frac{dx'}{dt'} = u'\frac{\dot{\sigma}}{1 - M^2} \tag{B.19}$$

in which $M = \frac{u'}{c_f}$ is the local Mach number of the flow and $\dot{\sigma}$ is often referred to as the thermicity parameter:

$$\dot{\sigma} = \sum_{i=1}^{N_s}\left(\frac{W}{W_i} - \frac{h_i}{C_p T}\right)\frac{dY_i}{dt'} \tag{B.20}$$

Using the conservation of mass and momentum equations B.10 and B.11, the derivative for other flow variable can be obtained as follows:

$$\frac{dp}{dt'} = -\rho {u'}^2 \frac{\dot{\sigma}}{1-M^2} \tag{B.21}$$

$$\frac{d\rho}{dt'} = -\rho \frac{\dot{\sigma}}{1-M^2} \tag{B.22}$$

Along with the chemical kinetic equation and prescribed boundary conditions, i.e.,

$$\frac{dY_i}{dt'} = \frac{\dot{\omega}_i W_i}{\rho} \qquad (i = 1, \ldots, N_s) \tag{B.23}$$

the system of equations can readily be integrated to obtain the steady ZND detonation structure.

Appendix C

Theoretical analysis of the shock-detonation collision problem

A class of shock wave interaction phenomena, such as the collision of a shock with wire screens (Franks 1957) or shock wave interaction with an abrupt area change (Oppenheim *et al.* 1959) has been studied extensively in the past. Solutions for the steady gasdynamic flow fields of these phenomena are generally obtained by guessing a self-similar wave pattern, which is then validated if the conservation laws of mass, momentum, and energy can be satisfied. However, it has been shown that multiple wave configurations might satisfy all the conservation laws for these problems considered, depending on different parameters such as incident shock strength or area ratio, etc. Accordingly, in this Appendix, the theoretical analysis recently carried out by Ng *et al.* (2004) on the head-on collision problem between a detonation and a planar shock to establish the correct steady gasdynamic flow field is summarized. Different possible steady wave configurations that can take place after the long-time evolution subsequent to the collision the head-on interaction of a detonation with a shock are presented.

C.1 Possible steady wave configurations

The interaction can be described by a schematic of the $x - t$ wave diagram shown in figure C.1. Upon the collision of a detonation with a shock wave, a shock is transmitted into the upstream product. A transmitted detonation continues to move downstream into the shocked reactant, which is followed by a contact surface separating the gas mixture behind each transmitted wave. Unlike the interaction of two plane shock waves, different gasdynamic flow field can be obtained depending on the nature of the transmitted detonation.

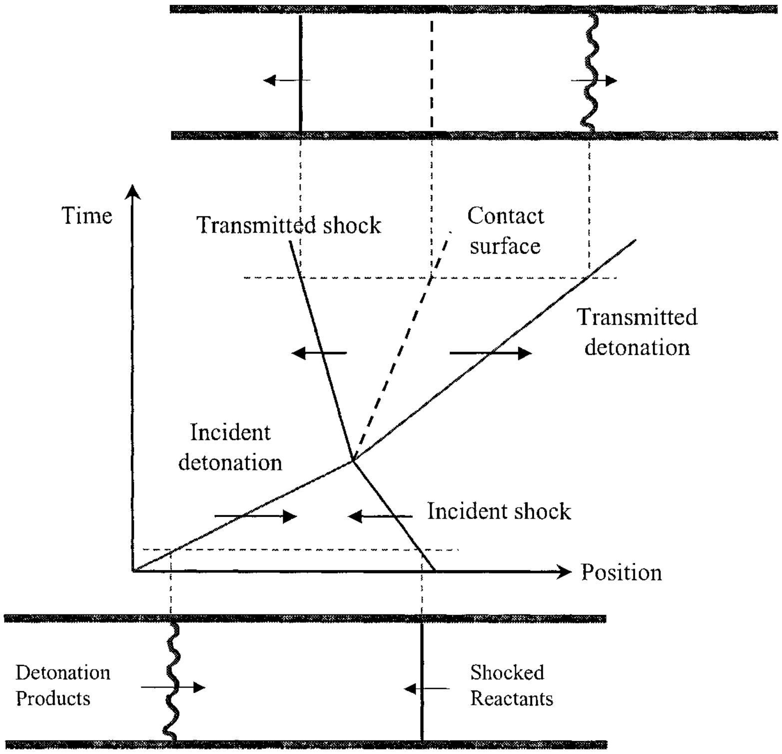

Figure C.1. Schematic of the first one-dimensional wave configuration model for the collision between a detonation with a shock wave.

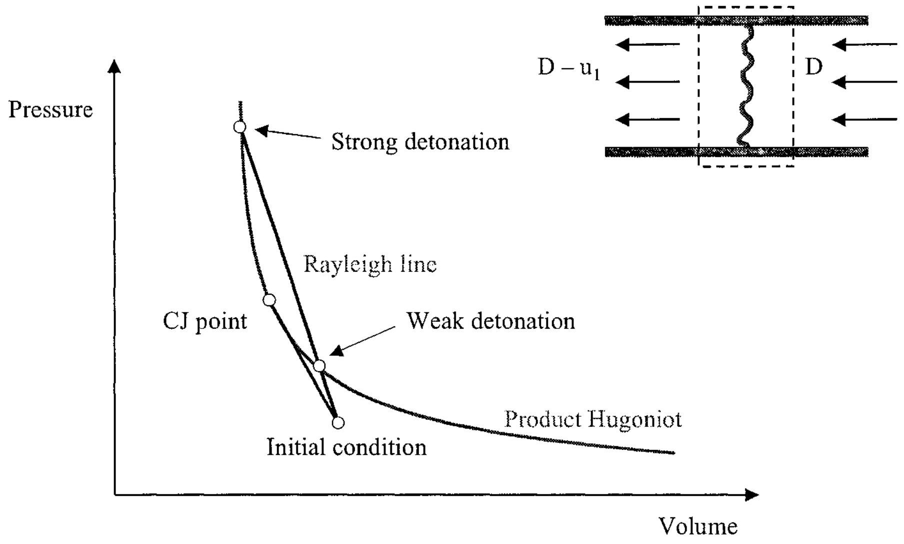

Figure C.2. Pressure - specific volume diagram illustrating different detonation solutions.

The classical Chapman-Jouguet theory assumes the detonation to be steady, planar and one-dimensional. The state behind the detonation can be determined using conservation equations applied to a control volume surrounding the wave, as shown in figure C.2. The possible solutions can be illustrated by graphical representation in the pressure - specific volume ($p - \nu$) plane. The figure displays the product Hugoniot curve obtained from the conservation of mass and energy, which determines the locus of the possible solutions behind the detonation. The Rayleigh line, which is a linear relationship between pressure and specific volume derived from the conditions of mass and momentum conservation, is also shown in the $p - \nu$ diagram. The intersection of product Hugoniot and Rayleigh line defines the steady detonation states. In general, the Rayleigh line crosses the Hugoniot curve in two distinct solutions. The high pressure solution is called the strong solution terminated on the subsonic branch of the equilibrium Hugoniot curve, while the lower pressure one is referred to as the weak solution with the flow being supersonic behind the wave. The particular case where the Rayleigh line and the product Hugoniot are tangent is called the Chapman-Jouguet detonation, which provides a unique minimum detonation speed. At the CJ point, the flow behind the detonation is sonic. In general, the $x - t$ wave diagram shown in figure C.1 can therefore yield three different gasdynamic flow fields according to whether the transmitted detonation is strong, weak or CJ from the matching across the contact surface.

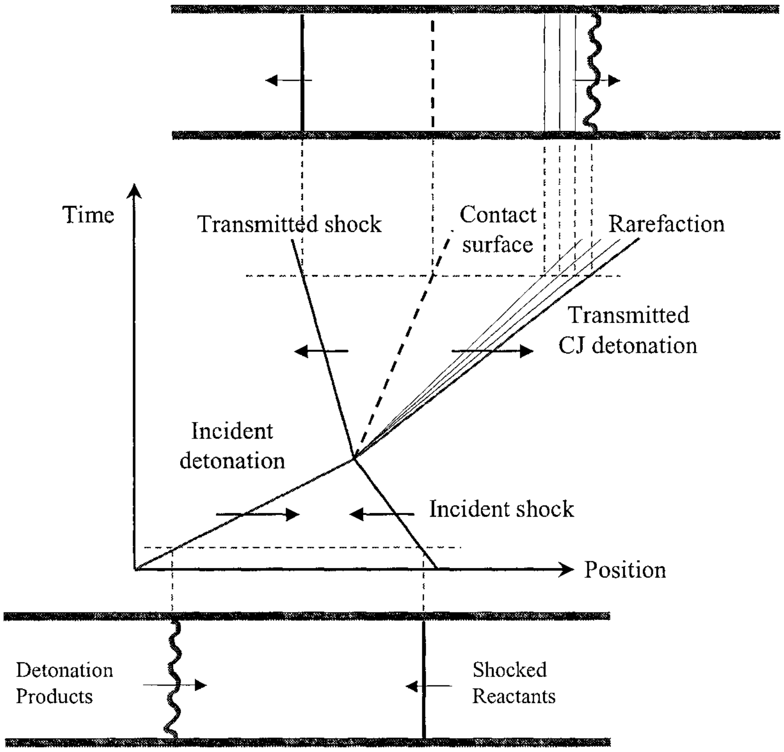

Figure C.3. Schematic of the second one-dimensional wave configuration model for the collision between a detonation with a shock wave.

Experimentally, it has been well observed that all self-sustained detonations in smooth tube propagate at the CJ velocity. For the present shock - detonation interaction problem, one may intuitively impose the transmitted detonation to be a CJ solution which depends only on the conditions ahead of it. In this case, an additional wave pattern may be necessary to relax this constraint on the transmitted detonation. To do so, a rarefaction may be needed behind the transmitted detonation to match the boundary condition in the flow field and it is totally valid due to the sonic condition behind the CJ detonation wave. This second wave configuration is shown schematically in figure C.3.

Based on all the above considerations, it appears that there exist multiple solutions to describe the steady wave configuration for the head-on collision of a detonation with a shock wave.

C.2 Theoretical analysis

A simple model is considered to determine analytically different flow properties after the head-on collision. It assumes a steady one-dimensional geometry and treats the detonation wave as a gasdynamic discontinuity, i.e. chemical energy is released immediately behind the wave front. The flow behind the incident shock and incident detonation are uniform.

To solve the complete flow field for each wave configuration discussed previously (figure C.4), the task is to seek a solution that satisfies the Rankine-Hugoniot (RH) relationships across each wave and the boundary conditions for the problem under consideration. For a non-reactive shock, the properties across its front are simply given by the normal shock relationships:

$$\frac{\rho_+}{\rho_-} = \frac{(\gamma+1)\,M_s^2}{2+(\gamma-1)\,M_s^2} \tag{C.1}$$

$$\frac{p_+}{p_-} = \frac{2\gamma M_s^2-(\gamma-1)}{(\gamma+1)} \tag{C.2}$$

$$\frac{u_+}{c_-} = \frac{2}{\gamma+1}\left(M_s-\frac{1}{M_s}\right) \tag{C.3}$$

For the detonation wave, the RH relationships can be written as:

$$\frac{\rho_-}{\rho+} = \frac{D-u_+}{D-u_-} = \frac{\gamma_+\left(\gamma_- + \eta \mp s\right)}{\gamma_-\left(\gamma_+ + 1\right)} \tag{C.4}$$

$$\frac{p_-}{p+} = \frac{\gamma_- + \eta \pm \gamma_+ s}{\eta\left(1+\gamma_+\right)} \tag{C.5}$$

where:

$$\eta = \frac{1}{M_d^2} \quad \text{and} \quad s = \left\{\left(\frac{\gamma_-}{\gamma_+} - \eta\right)^2 - k\eta\right\}^{\frac{1}{2}}$$

$$k = 2\left\{\frac{\gamma_-\left(\gamma_+ - \gamma_-\right)\left(\gamma_+ + 1\right)}{\gamma_+^2\left(\gamma_- - 1\right)} + \frac{\gamma_-^2\left(\gamma_+^2 - 1\right)}{\gamma_+^2}\frac{Q}{c_-^2}\right\}$$

The subscript '$-$' and '$+$' denote the state ahead and behind of the wave, respectively. Equivalently for the detonation wave, the '$-$' refers to the unburned reactant with $\gamma_- = \gamma_r$, while the '$+$' is for the burned product of $\gamma_+ = \gamma_p$ across the detonation. The parameter γ in the normal shock relationship depends on whether the shock is propagating in the reactant γ_r or product γ_p. For any given strength, it is discussed before that there exist two possible solutions represented by the two signs preceding s. The top sign denotes the strong solution, while the bottom sign denotes the weak detonation solution. The unique Chapman-Jouguet (CJ) solution is obtained where the two solutions coincide ($s = 0$). In all cases studied, an incident CJ detonation is generated upstream initially before the interaction and its strength for a given chemical heat release Q is given by:

$$\eta_{cj} = \frac{\gamma_r}{\gamma_p} + \frac{k}{2} - \left\{k\left(\frac{\gamma_r}{\gamma_p} + \frac{k}{4}\right)\right\}^{\frac{1}{2}} \tag{C.6}$$

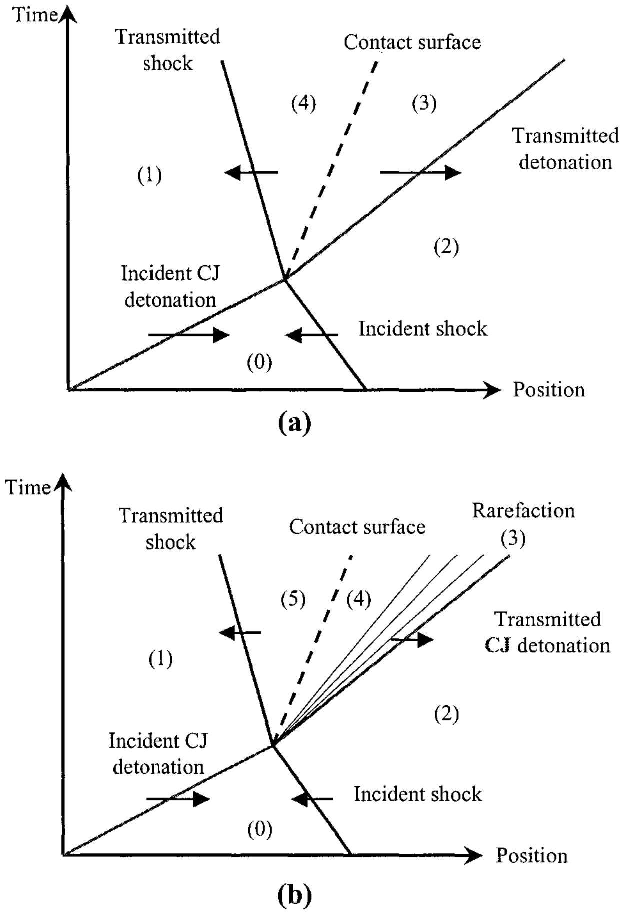

Figure C.4. Schematic of the two possible one-dimensional wave configuration models for the collision between a detonation with a shock wave.

This study begins to solve the first wave configuration as shown again schematically in figure C.4a. Upon the collision of a detonation with a planar shock, a transmitted detonation is generated downstream, which is followed by a contact surface, across which the pressure and particle velocity are uniform. A transmitted shock is also obtained, which continues to propagate into the detonation product. The properties behind the incident CJ detonation in region (1) and behind the incident shock wave in region (2) can be calculated directly from the CJ detonation solution of the Hugoniot and from the normal shock relations, respectively. Combining equations C.1-C.3 and equations C.4-C.5 across the transmitted detonation and the shock wave shown in figure C.4a and noting that pressure and particle velocity are uniform across the contact surface, the following equation is derived from which transmitted detonation Mach number can be found by an iteration procedure:

$$u_2 - \frac{c_2}{\sqrt{\eta_t}}\left(\frac{\gamma_p\left(\gamma_r+\eta_t \mp s\right)}{\gamma_r\left(\gamma_p+1\right)}-1\right) =$$
$$u_1 - c_1\left(\frac{p_2}{p_1}\left(\frac{\gamma_r+\eta_t \pm \gamma_p s}{\eta_t\left(1+\gamma_p\right)}\right)-1\right)\sqrt{\frac{2\eta_t}{\gamma_p\left(\eta_t\left(\gamma_p-1\right)+\left(\gamma_r+\eta_t \pm \gamma_p s\right)\frac{p_2}{p_1}\right)}} \tag{C.7}$$

Once the correct transmitted detonation strength η_t is found which satisfies all the boundary conditions, other flow properties in regions (3) and (4) can be easily obtained using the RH relationship.

Sample results obtained for the transmitted detonation using the first wave configuration are illustrated in figure C.5 for a gas mixtures with constant gas properties throughout (i.e.,$\gamma_r = \gamma_p = 1.2$ for simplicity without loss of generality). It shows that there can exist three possible regions of solutions, depending on the given incident detonation and incident shock strength. In the figure, the curve indicates a CJ solution for the transmitted detonation, which also provides the boundary separating the strong and weak solutions. For example, if a $M_{cj} = 6.0$ incident CJ detonation collides head on with a shock wave of strength $M_{s_i} = 2.0$, only the weak solution for the transmitted detonation can satisfy the boundary condition (i.e. the matching) across the contact surface.

Next is to consider the other possible configuration for the present wave interaction problem. It is possible to strictly replace the transmitted detonation by a

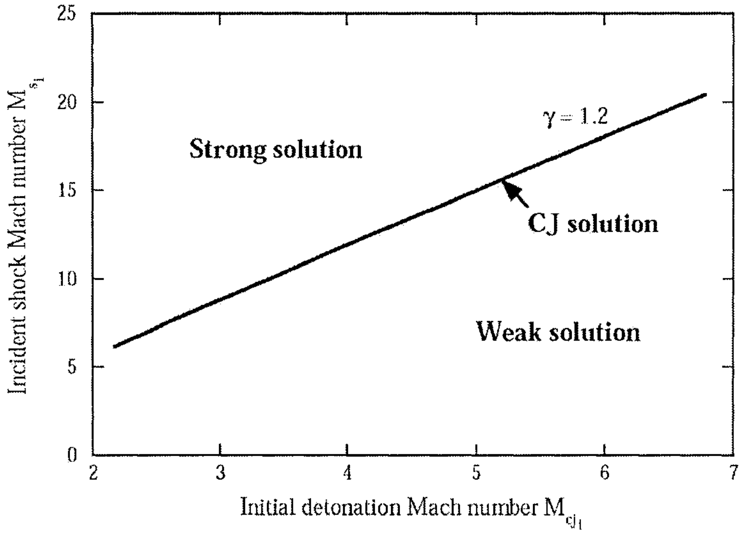

Figure C.5. Different regimes of solutions for the transmitted detonation with varying incident detonation and incident shock strength obtained using the first wave configuration shown in figure C.4a.

CJ detonation, and due to the sonic condition behind, it can be followed by a Taylor wave (or rarefaction wave) to match the condition across the contact surface, as shown in figure C.4b. In addition to the RH relationships across the shock and detonation wave, the basic isentropic relation across a rarefaction wave is needed and the flow properties inside the rarefaction fan can be obtained by marching along a C-minus characteristic:

$$\begin{aligned} u_+ - \frac{2}{\gamma-1}c_+ &= u_- - \frac{2}{\gamma-1}c_- \\ \frac{c_+}{c_-} = \left(\frac{p_+}{p_-}\right)^{(\gamma-1)/2\gamma} &= \left(\frac{\rho_+}{\rho_-}\right)^{(\gamma-1)/2} \end{aligned} \tag{C.8}$$

Combining equation C.1-C.5 and C.8 yields the following algebraic equation that is again solved by iteration to obtain the unique solution of wave strength (i.e. the transmitted shock Mach number M_{s_t}) resulting from the head-on collision between

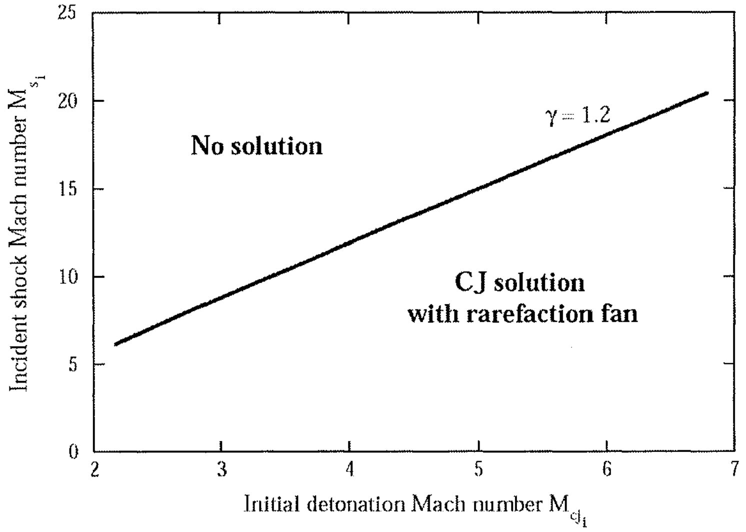

Figure C.6. Different regimes of solutions for the transmitted detonation with varying incident detonation and incident shock strength obtained using the second wave configuration shown in figure C.4b.

a detonation and a shock. (Note that η_{cj_t} can be readily found using equation C.6 from knowing the condition ahead of the detonation):

$$\begin{aligned} & u_1 - c_1 \left(\frac{2\gamma_p M_{s_t}^2 - (\gamma_p - 1)}{\gamma_p + 1} - 1 \right) \sqrt{\frac{2}{\gamma_p (\gamma_p - 1) \left(\frac{2\gamma_p M_{s_t}^2 - (\gamma_p - 1)}{\gamma_p - 1} \right)}} \\ = \; & u_2 - \frac{2c_2}{\sqrt{\eta_{cj_t}}} \frac{\gamma_p (\gamma_r + \eta_{cj_t})}{\gamma_r (\gamma_p^2 - 1)} \cdot \\ & \left[1 - \left(\frac{p_1}{p_2} \frac{\eta_{cj_t} \left(2\gamma_p M_{s_t}^2 - (\gamma_p - 1)\right)}{\eta_{cj_t} + \gamma_r} \right)^{\frac{(\gamma_p - 1)}{2\gamma_p}} + \frac{(\gamma_p - 1)(\gamma_p \eta_{cj_t} - \gamma_r)}{2\gamma_p (\gamma_r + \eta_{cj_t})} \right] \end{aligned} \tag{C.9}$$

It is found that solution to the above equation also exists and results are illus-

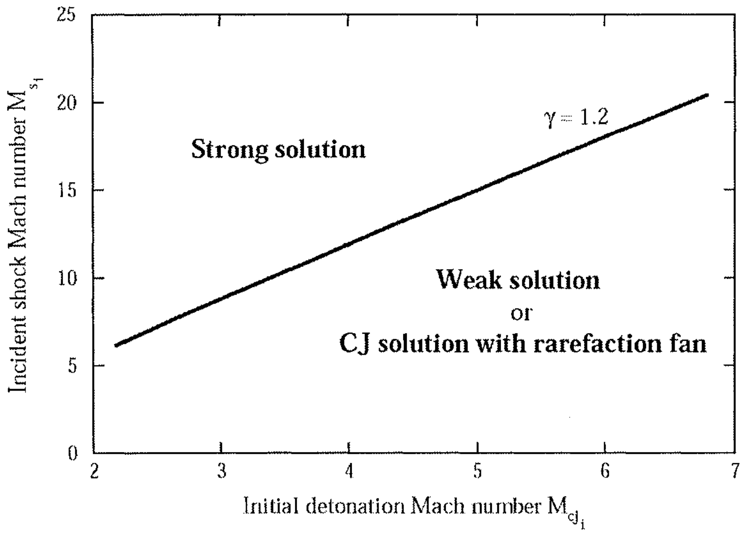

Figure C.7. Summary of possible solutions for the transmitted detonation with varying incident detonation and incident shock strength based on different wave configurations.

trated in figure C.6. The curve again indicates the specific incident detonation and incident shock strengths where a CJ solution for the transmitted detonation is obtained. For the initial conditions below this curve, solutions are also found in the above equation giving a CJ transmitted detonation followed by rarefaction fan as shown in figure C.4b. However, for conditions above this curve, no physical solution is possible. Figure C.6 therefore provides another set of solutions satisfying the conservation laws to describe the basic gasdynamics of a head-on collision between a detonation and a planar shock.

Using this simple analytical model, this Appendix mapped out different possible wave configurations that can take place resulted from the collision of a detonation with a shock over a wide range of incident wave strength. The gasdynamics flow field depends on the type of the transmitted detonation and its different solutions are summarized in figure C.7. It is interesting to point out that for typical gaseous combustible mixtures, the CJ detonation Mach number M_{cj_i} is about 4 - 7 and the initial conditions for the collision with a weak shock wave always lie in the region below the curve shown in figure C.7. One can see that in this region of initial conditions there exists multiple solutions within the context of the present simple model. The transmitted detonation can be either a weak or CJ solution. On the other hand, the strong solution can only be achieved if the incident detonation collides with a very strong shock wave $M_{s_i} \geq O\left[10\right]$, where the flow induced by the incident shock becomes significant and can overdrive the detonation after collision. However it is hardly achievable in practice because with such a strong incident shock strength, the mixture itself can be auto-ignited by shock compression and in this case, it is no longer possible to study the interaction problem.